SIMULATION OF HEAT TRANSFER PROCESSES IN TURBOCHARGERS

A DISSERTATION

*Submitted in partial fulfillment of the
requirements for the award of the degree*
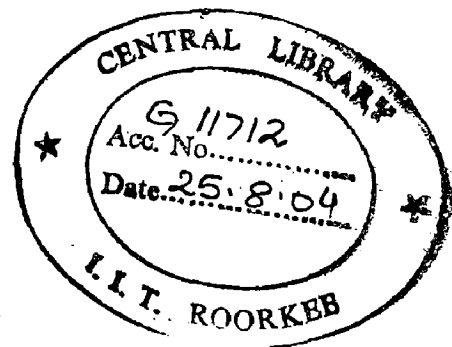of
MASTER OF TECHNOLOGY
in
MECHANICAL ENGINEERING
(With Specialization in Thermal Engineering)

By

HARMEET SINGH SALUJA

**DEPARTMENT OF MECHANICAL & INDUSTRIAL ENGINEERING
INDIAN INSTITUTE OF TECHNOLOGY ROORKEE
ROORKEE -247 667 (INDIA)
JUNE, 2004**

CANDIDATE'S DECLARATION

I hereby declare that the work which is being presented in the dissertation entitled **"Simulation of Heat Transfer Processes in a Turbochargers"** in the partial fulfilment of the requirement for the award of the degree of **Master of Technology** in Mechanical Engineering with specialization in **Thermal Systems** is an authentic record of my own work carried out from September 2003 to June 2004 under the combined supervision of Dr P.K.Sahoo, Assistant professor, Department of Mechanical and Industrial Engineering, Indian Institute of Technology, Roorkee and Dr-Ing-H Pucher, Professor, Institute of Internal Combustion Engine, TU Berlin.

I have not submitted the record embodied in this report for the award of any other degree or diploma.

Place: Roorkee

Date: 30-06-2004

(Harmeet Singh Saluja)

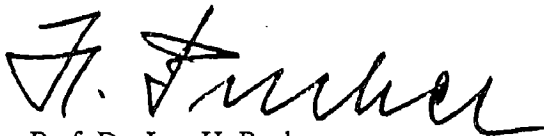This is to certify that the above statement made by the candidate is correct to the best of my knowledge.

(Dr P.K.Sahoo)

Assistant professor

Department of Mechanical

and Industrial Engineering

IIT Roorkee

Technische Universität Berlin

CERTIFICATE

This is to certify that the project report titled

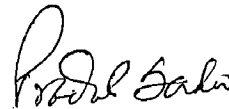**"SIMULATION OF HEAT TRANSFER PROCESSES IN TURBOCHARGERS"**

being submitted by **Harmeet Singh Saluja** is a record of bonafide work carried out under my guidance for the award of the degree **Master of Technology** in the Department of Mechanical and Industrial Engineering, Indian Institute of Technology, Roorkee.

Prof. Dr.-Ing. H. Pucher
Fachgebiet Verbrennungskraftmaschinen
Institut für Land- und Seeverkehr

Technische Universität Berlin

Technische Universität Berlin
Fak. V · Verbrennungskraftmaschinen
Prof. Dr.-Ing. Helmut Pucher
Carnotstraße 1 A, D-10587 Berlin
☎ (030) 314-233 53, Fax (030) 314-261 05

Dr. P. K. Sahoo
Assistant Professor
Department of
Mechanical and Industrial Engineering
IIT Roorkee

Dr. Pradeep K. Sahoo
Assis'   'rofessor
Dept. of Mechanical & Industrial Engg.
I.I.T. Roorkee, Roorkee-247 667

ACKNOWLEDGEMENT

Dated

Place: Roorkee   (Harmeet Singh Saluja)

Contents

List of figures and tables

Nomenclature

Letter	Physical entity	Units
A_{Sin}	Inside surface area of the turbine casing	m²
A_{Sout}	Outside surface area of the turbine casing	m²
A_{cb}	Cross-sectional area of the shaft and bearing housing assembly	m²
A_{Sb}	Outside surface area of a part of the shaft and bearing housing assembly	m²
A_{cc}	Cross-sectional area of the second part of the compressor casing	m²
A_{Sc1}	Outside surface area of the first part of the compressor casing	m²
A_{Sc2}	Outside surface area of the second part of the compressor casing	m²
A_{SinC}	Inside surface area of the compressor casing.	m²
c_p	Specific heat of the hot gases	J/Kg K
c_{pair}	Specific heat of air	J/Kg K
c	Specific heat of the compressor casing	J/Kg K
D_{in}	Inner diameter of the channel modelled as turbine casing	m
D_{out}	Outside diameter of the channel	m
D_b	Diameter of the shaft and bearing housing assembly	m
D_{outC}	Outside diameter of the compressor casing	m
k_b	Thermal conductivity of the shaft and bearing housing assembly.	W/m K
k	Thermal conductivity of the compressor casing	W/m K
k_f	Thermal conductivity of the hot gases	W/m K
k_{air}	Thermal conductivity of air	W/m K
L	Length of the channel modelled as turbine casing	m
l_b	Half the length of a part of the shaft and bearing housing assembly	m
l_{c1}	Length of the first part of the compressor casing	m
l_{c2}	Length of the second part of the compressor casing	m
$\overset{\bullet}{m}$	Mass flow rate of hot gases through the turbine	Kg/s

Symbol	Description	Units
$\dot{m}_{air}$	Mass flow rate of air through the compressor	Kg/s
n_{TBC}	Turbocharger speed	rpm
P_{inT}	Power entering the turbine with the hot gasses	W
P_{outT}	Power leaving the turbine with the exhaust gasses	W
P_{inC}	Power entering the compressor with the air	W
P_{outC}	Power leaving the compressor with the compressed air	W
P_{tur}	Mechanical power developed by the turbine	W
P_{comp}	Mechanical power absorbed by the compressor	W
P_1	Compressor inlet pressure	N/m²
P_2	Compressor outlet pressure	N/m²
P_{3t}	Total pressure at turbine inlet	N/m²
P_{4s}	Static pressure at turbine outlet	N/m²
$\dot{Q}_{inT}$	Convection heat transfer from the hot gases to the turbine casing	J/s
$\dot{Q}_{stT}$	Heat stored in the turbine casing	J/s
$\dot{Q}_{convT}$	Convection heat transfer from the turbine casing to the surroundings	J/s
$\dot{Q}_{radT}$	Radiation heat transfer from the turbine casing to the surroundings	J/s
$\dot{Q}_{in1}$	Conduction heat transfer from the turbine casing to the first part of the shaft and bearing housing assembly	J/s
$\dot{Q}_{st1}$	Heat stored in the first part of the shaft and bearing housing assembly	J/s
$\dot{Q}_{con1}$	Convection heat transfer from the first part to the surroundings	J/s
$\dot{Q}_{rad1}$	Radiation heat transfer from the part to the surroundings	J/s
$\dot{Q}_{in2}$	Conduction heat transfer from the first part to the second part of the shaft and bearing housing assembly	J/s
$\dot{Q}_{st2}$	Heat stored in the second part of the shaft and bearing housing assembly	J/s
$\dot{Q}_{con2}$	Convection heat transfer from the second part to the surroundings	J/s
$\dot{Q}_{rad2}$	Radiation heat transfer from the second part to the surroundings	J/s

$\dot{Q}_{oil}$	Heat transferred to the lubricating oil	J/s
$\dot{Q}_{in3}$	Conduction heat transfer from the second part to the third part of the shaft and bearing housing assembly	J/s
$\dot{Q}_{st3}$	Heat stored in the third part of the shaft and bearing housing assembly	J/s
$\dot{Q}_{con3}$	Convection heat transfer from the third part to the surroundings	J/s
$\dot{Q}_{rad3}$	Radiation heat transfer from the third part to the surroundings	J/s
$\dot{Q}_{c1}$	Conduction heat transfer from the third part of the shaft and bearing housing assembly to the first part of the compressor casing	J/s
$\dot{Q}_{stc1}$	Heat stored in the first part of the compressor casing	J/s
$\dot{Q}_{conc1}$	Convection heat transfer from the first part to the surroundings	J/s
$\dot{Q}_{radc1}$	Radiation heat transfer from the first part to the surroundings	J/s
$\dot{Q}_{c2}$	Conduction heat transfer from the first part to the second part of the compressor casing	J/s
$\dot{Q}_{stc2}$	Heat stored in the second part of the compressor casing	J/s
$\dot{Q}_{conc2}$	Convection heat transfer from the second part to the surroundings	J/s
$\dot{Q}_{radc2}$	Radiation heat transfer from the second part to the surroundings	J/s
$\dot{Q}_{inair}$	Convection heat transfer from the compressor casing to the air passing through it	J/s
R	Gas constant	J/Kg K
T_3	Turbine inlet temperature	K
T_m	Turbine casing temperature	K
T_4	Turbine outlet temperature	K
T_{b1}	Temperature of the first part of the shaft and bearing housing assembly.	K
T_{b2}	Temperature of the second part of the shaft and bearing housing assembly	K
T_{b3}	Temperature of the third part of the shaft and bearing housing assembly	K
T_{c1}	Temperature of the first part of the compressor casing	K

T_{c2}	Temperature of the second part of the compressor casing	K
T_1	Compressor inlet temperature	K
T_2	Compressor outlet temperature	K
T_{surr}	Surrounding temperature	K
V	Volume of the turbine casing	m³
V_b	Volume of a part of the shaft and bearing housing assembly	m³
V_{c1}	Volume of the first part of the compressor casing	m³
V_{c2}	Volume of the second part of the compressor casing	m³
V_{DC}	Velocity of cross flow in forced convection.	m/s

Symbol	Entity
ε	Emissivity
σ	Stefan-Boltzmann constant
f	Friction factor
η_{TT}	Turbine total efficiency
η_m	Transmission efficiency
μ	Dynamic viscosity of the hot gases (N/s.m²)
ν_{air}	Kinematic viscosity of air (m²/s)

Abstract

This thesis work deals with the simulation of heat transfer processes in a turbocharger using SIMULINK. A simplified model is designed which takes the turbine inlet conditions and the mechanical power absorbed by the compressor as input from the experimental data and gives the transient variation of the turbine exhaust temperature as the output. Subsequently an advanced model is designed which takes the turbine pressure ratio and inlet temperature and the compressor inlet conditions as input from the experimental data and gives the transient variation of the turbine exhaust temperature, turbine casing temperature, bearing housing temperature and the compressor outlet temperature as the output.

The correlations for the turbine total efficiency and the effective turbine throat areas as a function of the turbine pressure ratio are developed by performing dynamic experiments on the turbocharger test cell. The models are then validated by conducting experiments on the turbocharger test cell under forced and natural convection conditions with three different VTG positions (100%, 50% and 0%).

The simplified model gives a very close approximation of the turbine exhaust temperature under natural convection. The advanced model gives a close approximation of the transient variation of the bearing housing temperature and the compressor outlet temperature. The model works well with different VTG positions but the accuracy is decreased with 0% VTG position. The results show an over prediction of the turbine total efficiency and under prediction of the outside heat transfer coefficient under forced convection.

CHAPTER 1

Introduction

1.1 Problem description

Concern over air pollution is growing steadily. Vehicle emissions contribute between one third and one half of the total atmospheric burden of carbon monoxide (CO), nitrogen oxides (NOx), and hydrocarbon compounds (HC). The impact is even greater in urban areas. To solve these problems, cities, states and federal governments have created emission regulations (EU 4 and US 2007) to restrict the amount of pollution that vehicles can produce. To keep up with these laws, car manufacturers have developed a number of emission control techniques [3].

Emissions from a vehicle can be grouped into three categories. Those that are emitted from the crankcase, those that evaporate from the fuel system, rubber and plastic parts of the vehicle, and those that comes from the tail pipe.

Crankcase emissions have been reduced 100% since positive crankcase ventilation systems were introduced on passenger cars. This simple system used a hose from the crankcase to the engine intake manifold to pull fumes into the manifold. There the fumes could be reburned. A small check valve called the PCV valve (Positive Crankcase Ventilation) was placed in the hose to control the flow of fumes.

Evaporative emissions come from the fuels, oils, rubber, and plastic parts used on the automobiles. Most of the emissions come from the fuel and this has been controlled using a charcoal canister connected to the vent line from the fuel tank. The charcoal canister is filled with activated charcoal (carbon) that attracts the hydrocarbon fumes evaporating from the fuel. Each gram of activated charcoal can hold up to 1000 times its weight in hydrocarbon fumes. The canister can release the fumes when fresh air is pulled through the charcoal, so the canister can be used over and over again. Air is pulled through the canister by engine intake manifold vacuum and the hydrocarbon fumes are burned inside the engine instead of being released to the atmosphere.

Exhaust emissions are controlled using many different devices and designs. The shape of the combustion chamber inside the engine where the fuel and air ignite plays an important part in reducing the exhaust emissions. Better technology and research techniques have enabled the car manufacturers to change their engines to meet tougher emissions regulations. Fuel injection has played a major part in reducing emissions. The accurate computer control of fuel and ignition timing has also given better fuel economy and performance. The exhaust gas recirculation (EGR) system has been used to reduce the amount of nitrogen oxides (NOx) created by the engine during operating periods that usually result in high combustion temperatures. The system reduces NOx production by recirculating small amounts of exhaust gases into the intake manifold where it mixes with the incoming air/fuel charge. By diluting the air/fuel mixture under these conditions, peak combustion temperatures and pressures are reduced, resulting in an overall reduction of NOx output. Furthermore, the catalytic converters have also been

developed which treat the exhaust before it leaves the vehicle and reduces a lot of atmospheric pollution [5].

Today's converters eliminate up to 97% of CO and HC emissions. Unfortunately the effectiveness of a catalyst is greatly limited for the time that it takes to reach its operating temperature (also called light off temperature) of about 300°C. Between 60% to 80% of the toxic air emissions from automobiles occur during this cold-start period. The concern over cold-start emissions has lead to significant activity by car manufacturers and suppliers to develop new emissions treatment techniques. Leading approaches include heating the converter electrically or with a catalyzed fuel burner. This approach requires 10 to 20 Wh of electric energy, to be supplied by the alternator or battery. Furthermore, the fuel burner systems are fairly complex and may expose the converter to severe thermal gradients which may lead to a reduction in system durability. Another approach that has been used is to move the converter closer to the engine manifold to reach the operating temperature more quickly. However, in many cars this introduces additional unwanted heat into the engine compartment and also the catalyst is more susceptible to exhaust temperature excursions.

A recent approach that is being used is to use insulated converters located well downstream of the engine. Sufficient insulation around the converter can help the converter to maintain its temperature above the operating temperature for several hours after the engine is shut off. Unfortunately, to provide sufficient thermal insulation for holding heat for more than 3 hours, conventional refractory insulation must be extremely bulky and heavy. Also, during steady state operation of the engine, this insulation may allow the catalyst temperature to exceed the safe limits (approximately 1000°C), resulting in thermal degradation and loss of emission conversion efficiency. A better approach for the thermal management of the converter, that is being developed, is to use a compact insulation that could be continuously varied in thermal conductance, providing the very low conductivity needed to retain heat when engine is shut off but providing much higher conductivity for heat rejection from the converter during engine operation [3].

For the further improvement of the above mentioned emission treatment techniques it is desirable to have a clear understanding about the transient variation of the temperature of the exhaust gases from the engines. In the case of turbocharged engines the understanding about the transient variation of the temperature of the exhaust gases from the turbocharger turbine is desirable. Particularly variation of the exhaust gas temperature during cold-start period is of greater importance.

Secondly, simulation models, which simulate the complete engine cycle, are being used for the last few decades to assist in understanding the observed behaviour of engines and to predict engine performance and efficiency as a function of engine design parameters. Today engine systems are becoming more complicated to meet the increasing demands on fuel efficiency and emission legislation. Therefore it is desirable to have accurate engine system simulation models. In most of the engine system simulation models being used, it is a common practise to consider the compressor of the turbocharger as an adiabatic unit. This assumption gives an incorrect approximation of the temperature

2

rise across the compressor. For a better approximation of the temperature at the outlet of the compressor it is necessary to consider the heat transfer that takes place by conduction through the shaft and bearing housing, to the compressor of the turbocharger. Moreover, for the thermal management of the engine compartment it is desirable to have a clear understanding about the variation of the casing temperature of the turbine and the compressor of the turbocharger. The full analysis requires the modelling of various heats and power fluxes which occur within a turbocharger.

1.2 Objectives of the Thesis

The present thesis deals with mathematical modelling, simulation and validation of various heat and power fluxes, which occur within a turbocharger. The objectives of this thesis include the determination of transient variation of the exhaust gas temperature and the casing temperature of the turbine of a turbocharger under forced and natural convection conditions. The thesis also aims at providing an insight into the transient variation of compressor outlet temperature, impeller casing temperature and the pressure ratio across the compressor for a given range of turbine inlet temperature and pressure ratio.

The thesis consist of following parts

- Designing of a simplified and an improved MATLAB/SIMULINK heat transfer models.
- Conducting experiments with different convection conditions.
- Comparison and validation of the models with experimental data.

CHAPTER 2

State of the Art

2.1 Fundamentals of Heat Transfer

Heat transfer (or heat) is energy being transmitted due to a temperature difference. Whenever there exists a temperature difference in a medium or between media, heat transfer will occur. The different types of heat transfer processes or modes are conduction, convection and thermal radiation (shown in Fig 2.1 to 2.3). The term conduction refers to the heat transfer that occurs when a temperature gradient exists in a stationary medium, which may be a solid or a fluid. The term convection refers to the heat transfer that occurs between a surface and a moving fluid when they are at different temperatures. All surfaces of finite temperature emit energy in the form of electromagnetic waves. So in the absence of an intervening medium there is net heat transfer between two surfaces at different temperatures, this is referred to as heat transfer by thermal radiation [1].
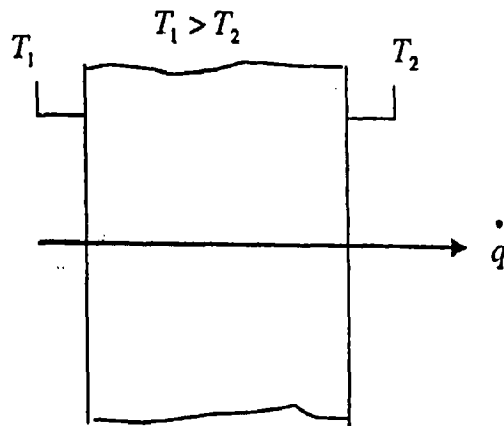
Figure 2.1 Conduction through a solid or a stationary fluid.
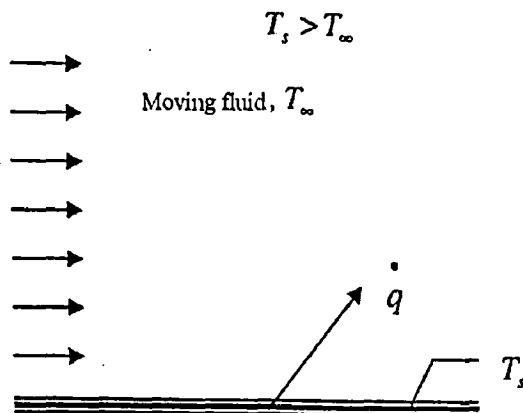
Figure 2.2 Convection from a surface to a moving fluid.
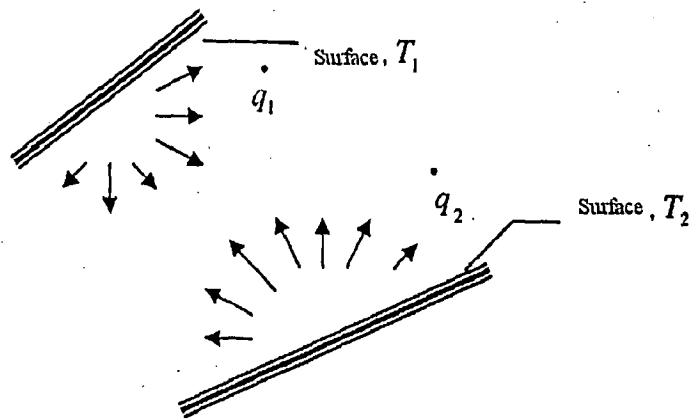
Figure 2.3 Net radiation heat exchange between two surfaces.

2.1.1 Conduction:

Conduction is heat transfer by means of molecular agitation within a material without any motion of the material as a whole. Heat energy in a substance is associated with random translational motion, as well as with the internal rotational and vibrational motions of the molecules making up the substance. Consider a gas in which there exists a temperature gradient and assuming that there is no bulk motion. As higher temperatures are associated with higher molecular energies so when the neighbouring molecules collide there occurs a transfer of energy from more energetic to less energetic molecules. In the presence of a temperature gradient, energy transfer occurs in the direction of decreasing temperature. In liquids, since the molecules are closely spaced the molecular interactions are stronger and more frequent. In solids the molecules themselves are bound and contribute to conduction of heat mainly by vibrating against neighbouring molecules. A more important mechanism, however, is the migration of energetic free electrons through the solid. Metals which have a high free -electron density are good conductors of heat, while non-metals, such as wood or glass, have few free electrons and are poor conductors of heat [6].

Appropriate rate equations are used to quantify heat transfer processes in the terms of amount of energy transferred per unit time. For heat conduction, the rate equation is known as Fourier's law. For a one dimensional plane wall shown in Fig 2.4, having a temperature distribution T(x) , the rate equation is expressed as

$$\overset{\bullet}{q}_x = -k\frac{dT}{dx}. \tag{2.1}$$

The heat flux $\overset{\bullet}{q}_x$ is the heat transfer rate in the x direction per unit area perpendicular to the direction of transfer and it is proportional to the temperature gradient, $\dfrac{dT}{dx}$ in this direction. The proportionality constant k is a transport property known as thermal conductivity and is a characteristic of the wall material. The minus sign is a consequence of the fact that heat is transferred in the direction of

decreasing temperature. Under steady state conditions, where the temperature distribution is linear, the temperature gradient may be expressed as
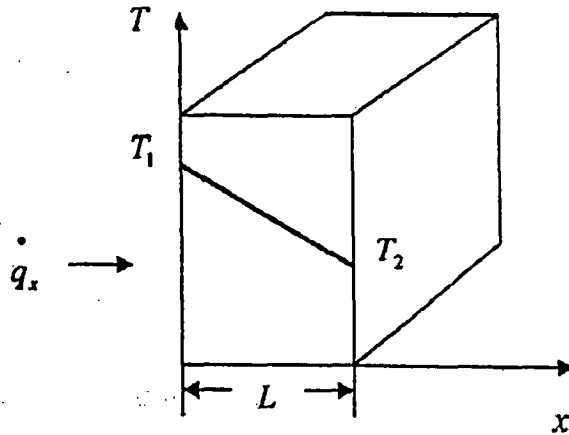
Figure 2.4 One-dimensional heat transfer by conduction.

$$\frac{dT}{dx} = \frac{T_2 - T_1}{L} \tag{2.2}$$

Substituting equation 2.1 in equation 2.2 gives heat flux as

$$\dot{q}_x = -k\frac{T_2 - T_1}{L}. \tag{2.3}$$

Or

$$\dot{q}_x = k\frac{T_1 - T_2}{L} = k\frac{\Delta T}{L} \tag{2.4}$$

This equation provides a heat flux, that is, the rate of heat transfer per unit area. The heat rate by conduction, $\dot{Q}_x$ through a plane wall of area A is then the product of the flux and the area,

$$\dot{Q}_x = \dot{q}_x A. \tag{2.5}$$

2.1.2 Convection:

The convection heat transfer mode is comprised of two mechanisms. In addition to energy transfer due to random molecular motion, there is also energy being transferred by the bulk, or macroscopic, motion of the fluid. This fluid motion is associated with the fact that, at any instant, large number of molecules are moving collectively or as aggregates. Such motion, in the presence of a temperature gradient, will give rise to heat transfer. Because the molecules in the aggregate retain their random motion, the total heat transfer is then due to a superimposition of energy transport by the random motion of the molecules and by the bulk motion of the fluid. The term convection is used to refer this cumulative transport and the term advection is used to refer transport due to bulk fluid motion [10].

Convective heat transfer is categorized into forced convection and natural convection according to the nature of flow. In forced convection flow is caused by some external means, such as by a fan, a pump, or atmospheric winds. In natural or free convection flow is induced by buoyancy forces in the fluid.

These forces arise from density variations caused by temperature variations in the fluid. An example is the free convection heat transfer that occurs from a hot pavement to the atmosphere on a still day. Air that is in contact with the hot pavement has a lower density than that of the cooler air above the pavement. Hence, a circular pattern exists in which the warm air moves up from the pavement and the cooler air moves downward [13].

The appropriate rate equation for the convection heat transfer mode is given by Newton's law of cooling that is of the form

$$\dot{q} = h(T_s - T_\infty).$$
(2.6)

Here, $\dot{q}$ the heat flux per unit surface area is proportional to the difference between surface and fluid temperatures, T_s and T_∞ respectively. The proportionality constant h is referred to as heat transfer coefficient. It encompasses all the effects that influence the convection mode. It depends on the conditions in the boundary layer which are influenced by surface geometry, nature of fluid motion, and number of fluid thermodynamic and transport properties [1].

2.1.2.1 Convection boundary layers:

Boundary layer effects are an integral part of convection heat transfer. Consider fluid flow over a heated surface as shown in Fig 2.5. A consequence of the fluid-surface interaction is the development of a region in the fluid through which the velocity varies from zero at the surface to a finite value u_∞ associated with the main flow. This region of the fluid is known as the hydrodynamic or velocity boundary layer. Moreover, if the surface and flow temperature differs, there will be a region of the fluid through which the temperature varies from T_s at $y = 0$ to T_∞ in the outer flow. This region, called the thermal boundary layer, may be smaller, larger, or the same size as that through which the velocity varies.
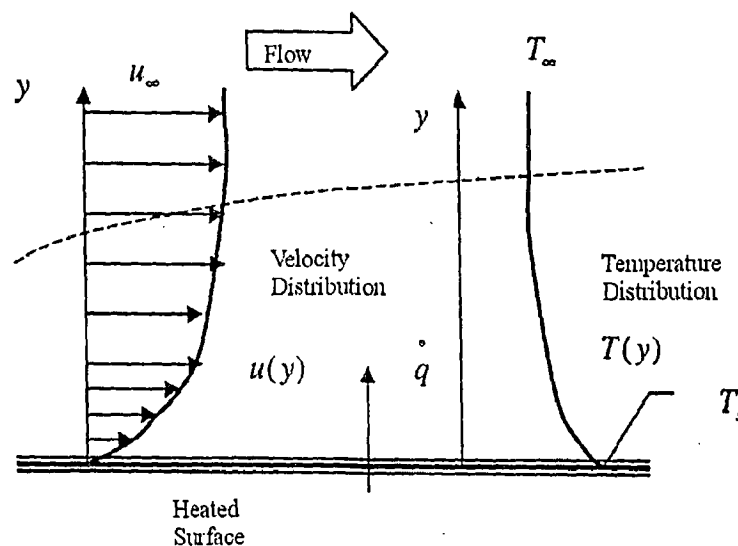
Fig 2.5 Boundary layer development in convection heat transfer

The convection heat transfer mode is sustained by both random molecular motion and the bulk motion of the fluid within the boundary layer. The contribution due to random molecular motion generally dominates near the surface where the fluid velocity is low. At the interface between the surface and the fluid, heat is transferred by this mechanism only. The contribution due to bulk fluid motion originates from the fact that boundary layers grow as the flow progresses in x direction [9].

2.1.2.2 Laminar and turbulent flows:

In the treatment of any convection problem it is essential to determine whether the boundary layer is laminar or turbulent. Surface friction and the convection heat transfer rates depend strongly on which of these conditions exists. As shown in Fig 2.6 there are sharp differences between laminar and turbulent flow conditions. In the laminar boundary layer, fluid motion is highly ordered and it is possible to identify streamlines along which particles move. In contrast, fluid motion in the turbulent boundary layer is highly irregular and is characterised by velocity fluctuations. These fluctuations enhance the transfer of momentum, energy, and species and hence increase surface friction as well as convection heat transfer rates. Fluid mixing resulting from fluctuations makes turbulent boundary layer thickness larger and boundary layer profiles flatter than in laminar flow [9].
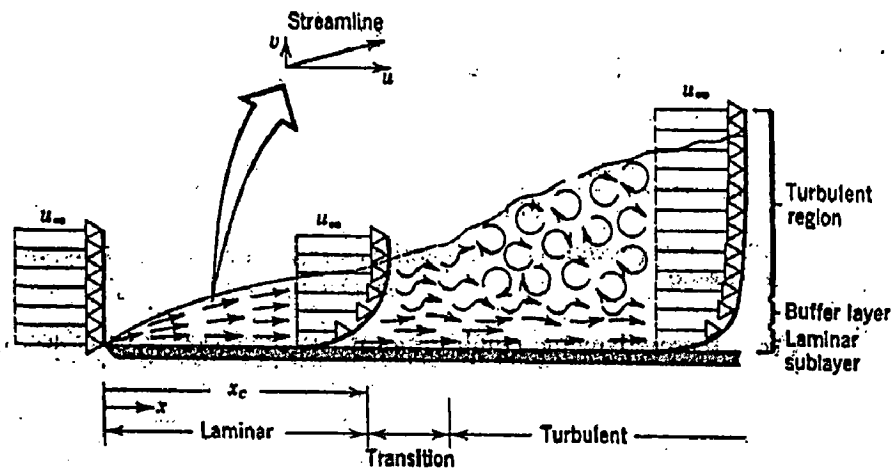
Figure 2.6 Velocity boundary layer development on a flat plate.

The boundary layer is initially laminar, but at some distance from the leading edge, transition to turbulent flow begins to occur. Fluid fluctuations begin to develop in the transition region and the boundary layer eventually becomes completely turbulent. In calculating boundary layer behaviour it is frequently reasonable to assume that transition begins at some location x_c. This location is determined by a dimensionless grouping of variables called the Reynolds number,

$$\text{Re}_x = \frac{\rho u_\infty x}{\mu}.$$
(2.7)

8

Here the characteristic length x is the distance from the leading edge. The critical Reynolds number is the value of Re_x for which transition begins, and for external flow it is known to vary from 10^5 to 3×10^5, depending on surface roughness, the turbulence level of the free stream and the nature of pressure variation along the surface.

2.1.3 Radiation:

Thermal radiation is energy emitted by matter that is at a finite temperature. Although in this thesis the focus is primarily on radiation from solid surfaces, emission may also occur from liquids and gases. Regardless of the form of matter, the emission may be attributed to changes in the electron configuration of the constituent atoms or molecules. The energy of radiation field is transported by electromagnetic waves (or alternatively, photons). The transfer of energy by radiation does not require the presence of any material medium. In fact it occurs most efficiently in vacuum.

There are two features which describe the nature of thermal radiation from a surface. One is spectral distribution and other is the directionality. Thermal radiation emitted by a surface encompasses a range of wavelengths and the magnitude of the radiation varies with wavelength, the term spectral is used to refer to the nature of this dependence. The second feature relates to its directionality, as a surface may emit preferentially in certain directions, creating a directional distribution of the emitted radiation [14]. The blackbody is an ideal surface which absorbs all incident radiation, regardless of wave length and direction. For a given temperature and wavelength, no surface can emit more energy than a blackbody and radiation emitted is independent of direction. The flux at which radiation is emitted by a blackbody is given by Stefan-Boltzmann law that is

$$\dot{q} = \sigma T_s^4. \tag{2.8}$$

Here T_s is the absolute temperature of the surface and σ is the Stefan-Boltzmann constant.

The heat flux emitted by a real surface is less than that of the ideal radiator and is given by

$$\dot{q} = \varepsilon \sigma T_s^4. \tag{2.9}$$

Here ε is a radiative property of the surface called the emissivity. This property indicates how efficiently the surface emits compared to an ideal radiator. The emissivity for a blackbody is 1 and for a real surface emissivity is always less than 1. Equation 2.8 determines the rate at which energy is emitted by a surface. Determination of the net rate at which radiation is exchanged between surfaces is more complicated. However, a special case that is considered in this thesis is the net exchange between a small surface and a much larger surface that completely surrounds the smaller one (Fig 2.6). The air which separates the surface and the surroundings has no effect on the radiation transfer and the surrounding is assumed to be a black body. The net rate of radiation heat exchange between the surface and its surroundings, expressed per unit area of the surface is given by

$$\dot{q} = \frac{q}{A} = \varepsilon \sigma (T_s^4 - T_{atm}^4). \tag{2.10}$$

Here A is the surface area and ε is its emissivity, while T_s and T_{atm} are the temperatures of the surface and the surrounding respectively. With the above assumption, the area and the emissivity of the surroundings do not influence the net heat exchange rate [14].
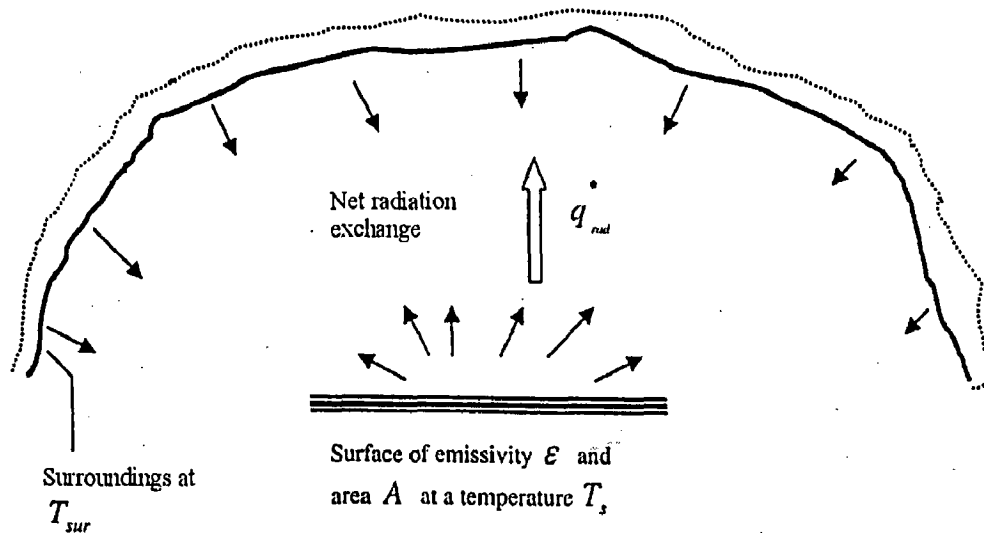
Figure 2.7 Radiation exchange between a surface and its surroundings.

2.1.4 Transient Conduction

2.1.4.1 The lumped capacitance method:

The lumped capacitance method is a model, which deals with transient conduction problems in which a solid experiences a sudden change in its thermal environment. Consider a hot metal forging that is initially at a uniform temperature T_i and is quenched by placing it in a free air stream of lower temperature $T_\infty < T_i$ (Fig 2.7). If the quenching is said to begin at time $t = 0$, the temperature of the solid will decrease for time $t > 0$ until it eventually reaches T_∞. This reduction is due to convection heat transfer occurring at the solid/air interface. The essence of the lumped capacitance method is the assumption that the temperature of the solid is spatially uniform at any instant during the transient processes. This implies that temperature gradients within the solid are negligible [8].

Transient temperature response of the solid is determined by formulating an energy balance over the solid which relates the rate of heat loss at the surface to the rate of change of the internal energy. This is of the form
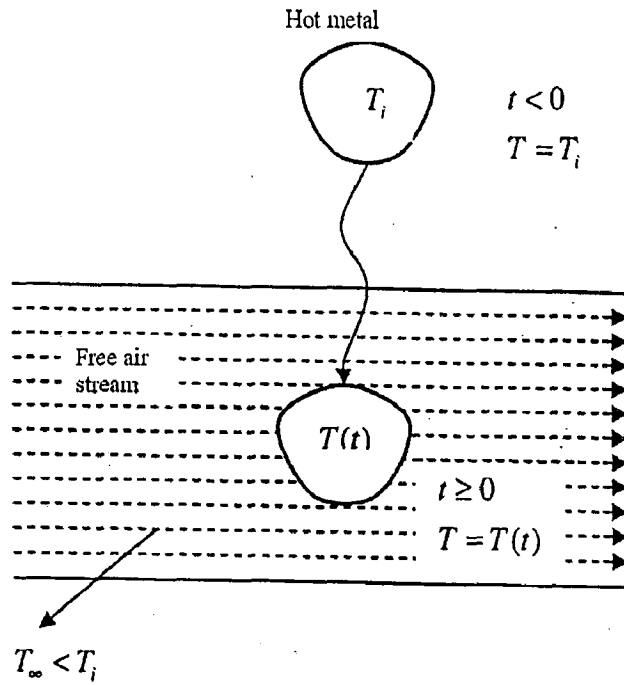
Figure 2.8 Cooling of a hot metal.

$$-\dot{E}_{out} = \dot{E}_{st}.$$ (2.11)

Or

$$-hA_s(T - T_\infty) = \rho V c \frac{dT}{dt}.$$ (2.12)

Here $\dot{E}_{out}$ is the rate at which energy is transferred by convection and negative sign shows that heat is

lost from the solid. E_{st} is the rate of change of internal energy of the solid.

Introducing the temperature difference

$$\theta = T - T_\infty$$ (2.13)

And recognizing that

$$\frac{d\theta}{dt} = \frac{dT}{dt}.$$ (2.14)

Substituting equations 2.12 and 2.13 in equation 2.11 gives

$$\frac{\rho V c}{hA_s} \frac{d\theta}{dt} = -\theta.$$ (2.15)

Separating variables and integrating from the initial condition that at $t = 0$ the temperature is

$T(0) = T_i$ gives

$$\frac{\rho\,Vc}{hA_s}\int_{\theta_i}^{\theta}\frac{d\theta}{\theta}=-\int_0^t dt.$$

(2.16)

Here $\theta_i = T_i - T_\infty$.

(2.17)

Evaluating the integrals it follows that

$$\frac{\rho Vc}{hA_s}\ln\frac{\theta_i}{\theta}=t.$$

(2.18)

$$\frac{\theta}{\theta_i}=\frac{T-T_\infty}{T_i-T_\infty}=\exp\left[-\left(\frac{\rho Vc}{hA_s}\right)t\right].$$

(2.19)

The above equation gives the transient temperature response of the solid.

2.1.4.2 Validity of Lumped Capacitance Method:

This analysis is valid if the resistance to conduction within the solid is much less than the resistance to convection across the fluid boundary layer. Thus the assumption of a uniform temperature distribution is reasonable if the following condition is satisfied

$$Bi=\frac{hL_c}{k}\le 0.1.$$

(2.20)

Here Bi is a dimension less parameter termed as Biot number, k is the thermal conductivity of the solid, h is the heat transfer coefficient of the surrounding air and L_c is the characteristic length given by

$$L_c=\frac{V}{A_s}.$$

(2.21)

Here V is the volume of the solid and A_s is the surface area of the solid exposed to the fluid [8].

2.2 Literature survey

"A Study of Rotor Cavities and Heat Transfer in a Cooling Processes in a Gas Turbine"

In this paper Prof R.S. Amano has presented a numerical study of thermal flow analysis in a two stage turbine in order to understand better the detailed flow and heat transfer mechanisms through the cavity and the rotating rotor disks. The numerical computations were performed to predict thermal fields through the rotating disks.

"Heat Transfer and Flow Phenomena in a Swirl Chamber Simulating Turbine Blade Internal Cooling"

In this paper Prof P.M.Ligrani has given heat transfer and fluid mechanics results for a swirl chamber whose geometry models an internal passage used to cool the leading edge of a turbine blade. The Reynolds number, based on inlet duct characteristics is investigated.

"Experimental and Theoretical Investigations of Heat Transfer in Closed Gas Filled Rotating Annuli"

In this paper Prof D. Bohn had made the experimental investigations to analyze the convective heat transfer in closed, gas filled annuli to rotating around their horizontal axes. The experimental setup is designed to establish a pure centripetal heat flux inside these annular cavities. A computer programme

12

to simulate flow and heat transfer in closed rotating cavities has been developed and tested successfully for annuli with isothermal side walls with different temperatures giving an axial heat flux.

"Effect of Velocity and Temperature Distribution at the hole exit on Film Cooling of Turbine Blades"

In this paper Prof V.K Garg has used an existing three–dimensional Navier–Stokes code, modified to include film cooling considerations, to study the effect of coolant velocity and temperature distribution at the hole exit on the heat transfer coefficient on three film cooled turbine blades, namely, the C3X vane, the VKI rotor, and the ACE rotor. Results are also compared with the experimental data for all the blades.

"The Influence of Film Cooling on the efficiency of an Annular Nozzle Guide Vane Cascade"

In this paper Prof C.R.B Day examines the effect of aerofoil surface film cooling on the aerodynamic efficiency of an annular cascade of transonic nozzle guide vane. A dense foreign gas (SF6/Ar mixture) is used to simulate engine representative coolant to mainstream density ratios under ambient conditions.

"Heat Transfer in a Rotating Cavity with a Peripheral Inflow and Outflow of Cooling air"

In this paper Prof I Mirzaee describes a combined computational and experimental of the heat transfer in a rotating cavity with a peripheral inflow and outflow of cooling air for a range of rotational speeds and flow rates.

"Heat Transfer in a Rotating Cavity with a Stationary Stepped Casing"

In this paper Prof I Mirzaee has considered a system in which co rotating turbine disks are cooled by the air supplied at the periphery of the system. The system comprises two co rotating disks, connected by a rotating cylindrical hub and shrouded by a stepped ,stationary cylindrical outer casing .Cooling air enters the system through holes in the periphery of one disk, and leaves through the clearances between the outer casing and the disks. The paper describes a combined computational and experimental study of heat transfer in the above described system.

"Simulation of Heat Transfer from Flow with High Free-Stream Turbulence to Turbine Blades"

In this paper Prof E.Fridman has applied the relaxation model to simulate the momentum and thermal boundary layers for laminar, transitional, and turbulent flows when turbulent fluctuations are present in the free stream.

"Local Heat Transfer in a Rotating Two Pass Triangular Duct with Smooth Walls"

In this paper Prof S.Dutta has conducted heat transfer studies on a triangular duct with orthogonal rotation. This paper presents turbulent heat transfer characteristics of a two pass smooth walled triangular duct. One pass is for radial outward flow and the other pass is for radial inward flow. With rotation radial outward and inward flow directions show different surface heat transfer characteristics.

"The Influence of Endwall Contouring on the Performance of a Turbine Nozzle Guide Vane"

In this paper Prof V.Dossena has presented the results of a detailed investigation of the flow field in a gas turbine linear cascade. A comparison between a contoured and a planar configuration of the same

cascade has been performed, and differences in the three dimensional flow field were analyzed and discussed.

"Experimental and Theoretical Investigations of Heat Transfer in Closed Gas Filled Rotating Annu II"

In this paper Prof D. Bohn had made the experimental investigations to analyze the convective heat transfer in closed, gas filled annuli to rotating around their horizontal axes. The experimental setup designed to setup is designed to establish a pure axially directed heat flux inside these annular cavitie Parallel to the experiments, numerical calculations have been conducted.

CHAPTER 3
Modelling the Heat Transfer in a Turbocharger

3.1 Description of Heat and Power Transfer in a Turbocharger
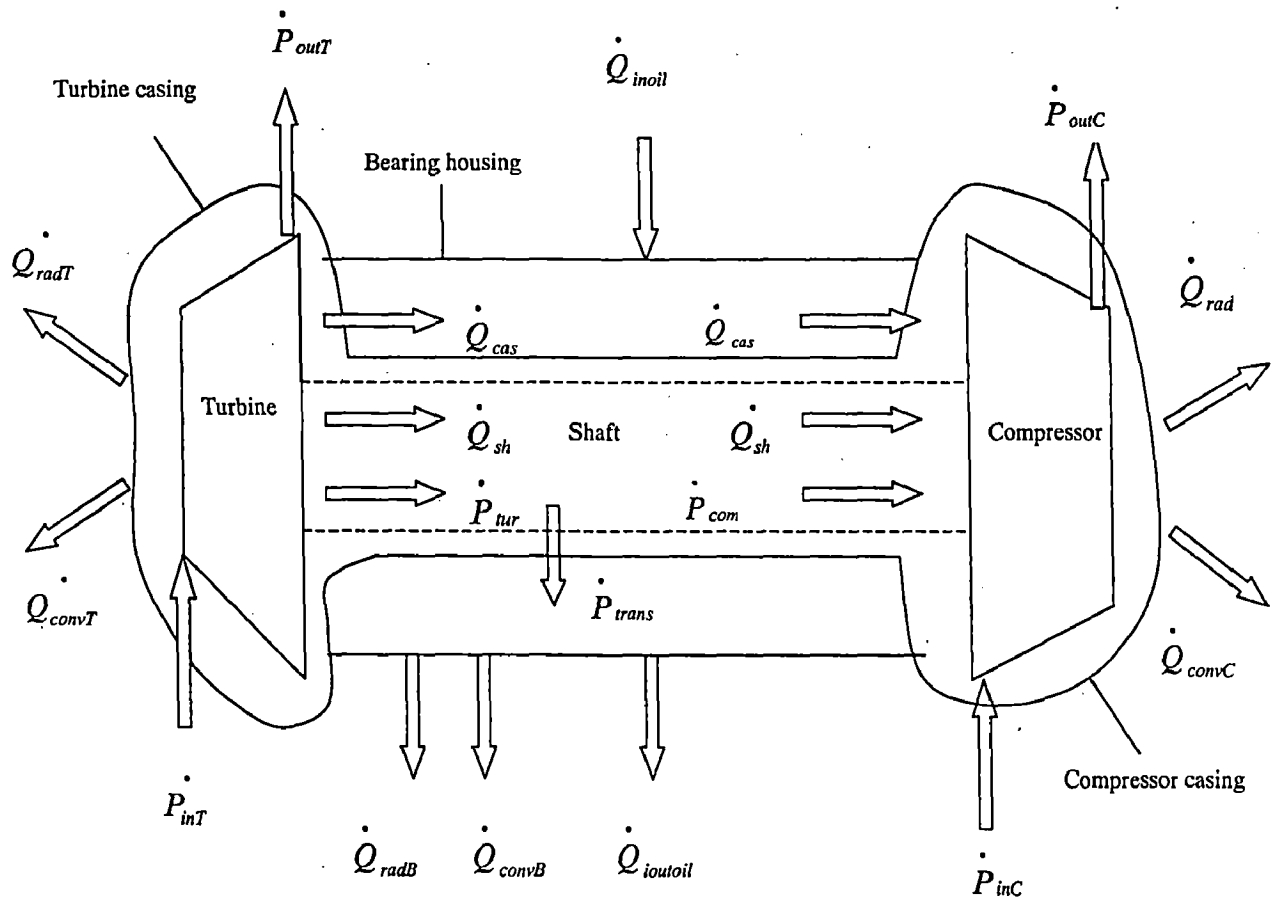
Figure 3.1 Heat and power fluxes in a turbocharger

The schematic figure 3.1 shows a turbocharger comprising of turbine, turbine casing, shaft, bearing housing, compressor and compressor casing. The figure shows the various heat and power fluxes which occur within a turbocharger. The fluxes are listed below

1. The transfer of heat by convection from the hot gases to the turbine casing.

2. The transfer of heat by convection from the turbine casing to the surroundings ($\dot{Q}_{convT}$).

3. The transfer of heat by radiation from the turbine casing to the surroundings ($\dot{Q}_{radT}$).

4. The storage of heat in the turbine casing.

5. The transfer of heat by conduction from the turbine casing to the shaft and bearing housing assembly ($\dot{Q}_{cas}$).

15

6. The transfer of heat by convection from the bearing housing to the surroundings ($\dot{Q}_{convB}$).

7. The transfer of heat by radiation from the bearing housing to the surroundings ($\dot{Q}_{radB}$).

8. The storage of heat in the shaft and bearing housing assembly.

9. The transfer of heat to the lubricating oil.

10. The transfer of heat by conduction from the shaft and bearing housing assembly to the compressor casing.

11. The storage of heat in the compressor casing.

12. The transfer of heat by convection from the compressor casing to the surroundings ($\dot{Q}_{convC}$).

13. The transfer of heat by radiation from the compressor casing to the surroundings ($\dot{Q}_{radC}$).

14. The transfer of heat by convection from the compressor casing to the air passing through it.

15. Power entering the turbine with hot gases ($\dot{P}_{inT}$).

16. The mechanical power developed by expansion of the gases through the turbine.

17. Power leaving the turbine with the exhaust gases ($\dot{P}_{outT}$).

18. The mechanical power lost in transmission from turbine to compressor.

19. Power entering the compressor with the air to be compressed ($\dot{P}_{inC}$).

20. The mechanical power absorbed by the compressor for compression of the air.

21. Power leaving the compressor with the compressed air ($\dot{P}_{outC}$).

3.2 Design of a simplified MATLAB model

3.2.1 Introduction

This model is designed to determine the transient variation of turbine casing temperature and the temperature of the exhaust gases leaving the turbine. The model will calculate these temperatures for given turbine inlet conditions and the power absorbed by the compressor under forced and natural convection conditions. The reason for designing this simplified model is that it can be easily parameterized and can be easily plugged into the complete engine cycle simulation model.

The following list contains the heat and power transfer effects considered in this model

1. Energy transferred by convection from the hot gases to the turbine casing.

2. Energy stored in the turbine casing

3. Energy lost due to convection to the atmosphere.

4. Energy lost due to radiation to the atmosphere.

5. Power entering the turbine with the hot gases.

6. The mechanical power absorbed by the compressor for compression of the air.

7. Power leaving the turbine with the exhaust gases.

The effects are described in detail below

3.2.2 Energy transferred by convection from the hot gases to the turbine casing

The transfer of heat by convection is governed by *Newton's Law of Cooling* which states that convective heat flux is proportional to the difference between the surface and the fluid temperatures (explained in detail in section 2.1.2)[10]. The heat transferred by convection from the hot gases to the turbine casing is given by

$$\dot{Q}_{inT} = h_{in} A_{Sin}(T_3 - T_m) \qquad (3.1)$$

Here $\dot{Q}_{inT}$ is the heat transferred by convection from the hot gases to the turbine casing, T_3 is the temperature of the hot gases entering the turbine and T_m is the temperature of the turbine casing. To calculate the heat transfer coefficient h_{in} the turbine casing is assumed to be a channel with a circular cross-section. The length of the channel is taken equal to the length of the spiral. In equation 3.1 A_{Sin} is the inside surface area of the channel exposed to the hot gases and is given by

$$A_{Sin} = \pi D_{in} L. \qquad (3.2)$$

Here L is the length of the channel and D_{in} is the inner diameter. The inner diameter of the channel is taken as the mean of turbine casing inner inlet and exit diameter as shown in the figure 3.2 below. The inner diameter at the inlet of the turbine casing is taken as the mean of horizontal and vertical diameters at the inlet section of the turbine casing.
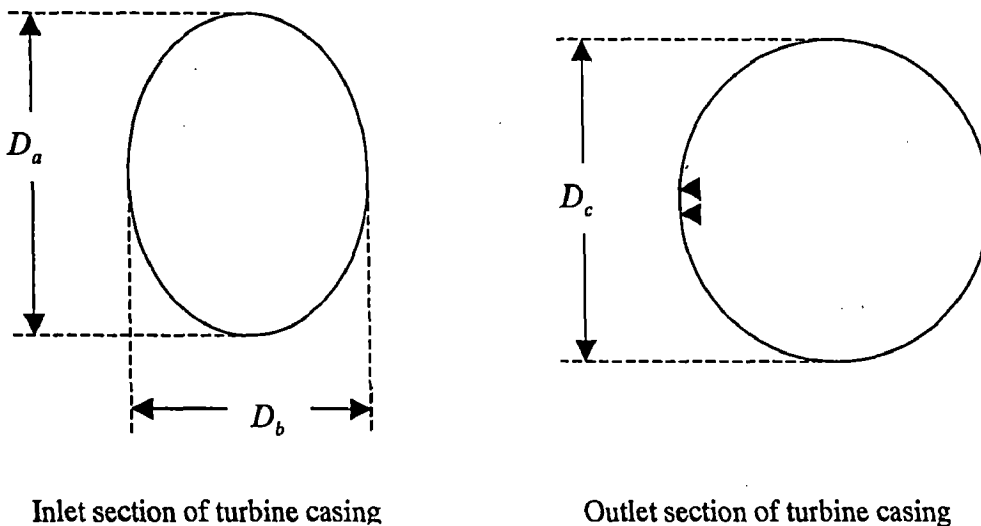

Inlet section of turbine casing   Outlet section of turbine casing

Figure 3.2 Inlet and outlet section of turbine casing

$$D_m = \frac{D_a + D_b}{2}. \qquad (3.3)$$

$$D_{in} = \frac{D_{mi} + D_c}{2}.$$ (3.4)

The outer diameter of the circular channel is calculated by adding twice the thickness of the turbine casing to the inner diameter. The Chilton–Colburn analogy[11] is used for computing the average Nusselt number for fully developed turbulent flow in a circular tube which is then used to calculate the heat transfer coefficient h_{in}. The analogy is of the form

$$\frac{f}{8} = \frac{Nu_D}{Re_D \, Pr^{1/3}}$$ (3.5)

Here Nu_D is the average Nusselt number, Re_D is the Reynolds number and Pr is the Prandlt number and are given by

$$Nu_D = h_{in} D_{in} / k_f.$$ (3.6)

$$Re_D = 4 D_{in} \dot{m} / \pi \mu.$$ (3.7)

Here μ is the dynamic viscosity, Pr is the Prandtl number and k_f is the thermal conductivity of the hot gases entering the turbine. These properties are measured at the temperature T_3. The corelations used are given in the appendix A1.

Subsituting equations 3.6 and 3.7 in equation 3.5 gives

$$\frac{f}{8} = \frac{h_{in} D_{in} / k_f}{(4 D \dot{m} / \Pi \mu)(Pr)^{1/3}}.$$ (3.8)

Here f refers to friction factor. Its value is taken as .038 for cast iron within the Reynolds number ranging from 20000 to 70000.

The equation 3.9 gives the heat transfer coefficient h_{in}.

3.2.2 Energy stored in casing of turbine:

This effect is accounted by using the *Lumped Capacitance Analysis* as it deals with the transient conduction problem in which a solid experiences a sudden change in its thermal environment (explained in detail in section 2.1.4)[1]. The rate at which energy is stored in the casing is equal to the rate of change of internal energy of the casing and is given by

$$\dot{Q}_{stT} = \rho V c \frac{dT_m}{dt}.$$ (3.9)

Here $\dot{Q}_{stT}$ is the heat stored in the casing, T_m is the temperature of the casing and V is the volume of the casing given by

$$V = \frac{\pi}{4} \left(D_{out}^2 - D_{in}^2 \right) L.$$ (3.10)

18

Here D_{out} is the outside diameter of the channel modelled as turbine casing.

3.2.3 Energy lost due to convection to the atmosphere:

The heat transfer by convection is governed by the *Newton's Law of Cooling* explained in detail in section (2.1.2)[10]. The heat transferred by convection from the turbine casing to the surroundings is given by

The appropriate rate equation is of the form

$$\dot{Q}_{convT} = h_{atm}A_{Sout}(T_m - T_{surr}).$$ (3.11)

Here $\dot{Q}_{convT}$ is the heat transferred by convection, T_{surr} is the temperature of the surroundings, h_{atm} is the surrounding heat transfer coefficient assumed to be 5W/(m²K) for natural convection condition and A_{Sout} is the outside surface area of the turbine casing exposed to the surroundings given by

$$A_{Sout} = \pi D_{out}L.$$ (3.12)

3.2.4 Energy lost due to radiation:

The heat transferred by radiation is governed by the *Stefan-Boltzmann law* explained in detail in section (2.1.3)[14]. The radiation heat transfer from the turbine casing to the surroundings is given by

$$\dot{Q}_{radT} = \varepsilon\sigma A_{Sout}(T_m^4 - T_{surr}^4).$$ (3.13)

Here $\dot{Q}_{radT}$ is the radiation heat transfer, ε is the emmisivity of the turbine casing metal that is cast iron and its value is taken as 0.85.

3.2.5 Energy balance over the turbine casing:

Initially the energy balance applied was only the Lumped capacitance method(explained in section 2.1.4), that was

$$h_{in}A_{Sin}(T_3 - T_m) = \rho Vc\frac{dT_m}{dt}.$$ (3.14)

Now considering the three factors illustrated above the corrected energy balance over the casing of the turbine is formulated as

$$\dot{Q}_{inT} = \dot{Q}_{stT} + \dot{Q}_{convT} + \dot{Q}_{radT}.$$ (3.15)

Substituting equations 3.1, 3.9, 3.11, and 3.13 in equation 3.15 gives

$$h_{in}A_{Sin}(T_3 - T_m) = \rho Vc\frac{dT_m}{dt} + h_{atm}As_{out}(T_m - T_{surr}) + \varepsilon\sigma A_{Sout}(T_m^4 - T_{surr}^4).$$ (3.16)

The above equation is modelled in SIMULINK. The processes of modelling is shown in figure below

$$\frac{dT_m}{dt} = [(h_{in}A_{Sin}(T_3 - T_m) - h_{atm}As_{out}(T_m - T_{surr}) - \varepsilon\sigma A_{Sout}(T_m^4 - T_{surr}^4))\frac{1}{\rho Vc}].$$ (3.17)

The above equation is then integrated over time with initial condition at time $t = 0$ temperature
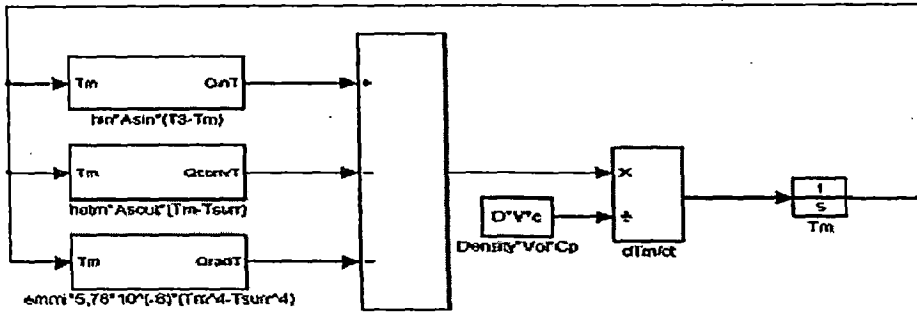
$$T_m = 298°\text{K}$$

Fig 3.3 Simulink model.

The solution of the equation gives the transient variation of turbine casing temperature.

3.2.6 Power entering the turbine:

The power absorbed by the turbine is

$$P = \dot{m}\,\Delta h_T = \dot{m}\,c\Delta T = \dot{m}\,c(T_3 - T_4). \tag{3.18}$$

Splitting the power with the enthalpy at absolute Zero as reference the power entering the turbine with the hot gases is given by

$$P_{inT} = \dot{m}\,c_p T_3 \tag{3.19}$$

Here the mass flow rate $\dot{m}$ and temperature T_3 of the hot gases entering the turbine are given as input to the system model from the experimental data.

3.2.7 Power absorbed by the compressor:

The power absorbed by the compressor in compressing air through it is given by

$$P_{comp} = \dot{m}_{air}\, c_{pair}\,\Delta T_{comp}. \tag{3.20}$$

Here, $\dot{m}_{air}$ is the mass flow rate of air through the compressor and ΔT_{comp} is the temperature rise across the compressor. Both the values are given as input to the system model from the experimental data.

3.2.8 Power leaving the turbine:

The power leaving the turbine along with the exhaust gases is given by

$$P_{outT} = \dot{m} c_p T_4 .$$
(3.21)

Here T_4 is the temperature of the exhaust gases leaving the turbine.

3.2.9 Overall energy balance over the turbocharger turbine:

The over all energy balance applied over the turbine is

$$P_{inT} = \dot{Q}_{inT} + P_{comp} + P_{outT} .$$
(3.22)

Substituting equation 3.1, 3.19, 3.20 and 3.21 in equation 3.22 yields

$$\dot{m} c_p T_3 = h_{in} A_{Sin} (T_3 - T_m) + \dot{m}_{air} c_{pair} \Delta T_{comp} + \dot{m} c_p T_4 .$$
(3.23)

This equation is then modelled in SIMULINK (in a similar manner as explained in section 3.2.5) and the variation of turbine exhaust gas temperature with time is determined as the system output.

3.3 Design of an improved MATLAB/SIMULINK model:

3.3.1 Introduction

The improved model is designed to determine the transient variation of the bearing housing temperature and the compressor outlet temperature in addition to the parameters determined in the simplified model for different convection conditions. In this model the inlet temperature and pressure of the hot gases and the pressure ratio across the turbine are taken as input from the experimental data. The model increases the overall accuracy of the system by considering the following heat and power transfer effects in addition to the effects considered in the simplified model

1. The transfer of heat by conduction from the turbine casing to the shaft and bearing housing assembly.
2. The transfer of heat by convection from the bearing housing to the surroundings.
3. The transfer of heat by radiation from the bearing housing to the surroundings.
4. The storage of heat in the shaft and bearing housing assembly.
5. The transfer of heat to the lubricating oil.
6. The transfer of heat by conduction from the shaft and bearing housing assembly to the compressor casing.
7. The storage of heat in the compressor casing.
8. The transfer of heat by convection from the compressor casing to the surroundings.
9. The transfer of heat by radiation from the compressor casing to the surroundings.
10. The transfer of heat by convection from the compressor casing to the air passing through it.
11. The mechanical power developed by the expansion of gases through the turbine.
12. The mechanical power lost in transmission from the turbine to the compressor.
13. Power entering the compressor with the air to be compressed.
14. Power leaving the compressor with the compressed air.

3.3.2 Energy balance over turbine casing:

In this model the energy balance applied over the turbine casing, considering the transfer of heat by conduction from turbine casing to the shaft and the bearing housing assembly is given by

$$\dot{Q}_{inT} = \dot{Q}_{stT} + \dot{Q}_{convT} + \dot{Q}_{radT} + \dot{Q}_{in1}. \tag{3.24}$$

Here $\dot{Q}_{in1}$ is the heat transferred by conduction from turbine casing to the shaft and bearing housing assembly (explained in detail in section below) and is given by[1]

$$\dot{Q}_{in1} = \frac{k_b A_{cb}}{l_b}(T_m - T_{b1}). \tag{3.25}$$

Substituting equations 3.1, 3.9, 3.11, 3.13 and 3.25 in equation 3.24 gives

$$h_{in} A_{Sin}(T_3 - T_m) = \rho V c \frac{dT_m}{dt} + h_{atm} A S_{out}(T_m - T_{surr}) + \varepsilon \sigma A_{Sout}(T_m^4 - T_{surr}^4) + \frac{k_b A_{cb}}{l_b}(T_m - T_{b1}) \tag{3.26}$$

The above given equation is modelled in SIMULINK. The solution of the equation gives transient variation of the turbine casing temperature.

3.3.3 Energy balance over the turbocharger turbine:

In this model the energy balance applied over the turbine, considering the mechanical power developed by it is

$$P_{inT} = \dot{Q}_{inT} + P_{tur} + P_{outT}. \tag{3.27}$$

Here P_{tur} is the mechanical power developed by the expansion of hot gases through the turbine and is given by

$$P_{tur} = \dot{m} \Delta h_{st} \eta_{st}. \tag{3.28}$$

Here $\dot{m}$ is the mass flow rate of the hot gas through the turbine and is given by

$$\dot{m} = A_{eff} P_{3t} \sqrt{\frac{2}{1-\frac{1}{\gamma}} \frac{1}{RT_3} \left[\left(\frac{P_{4s}}{P_{3t}}\right)^{\frac{2}{\gamma}} - \left(\frac{P_{4s}}{P_{3t}}\right)^{1+\frac{1}{\gamma}} \right]}. \tag{3.29}$$

Here P_{3t} is the total pressure of the gases entering the turbine, P_{4s} is the static pressure of the gases leaving the turbine and A_{eff} is the effective turbine cross-section area and is correlated to the pressure ratio across the turbine. The derivation of equation 3.27 is given in appendix section A5.

Δh_{st} is the isentropic enthalpy drop across the turbine and is given by

$$\Delta h_{st} = c_p T_3 \left[1 - \left(\frac{P_{4s}}{P_{3t}}\right)^{\frac{\gamma-1}{\gamma}} \right]. \tag{3.30}$$

η_{st} is the isentropic efficiency of the turbocharger turbine and is given by

22

$$\eta_{st} = \frac{\eta_{Tt}}{\eta_{Tm}}.$$

Here η_{Tt} is the total turbine efficiency and η_{Tm} is the transmission efficiency.

Substituting equation 3.1, 3.19, 3.21 and 3.28 in equation 3.27 yields

$$\dot{m}c_pT_3 = h_{in}A_{Sin}(T_3 - T_m) + \dot{m}\Delta h_{st}\eta_{st} + \dot{m}c_pT_4. \tag{3.31}$$

This equation is then modelled in SIMULINK and the transient variation of turbine exhaust gas temperature is determined.

3.3.4 Modelling of the shaft and bearing housing assembly:

The shaft and bearing housing assembly is modelled together as a solid cylindrical lump. Here for the purpose of simplification and easy parameterization transient one-dimensional partial differential equations are not used as it is practically difficult to model these equations on SIMULINK. The lump is again modelled in three parts as shown in figure below. Th e length of each part is equal to one third of the length of the assembly and diameter equal to the outside diameter of the bearing housing. The various heat transfer effects involved are shown below
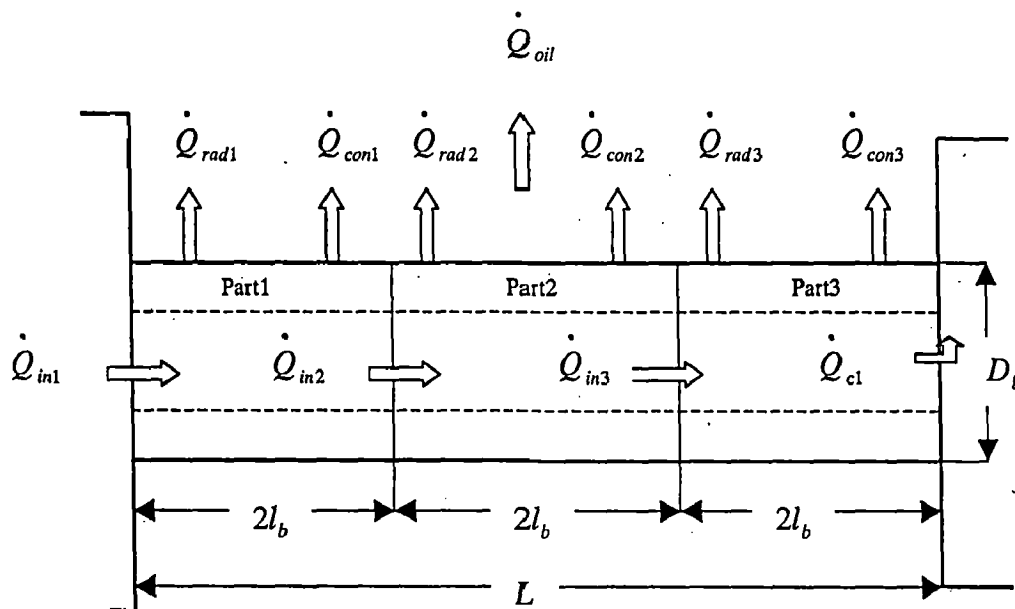

Figure 3.4 Heat fluxes through shaft and bearing housing assembly

3.3.4.1 Energy balance applied over part1:

The energy balance applied over the first part of the cylindrical lump is given by

$$\dot{Q}_{in1} = \dot{Q}_{st1} + \dot{Q}_{rad1} + \dot{Q}_{con1} + \dot{Q}_{in2}. \tag{3.33}$$

Here $\dot{Q}_{in1}$ is the heat transferred by conduction from turbine casing to the first part shaft and bearing housing assembly and is given by

$$\dot{Q}_{in1} = \frac{k_b A_{cb}}{l_b}(T_m - T_{b1}).$$ (3.34)

Here T_{b1} is the temperature of the first part of the lump, k_b is the thermal conductivity of the lump, l_b is half the length and A_{cb} is the cross-sectional area of a part of the lump and is given by

$$A_{cb} = \frac{\pi}{4}D_b^2.$$ (3.35)

In equation 3.30 $\dot{Q}_{st1}$ is the heat stored in the first part of the lump and is given by

$$\dot{Q}_{st1} = \rho V_b c \frac{dT_{b1}}{dt}.$$ (3.36)

Here V_b is the volume of a part of the lump and is given by

$$V_b = \frac{\pi}{4}D_b^2 \cdot 2l_b.$$ (3.37)

$\dot{Q}_{rad1}$ is the heat transferred by radiation from first part to surroundings and is given by

$$\dot{Q}_{rad1} = \varepsilon \sigma A_{Sb}(T_{b1}^4 - T_{surr}^4).$$ (3.38)

Here A_{sb} is the surface area of a part of the lump exposed to surroundings and is given by

$$A_{sb} = \pi D_b 2l_b.$$ (3.39)

$\dot{Q}_{con1}$ is the heat transferred by convection from first part to surroundings and is given by

$$\dot{Q}_{con1} = h_{atm}A_{Sb}(T_{b1} - T_{surr}).$$ (3.40)

$\dot{Q}_{in2}$ is the heat transferred by conduction from the first part to the second part of the lump and is given by

$$\dot{Q}_{in2} = \frac{k_b A_{cb}}{l_b}(T_{b1} - T_{b2}).$$ (3.41)

Here T_{b2} is the temperature of the second part of the lump.

Substituting equation 3.34, 3.36, 3.38, 3.40 and 3.41 in equation 3.33 yields

$$\frac{k_b A_{cb}}{l_b}(T_m - T_{b1}) = \rho V_b c \frac{dT_{b1}}{dt} + \varepsilon \sigma A_{Sb}(T_{b1}^4 - T_{surr}^4) + h_{atm}A_{Sb}(T_{b1} - T_{surr}) + \frac{k_b A_{cb}}{l_b}(T_{b1} - T_{b2})$$ (3.42)

The equation 3.39 gives the transient variation of T_{b1}.

3.3.4.2 Energy balance applied over part2:

The energy balance applied over the second part of the cylindrical lump is given by

$$\dot{Q}_{in2} = \dot{Q}_{st2} + \dot{Q}_{rad2} + \dot{Q}_{con2} + \dot{Q}_{oil} + \dot{Q}_{in3}.$$ (3.43)

Here $\dot{Q}_{st2}$ is the heat stored in the second part of the lump and is given by

$$\dot{Q}_{st2} = \rho V_b c \frac{dT_{b2}}{dt}.$$ (3.44)

$\dot{Q}_{rad2}$ is the heat transferred by radiation from second part to surroundings and is given by

$$\dot{Q}_{rad2} = \varepsilon \sigma A_{Sb}(T_{b2}^4 - T_{surr}^4).$$ (3.45)

$\dot{Q}_{con2}$ is the heat transferred by convection from second part to surroundings and is given by

$$\dot{Q}_{con2} = h_{atm} A_{Sb}(T_{b2} - T_{surr}).$$ (3.46)

$\dot{Q}_{oil}$ is the heat transferred to the lubricating oil and is co-related with the pressure ratio across the turbine. The co-relation is given in the appendix.A2.

$\dot{Q}_{in3}$ is the heat transferred by conduction from the second part to the third part of the lump and is given by

$$\dot{Q}_{in3} = \frac{k_b A_{cb}}{l_b}(T_{b2} - T_{b3}).$$ (3.47)

Here T_{b3} is the temperature of the third part of the lump.

Substituting equations 3.41, 3.44, 3.42, 3.46 and 3.47 in equation 3.43 yields

$$\frac{k_b A_{cb}}{l_b}(T_{b1} - T_{b2}) = \rho V_b c \frac{dT_{b2}}{dt} + \varepsilon \sigma A_{Sb}(T_{b2}^4 - T_{surr}^4) + h_{atm} A_{Sb}(T_{b2} - T_{surr}) + \dot{Q}_{oil} +$$

$$\frac{k_b A_{cb}}{l_b}(T_{b2} - T_{b3})$$ (3.48)

The equation 3.45 gives the transient variation of T_{b2}.

3.3.4.3 Energy balance applied over part3:

The energy balance applied over the third part of the cylindrical lump is given by

$$\dot{Q}_{in3} = \dot{Q}_{st3} + \dot{Q}_{rad3} + \dot{Q}_{con3} + \dot{Q}_{cc1}.$$ (3.49)

Here $\dot{Q}_{st3}$ is the heat stored in the third part of the lump and is given by

$$\dot{Q}_{st3} = \rho V_b c \frac{dT_{b3}}{dt}.$$ (3.50)

$\dot{Q}_{rad3}$ is the heat transferred by radiation from third part to surroundings and is given by

$$\dot{Q}_{rad3} = \varepsilon \sigma A_{Sb}(T_{b3}^4 - T_{surr}^4).$$ (3.51)

$\dot{Q}_{con3}$ is the heat transferred by convection from third part to surroundings and is given by

$$\dot{Q}_{con3} = h_{atm}A_{Sb}(T_{b3} - T_{surr}).$$ (3.52)

$\dot{Q}_{c1}$ is the heat transferred by conduction from the third part of the lump to the compressor casing (explained in detail in section below) and is given by[1]

$$\dot{Q}_{c1} = \frac{2\pi k l_{c1}}{\ln(D_m/D_b)}(T_{b3} - T_{c1}).$$ (3.53)

Here T_{c1} is the temperature of the third part of the lump.

Substituting equation 3.47, 3.50, 3.51, 3.52 and 3.53 in equation 3.49 yields

$$\frac{k_b A_{cb}}{l_b}(T_{b2} - T_{b3}) = \rho V_b c \frac{dT_{b3}}{dt} + \varepsilon\sigma A_{Sb}(T_{b3}^4 - T_{surr}^4) + h_{atm}A_{Sb}(T_{b3} - T_{surr}) + \frac{2\pi k l_{c1}}{\ln(D_m/D_b)}(T_{b3} - T_{c1})$$ (3.54)

The equation 3.45 gives the transient variation of T_{b3}.

3.3.5 Modelling of the compressor casing:

To consider the heat transfer by conduction from shaft and bearing housing assembly to the compressor casing it is modelled as a hollow cylindrical lump with inside diameter equal to the diameter of the bearing housing and outside diameter equal to the outer diameter of the compressor casing The length of the cylindrical lump is taken equal to the width of the compressor casing. The hollow cylindrical lump is again modelled in two parts as shown in figure below. The transfer of heat from the third part of the shaft and bearing housing to the first part of the hollow cylindrical lump is simulated as radial conduction of heat through concentric cylinders.
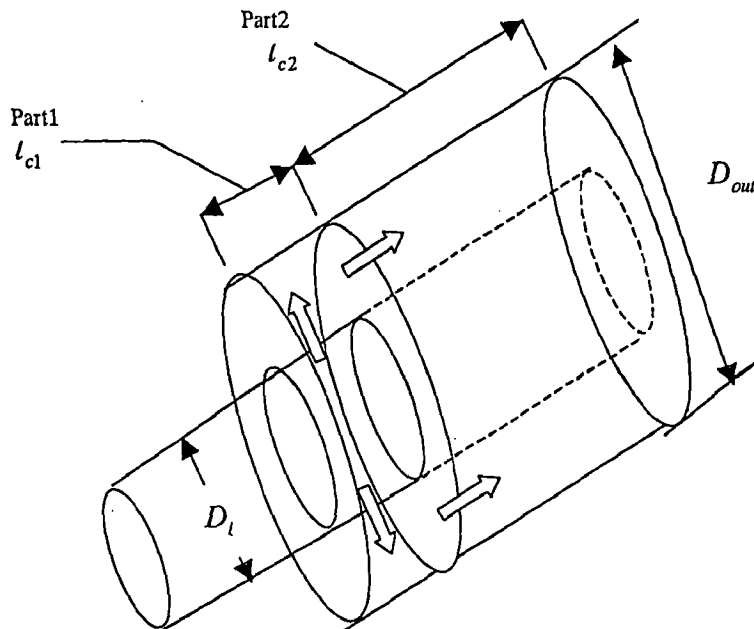

Figure 3.5 Heat transfer model of compressor casing.

3.3.5.1 Energy balance applied over first part of compressor casing:

The energy balance applied over the first part of the hollow cylindrical lump is given by

$$\dot{Q}_{c1} = \dot{Q}_{stc1} + \dot{Q}_{radc1} + \dot{Q}_{conc1} + \dot{Q}_{c2}.$$ (3.55)

Here $\dot{Q}_{c1}$ is the heat transferred by conduction from third part of the shaft and bearing housing assembly to first part of the hollow cylindrical casing and is given by

$$\dot{Q}_{c1} = \frac{2\pi k l_{c1}}{\ln(D_m/D_b)}(T_{b3} - T_{c1}).$$ (3.56)

Here D_m is the mean diameter and is given by

$$D_m = \frac{D_b + D_{out}}{2}.$$ (3.57)

l_{c1} is the length of first part and is calculated by equating the area of contact for conduction heat transfer

$$\frac{\pi}{4}D_b^2 = \pi D_b l_{c1}.$$ (3.58)

In equation 3.52 $\dot{Q}_{stc1}$ is the heat stored in the first part of the lump and is given by

$$\dot{Q}_{stc1} = \rho V_{c1} c \frac{dT_{c1}}{dt}.$$ (3.59)

Here V_{c1} is the volume of the first part and is given by

$$V_{c1} = \frac{\pi}{4}(D_{out}^2 - D_b^2)l_{c1}.$$ (3.60)

$\dot{Q}_{radc1}$ is the heat transferred by radiation to surroundings and is given by

$$\dot{Q}_{radc1} = \varepsilon \sigma A_{Sc1}(T_{c1}^4 - T_{surr}^4).$$ (3.61)

Here A_{sc1} is the surface area of the part exposed to surroundings and is given by

$$A_{sc1} = \pi D_{out} l_{c1} + \frac{\pi}{4}(D_{out}^2 - D_b^2).$$ (3.62)

$\dot{Q}_{conc1}$ is the heat transferred by convection to the surroundings and is given by

$$\dot{Q}_{conc1} = h_{atm} A_{Sc1}(T_{c1} - T_{surr}).$$ (3.63)

$\dot{Q}_{c2}$ is the heat transferred by conduction from the first part to the second part of the hollow cylindrical lump and is given by

$$\dot{Q}_{c2} = \frac{k A_{cc}}{l_{c2}/2}(T_{c1} - T_{c2}).$$ (3.64)

Here T_{c2} is the temperature and A_{cc} is the cross-sectional area of the second part of the hollow cylindrical lump for conduction heat transfer and is given by

$$A_{cc} = \frac{\pi}{4}(D_{out}^2 - D_b^2).$$

(3.65)

Substituting equations 3.56, 3.59, 3.61, 3.63and 3.64 in equation 3.55 yields

$$\frac{2\pi k l_{c1}}{\ln(D_m/D_b)}(T_{b3} - T_{c1}) = \rho V_{c1} c \frac{dT_{c1}}{dt} + \varepsilon \sigma A_{Sc1}(T_{c1}^4 - T_{surr}^4) + h_{atm} A_{Sc1}(T_{c1} - T_{surr}) +$$

$$\frac{k A_{cc}}{l_{c2}/2}(T_{c1} - T_{c2}).$$

(3.66)

The equation 3.64 gives the transient variation of T_{c1}.

3.3.5.2 Energy balance applied over second part of compressor casing:

The energy balance applied over the second part of the hollow cylindrical lump is given by

$$\dot{Q}_{c2} = \dot{Q}_{stc2} + \dot{Q}_{rad2} + \dot{Q}_{conc2} + \dot{Q}_{inair}.$$

(3.67)

Here $\dot{Q}_{stc2}$ is the heat stored in the second part of the lump and is given by

$$\dot{Q}_{stc2} = \rho V_{c2} c \frac{dT_{c2}}{dt}.$$

(3.68)

Here V_{c2} is the volume of the second part and is given by

$$V_{c1} = \frac{\pi}{4}(D_{out}^2 - D_b^2) l_{c1}.$$

(3.69)

$\dot{Q}_{radc2}$ is the heat transferred by radiation from the part to surroundings and is given by

$$\dot{Q}_{radc2} = \varepsilon \sigma A_{Sc2}(T_{c2}^4 - T_{surr}^4).$$

(3.70)

Here A_{sc2} is the surface area of the part exposed to surroundings and is given by

$$A_{sc2} = \pi D_{out} l_{c2} + \frac{\pi}{4}(D_{out}^2 - D_b^2).$$

(3.71)

$\dot{Q}_{conc2}$ is the heat transferred by convection to the surroundings and is given by

$$\dot{Q}_{conc2} = h_{atm} A_{Sc2}(T_{c2} - T_{surr}).$$

(3.72)

$\dot{Q}_{inair}$ is the heat transferred by convection from the compressor casing to the air passing through it and is given by

$$\dot{Q}_{inair} = h_{inC} A_{SinC}(T_{c2} - T_1).$$

(3.73)

Here h_{inC} is the heat transfer coefficient of the air passing through the compressor casing. To calculate this heat transfer coefficient a similar procedure, as used for turbine casing (explained in section 3.2.2)

28

is used considering compressor casing as a channel of circular cross-section of inside surface area A_{SinC}. T_1 is the temperature of the air entering the compressor casing.

Substituting equations 3.64, 3.68, 3.70, 3.72 and 3.73 in equation 3.67 yields

$$\frac{k \ A_{cc}'}{l_{c2}/2}(T_{c1} - T_{c2}) = \rho V_{c2}c\frac{dT_{c2}}{dt} + \varepsilon\sigma A_{Sc2}(T_{c2}^4 - T_{surr}^4) + h_{atm}A_{Sc2}(T_{c2} - T_{surr}) + h_{inC}A_{SinC}(T_{c2} - T_1).$$

(3.74)

3.3.6 Energy balance over the turbocharger compressor:

The energy balance applied over the turbocharger compressor is

$$\dot{P}_{inC} + \dot{Q}_{inair} + \dot{P}_{comp} = \dot{P}_{outC}.$$

(3.75)

Here $\dot{P}_{inC}$ power entering the compressor with the air to be compressed and is given by

$$\dot{P}_{inC} = \dot{m}_{air} \ c_{pair}T_1$$

(3.76)

Here $\dot{m}_{air}$ is the mass flow rate of the air entering the turbine and is taken as equal to the mass flow rate of the hot gases entering the turbine. c_{pair} is the specific heat of air.

$\dot{P}_{comp}$ is the power absorbed by the compressor in compressing the air through it and is taken as

$$\dot{P}_{comp} = \eta_m \ \dot{P}_{tur}.$$

(3.77)

Here η_m is the transmission efficiency for power transmission from turbine to the compressor and is taken as .9.

Substituting equation 3.26 in equation 3.74 gives

$$\dot{P}_{comp} = \eta_m \ \dot{m}\Delta h_{st}\eta_{st}.$$

(3.78)

$\dot{P}_{outC}$ is the power leaving the compressor with the hot gases and is given by

$$\dot{P}_{outC} = \dot{m}_{air} \ c_{pair}T_2.$$

(3.79)

Here T_2 is the temperature of the compressed air leaving the compressor.

Substituting equations 3.73, 3.76, 3.77, 3.78 in equation 3.75 gives

$$\dot{m}_{air} \ c_{pair}T_1 + h_{inC}A_{SinC}(T_{c2} - T_1) + \eta_m \ \dot{m}\Delta h_{st}\eta_{st} = \dot{m}_{air} \ c_{pair}T_2.$$

(3.80)

This equation gives the transient variation of temperature T_2.

3.3.5 Forced convection heat transfer coefficient

To calculate the heat transfer coefficient for forced convection over the turbocharger the flow is modelled as a cross flow over a circular cylinder[16]. The Zhukauskas correlation is used which is of the form

$$Nu_{DC} = C\,Re_{DC}^{m}\,Pr_{\infty}^{n}(Pr_{\infty}/Pr_{s})^{1/4}.$$

(3.81)

And is valid in the following range

$$.7 < Pr_{\infty} < 500$$

$$1 < Re_{DC} < 10^{6}$$

Here Nu_{DC} is the average Nusselt number and Re_{DC} is the Reynolds number for the cross flow and are given by

$$Nu_{DC} = h_{air}D_{C}/k_{air}.$$

(3.82)

$$Re_{DC} = V_{DC}D_{C}/v_{air}.$$

(3.83)

Here D_{C} is the diameter of the cylinder and V_{DC} is the velocity of the cross flow. In the above correlation all the properties are evaluated at upstream temperature of the air and Pr_{s} the Prandtl number of air at cylinder surface temperature is taken as 0.686. The value of $n = 0.37$ for $Pr_{\infty} \leq 10$ and the values of C and m used in above correlation are given in appendix section A4.
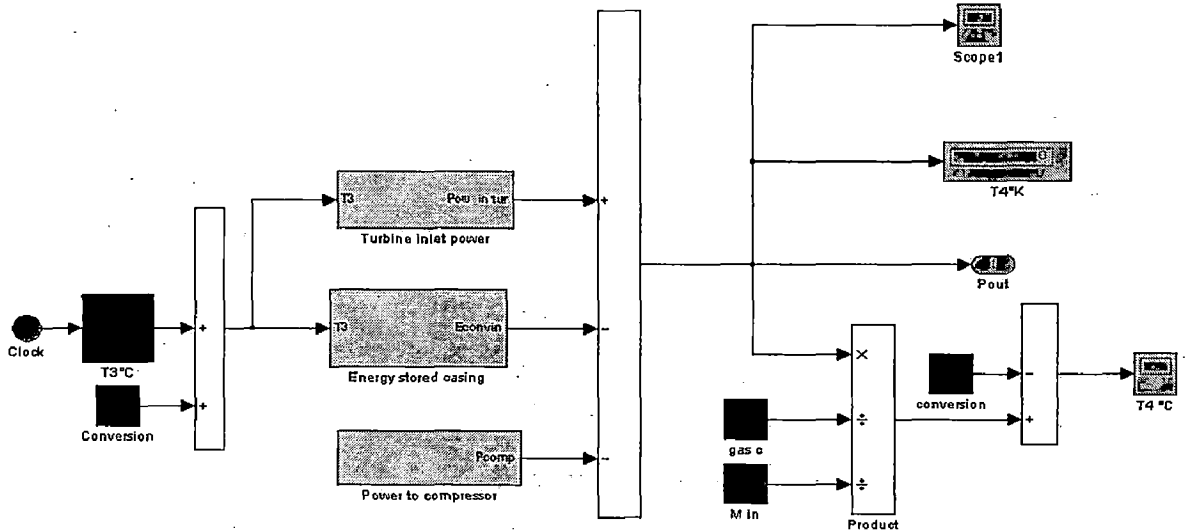
Fig 3.6 Simulink simplied model main system.
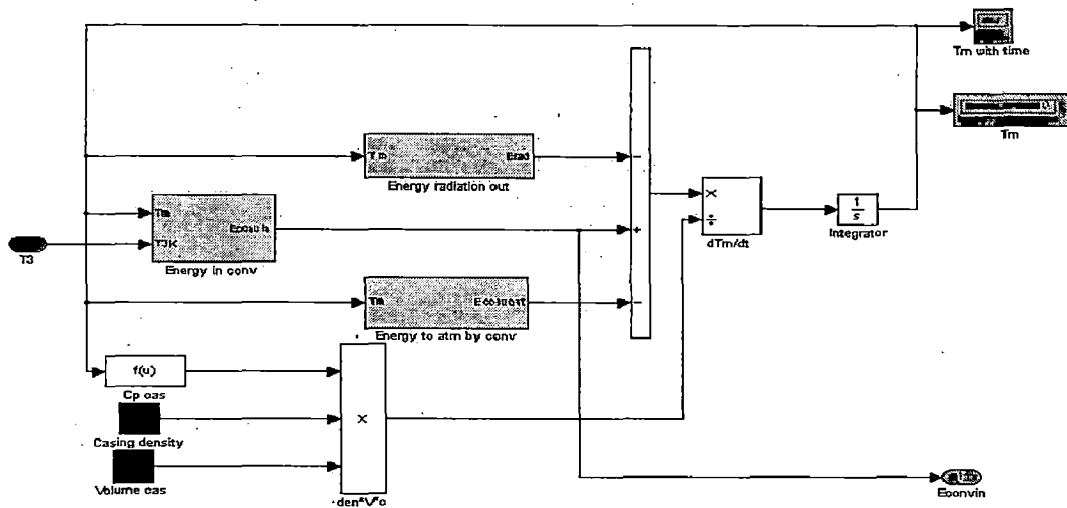
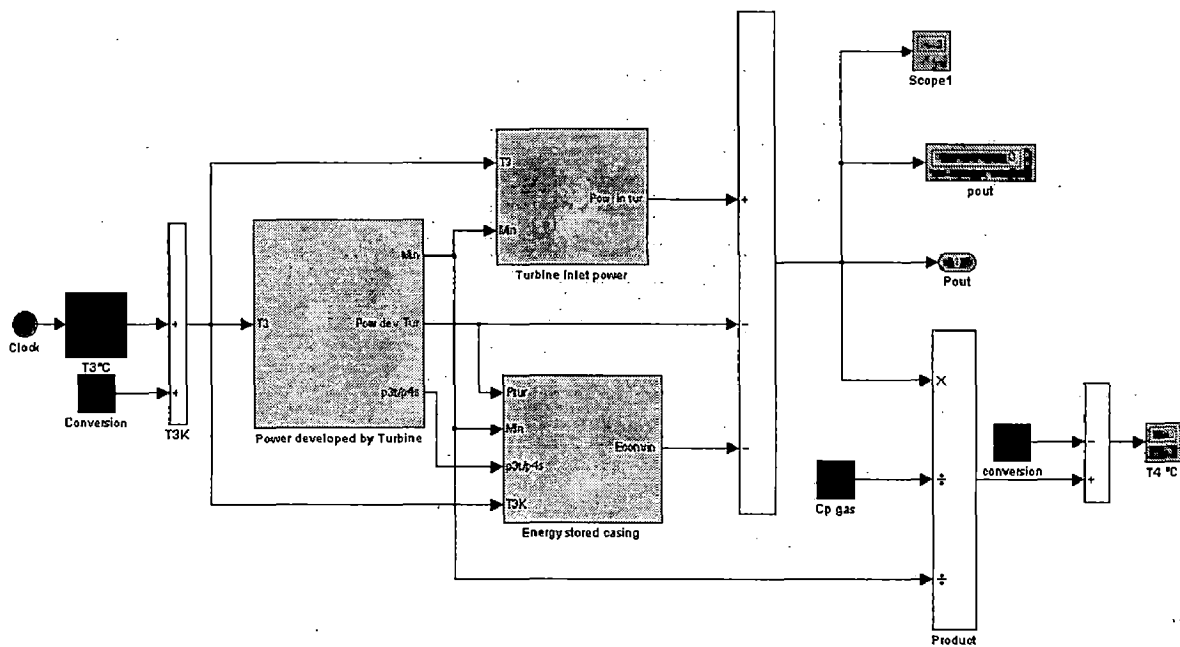**Fig 3.7** Simulink simplied model subsystem..

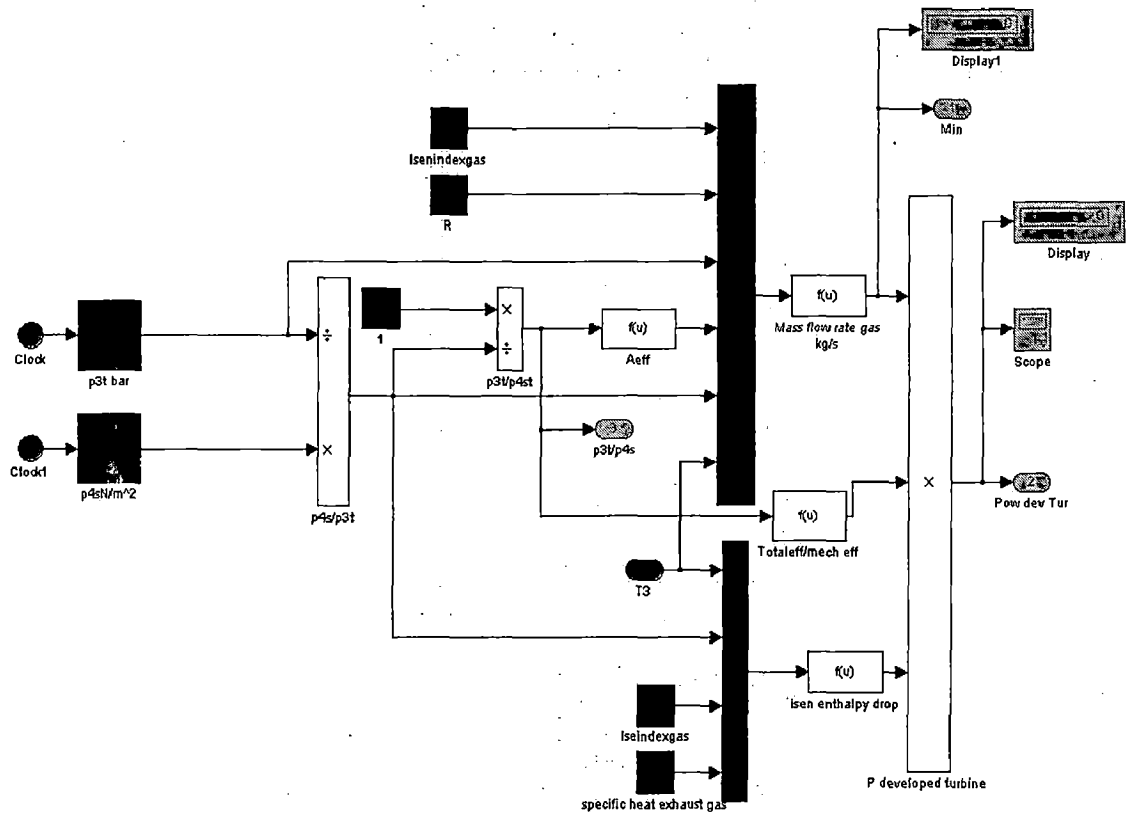**Fig 3.8** Simulink advanced model main system.
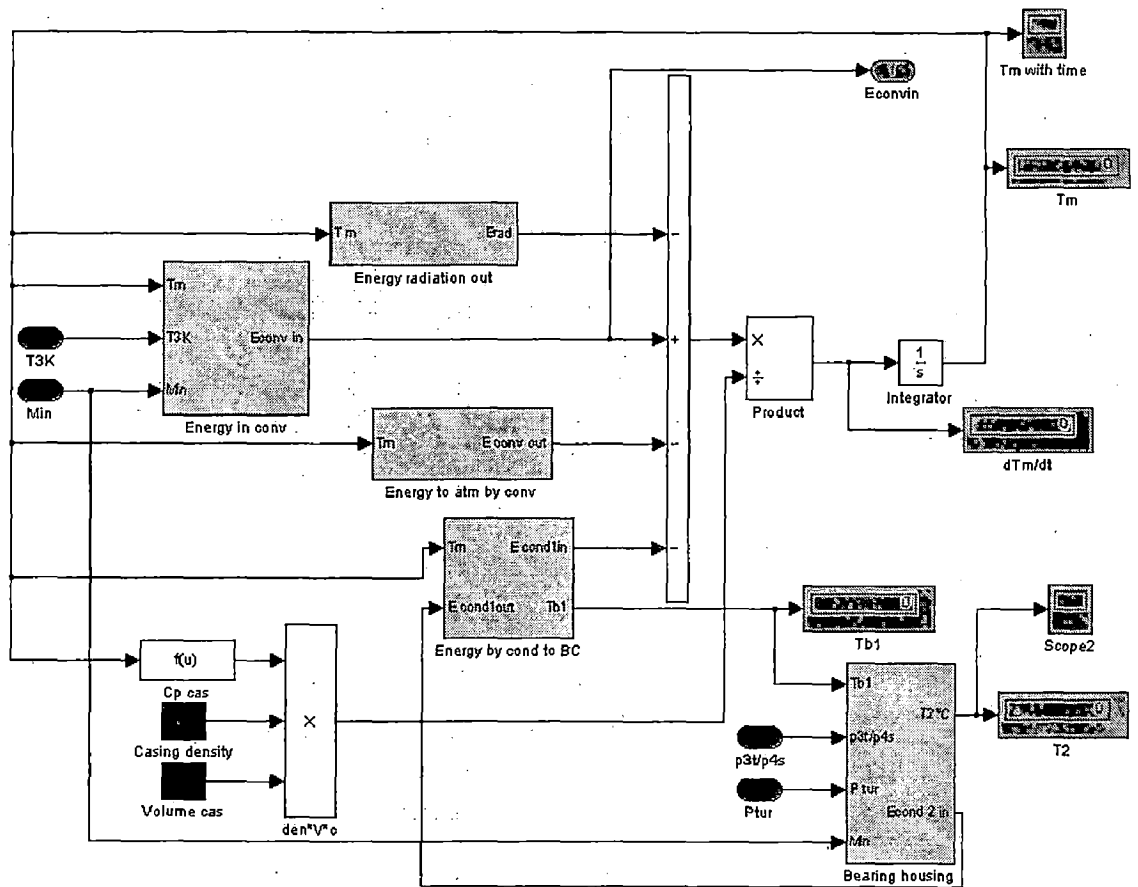
Fig 3.9 Simulink advanced model subsystem 1

Fig 3.10 Simulink advanced model subsystem 2.
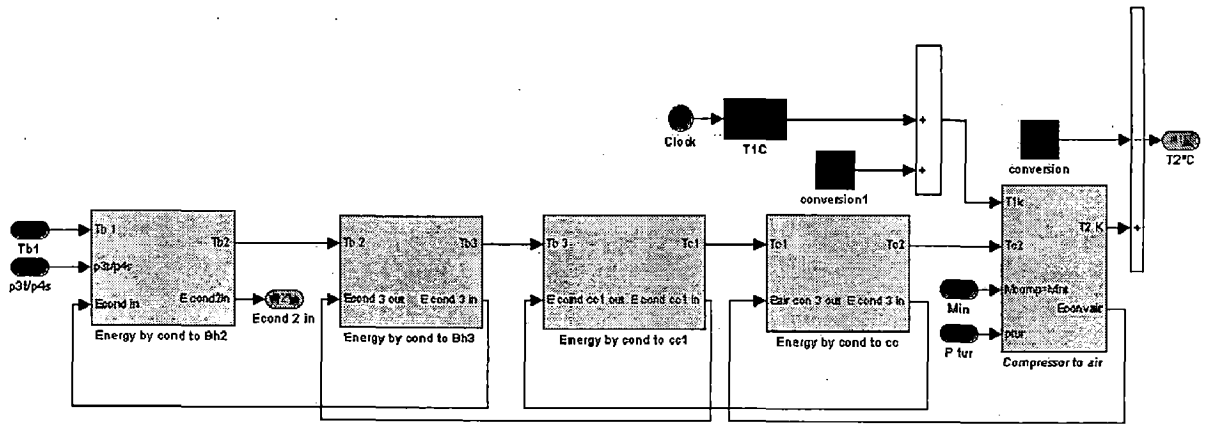
Fig 3.11 Simulink advanced model subsystem 3

CHAPTER 4
Heat Transfer Experiment on a TC Test Cell

4.1 Description of the test cell

4.1 1 Test cell introduction:

The purpose of the test cell is to perform measurements required for generating the operational characteristic maps of the turbine and the compressor of the turbocharger. For this pressure and temperature at the inlet and exit of the turbine and the compressor is measured. The mass flow rate of hot gases through the turbine and the mass flow rate of air through the compressor is also measured. These measurements are then used to generate the operational characteristics maps for the turbine and the compressor.

4.1.2 Operating methods

There are two different methods to operate the test cell, one is the characteristic map operating mode and the other is the gas turbine operating mode, depending on the external compressors, valves, sliders and tabs used.

4.1.2.1 Characteristic map operating mode

Fig 4.1 and 4.2 shows the gas flow diagram in this mode with the combustion air being supplied through compressor 1 and 2 respectively. This method is most commonly used for measuring the operating characteristic maps of the turbine and compressor of the turbocharger.
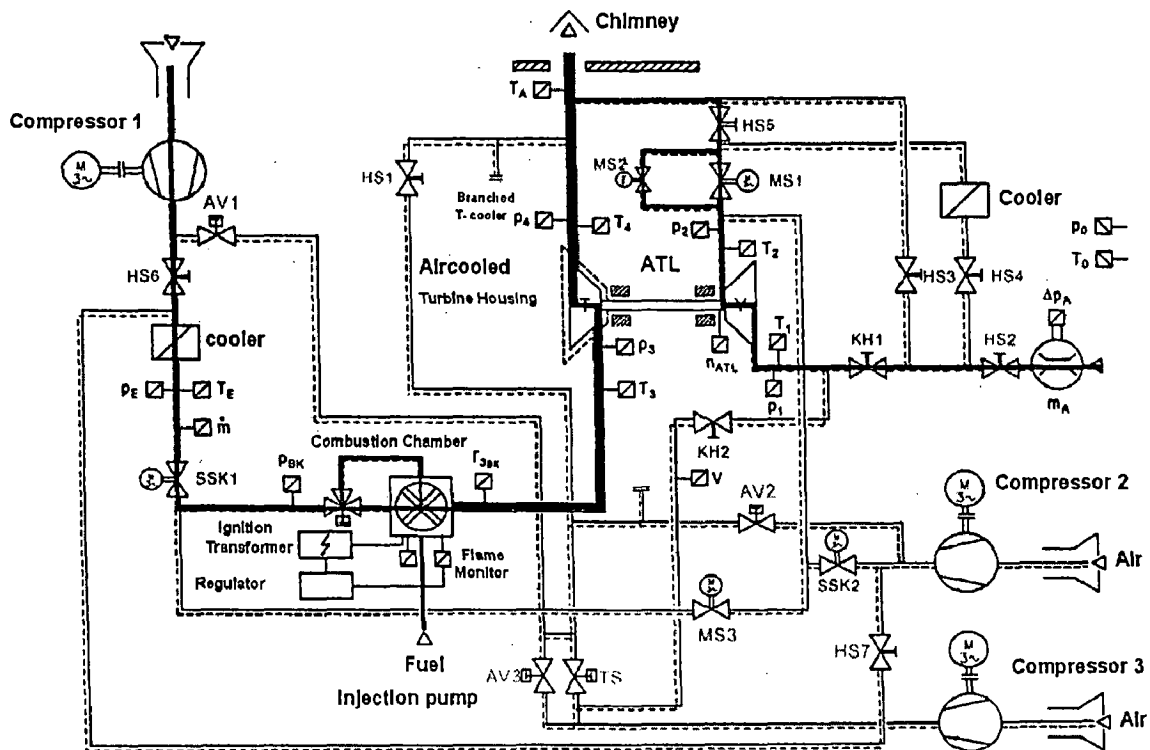

Figure 4.1: Gas flow diagram of test cell operating through compressor 1

The air is sucked in and compressed by the external compressor. The compressed air from the compressor passes through the charge air cooler. The cooler reduces the temperature of the

34

compressed air. The hot film anemometer (SENSYFLOW P) measures the mass flow rate of the air through the external compressor. The air then passes through the shut-off valve SSK1 to the combustion chamber through a three way valve (slider). The slider distributes the air to the primary and the secondary zone of the combustion chamber .Consequently it allows to control the required turbine inlet temperature T_3. The slider has to be operated carefully as the flame should not be extinguished and at the same time the temperature of the primary zone of the combustion chamber should not exceed $T_{BK\,max}$ = 1450° C. The fuel is then injected in the primary zone which on mixing with the compressed air results in combustion .The hot gases from the combustion chamber then expands through the turbine of the turbocharger and passes to the chimney.
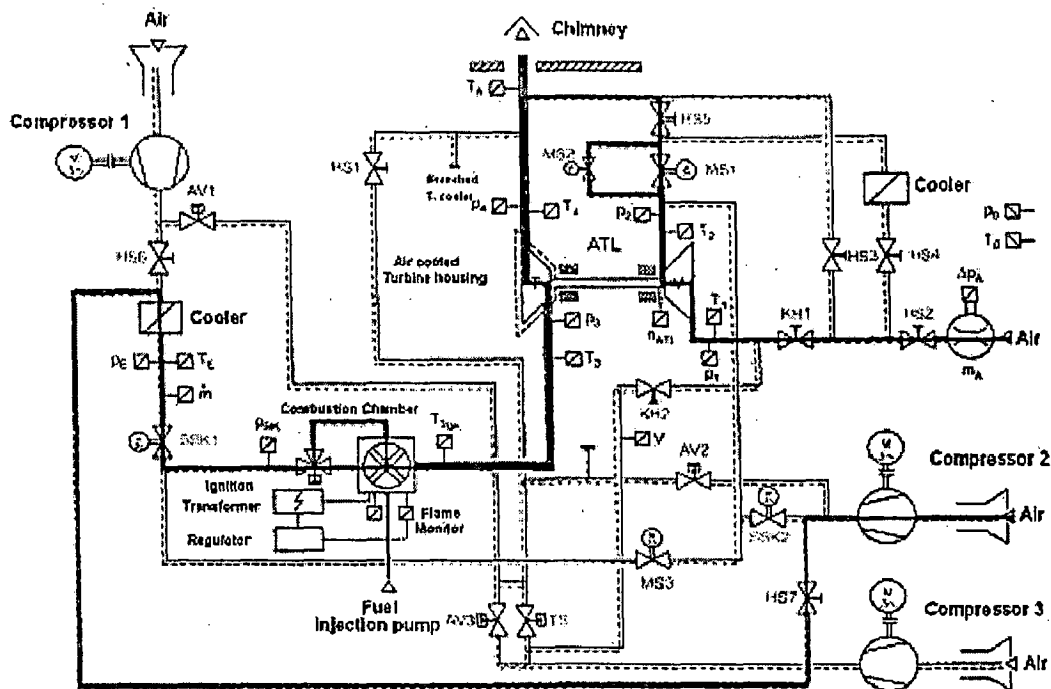

Figure 4.2 Gas flow diagram of test cell operating through compressor 2

The turbine drives the compressor of the turbocharger. The pressure difference across the inlet valve is used to compute the compressor mass flow rate. There are two motor driven valves MS1 and MS2, for regulating the air flow rate through the turbocharger compressor. MS1 is for coarse control and MS2 is for fine control. The operating state of the turbocharger is varied, by closing these valves, from maximum compressor mass flow rate to surge limit (minimum possible mass flow rate). The air then passes through the chimney.

4.1.2.2 Open cycle gas turbine operating mode

Fig 4.3 shows the gas flow diagram of the test cell in this mode. To run the turbocharger, in this mode of operation, the external compressors are not necessary. After being compressed the air from the turbocharger compressor is fed through the valve MS3 to the combustion chamber. There the air is heated by the combustion of the fuel and then expanded through the turbine of the turbocharger and

finally goes to the chimney. In this mode additional power for the external compressors is not required, as the power developed by the turbine itself is sufficient to drive the compressor of the turbocharger. This mode is less flexible than the characteristic map operating mode. As for example the only way to control the speed of the turbocharger is to increase or decrease the amount of fuel injected into the combustion chamber.
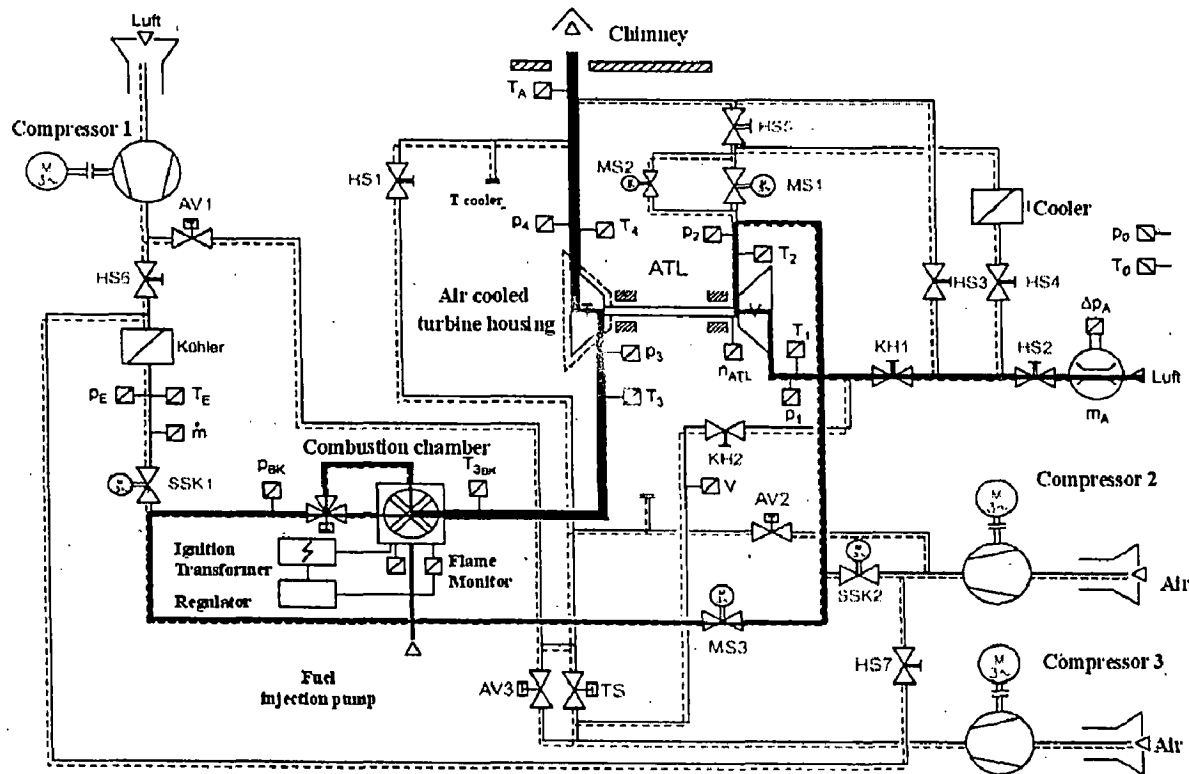

Fig 4.3 Gas flow diagram in the open cycle gas turbine opereation mode.

To start the operation by this mode first the air is supplied by an external compressor to the combustion chamber until the pressure at the outlet of the turbocharger compressor becomes equal to the pressure before the combustion Chamber. Then the motor operating valve MS3 is opened and the valves MS1 and MS2 are completely closed, at the same time the shut-off valve SSK1 is closed.

4.1.3 Components description

4.1.3.1 The External compressors

The external compressors 1 and 2 supply the air for the turbine of the turbocharger. The back pressure of the turbine determines that which compressor is to be used. compressor 1 is used for lower and compressor 2 is for higher back pressure of the turbine. The following gives the details of the external compressors used in the test cell.

Table 4.1

	COMPRESSOR 1	COMPRESSOR 2	COMPRESSOR 3
TYPE	AERZENER		
MOTOR SPEED	2950 min^{-1}		
COMPRESSOR SPEED	6200 to 14400 min^{-1}		
VOLUME FLOW RATE	20.2m^3/min	20.8 m^3/min	20.8m^3/min
PRESSURE DIFFERENCE	2.0 bar	3.0 bar	2.0 bar
COMPRESSOR POWER	64kw	85 kw	64 kw
ACTUATION POWER	90kw	110kw	90 kw
INLET PRESSURE	1.0 bar(abs)		
OUTLET PRESSURE	2.0 bar(rel)	3.0 bar (rel)	

4.1.3.2 Combustion chamber

The Combustion chamber provides the turbine with hot gas .It consist of three parts primary zone, dilution zone, and secondary zone. In order to achieve a quasi variable geometry combustor, the design comprises a single can type combustion chamber with variable air distribution between primary and dilution zone by introducing a pneumatic three way valve into the main compressed air supply pipe.

This concept allows an optimum combustion at all operating conditions since the combustion temperature in the primary zone can be set to a fixed value that is favourable for a stable combustion and additionally due to quasi variable geometry concept independent from the desired turbine inlet temperature. The turbine inlet temperature is exclusively controlled by the amount of secondary air added into the dilution zone. Furthermore an extremely wide operating range with respect to turbine inlet temperature can be achieved. The lower limit for a stable combustion is a turbine inlet temperature of about 400°C and the upper limit is given by maximum use temperature (1400°C) of the fibrous ceramic.

The ceramic liner segments serve as a thermal barrier for the metal housing which, for safety reasons, is additionally water cooled. The secondary air is added to the dilution zone through eight dilution holes. In order to achieve a uniform temperature pattern at the exit of the combustion chamber, the flow through each dilution hole can be adjusted by separate valves .Moreover, a ceramic straightening plate (bushing) right behind the dilution zone is used to increase the turbulence intensity, which improves the mixing quality and holds down the variance in turbine inlet temperature profile.
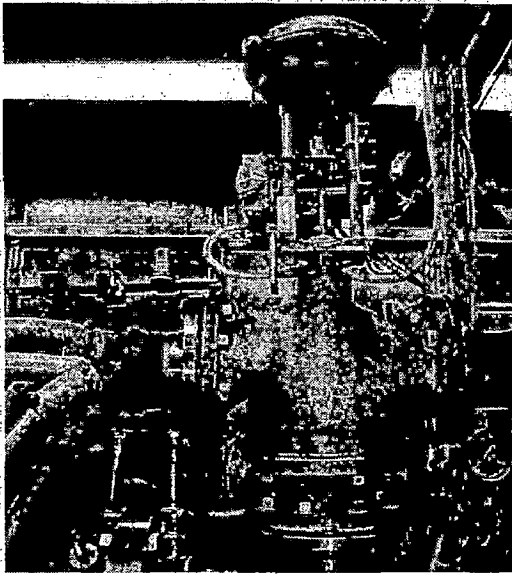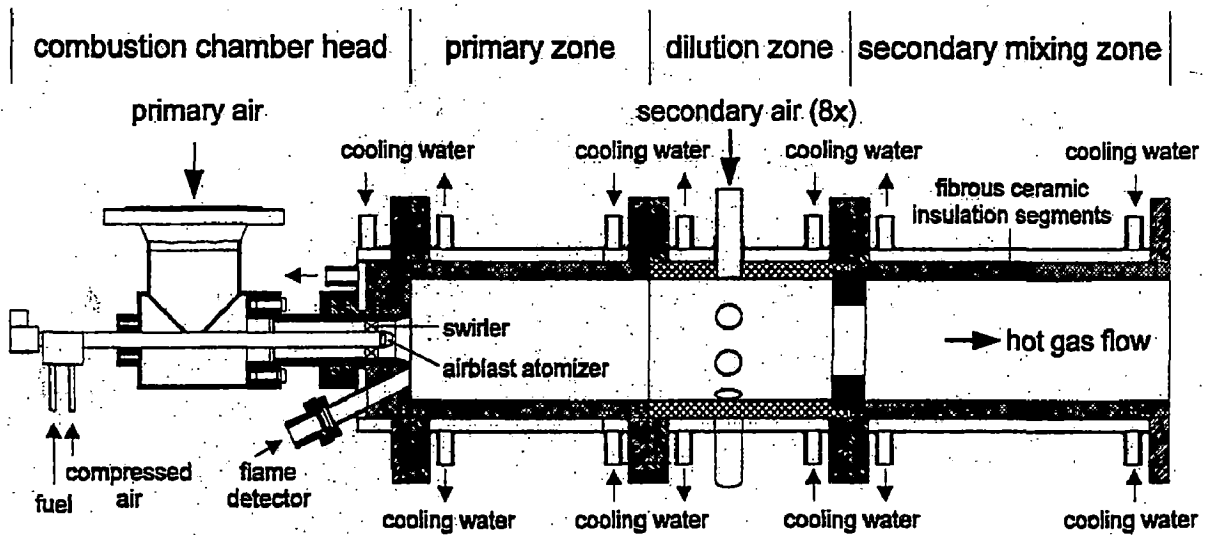
Fig 4.4 Combustion chamber slider

Fig 4.5 Combustion chamber

4.1.3.3 Injection system

Diesel fuel is injected by a gear pump used for fuel injection in domestic heating systems. An air blast fuel nozzle is used to atomize the fuel. The advantage of air blast nozzles is the broad operating range with respect to fuel flow rate. Therefore, stable combustion chamber over a wide air flow rate and turbine inlet temperature range can be realized, which would be quite difficult to achieve using standard simplex pressure swirl atomizers.

For the test cell a variety of fuel atomizers are available. The ones which are used are designed for the mass flow rate ranging from 4.0 to 10 kg/h. All the atomizers are having a servo ratio of 1:10, it means that the one which is designed for 5kg/h can deliver from 0.5 to 5 kg/h.
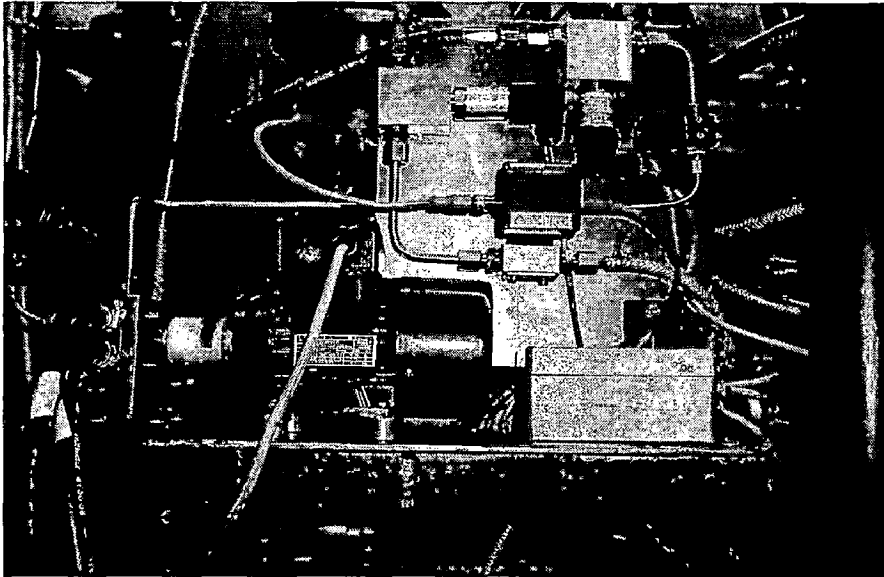
Fig 4.6 Injection system.

4.1.3.4 Exhaust gas turbocharger

The exhaust gas turbocharger is the component under investigation. It consists of a compressor and a turbine mounted on a shaft. The turbine receives the hot gases from the combustion chamber which on expansion develops power which is used to run the compressor. The compressor then compresses air through it.
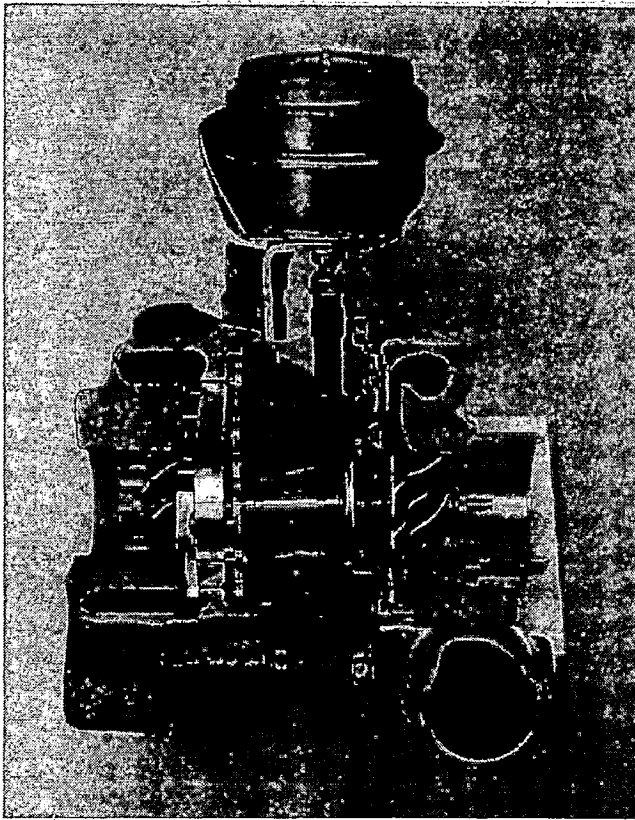

Fig 4.7 Sectioned model

Compressor air flow

Engine cylinder

Oil inlet

Charge air cooler

Compressor housing

Turbine wheel

Air inlet

Exhaust-gas outlet

Compressor wheel

Charge pressure control valve
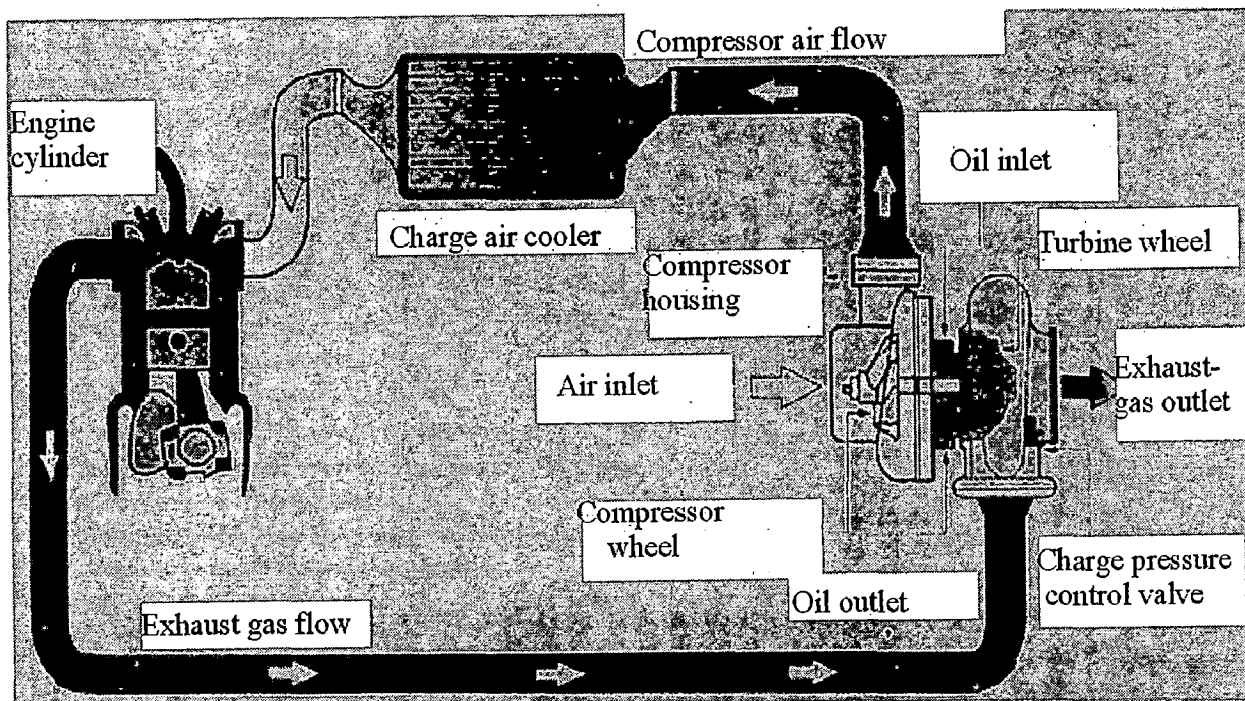
Oil outlet

Exhaust gas flow

Fig 4.8 Functioning of exhaust gas turbocharger.

4.1.3.5 Valves, sliders and piping

The motor sliders MS1 and MS2 are operated during the test run to vary the mass flow rate of air through the compressor of the turbocharger. The motor slider MS3 is provided in the circuit between pressure side of the turbocharger compressor and combustion chamber so that during open cycle gas turbine operation of the test cell, the air from turbocharger compressor can pass to the combustion chamber. The blow off valves AV1, AV2 and A V3 are operated to vary the mass flow rate of air through the combustion chamber .As the blow off valves are opened some of the compressed air from the external compressor passes through the hand operated valve HS1 to the exhaust gas stack. The hand-operated sliders from HS 1 to HS7 are adjusted according to the gas flow scheme of various operating methods. The position of these sliders are such that either they are fully opened or fully closed. The shut-off valves SSK1 and SSK2 are operated in case of a fault occur in operation and the air supply is to be cut off suddenly. The valve SSK1 is normally opened in characteristic map operating mode and is used to reduce the air mass flow rate below the minimum value that can be supplied by the external compressor. In free wheel operating method the valve SSK1 is closed so that the compressed air from the pressure side of the turbocharger compressor can move to the combustion chamber slider. The valve SSK2 is normally closed.
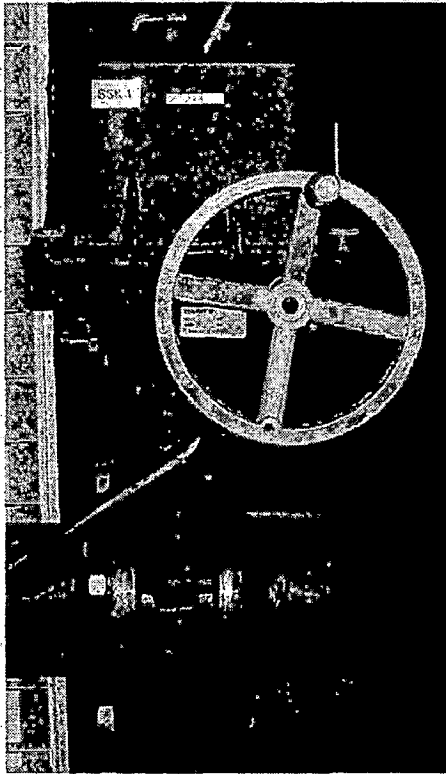
Fig 4.9 SSK1

4.1.4 Measurement techniques

The measurement systems includes the measurement of temperature, pressure, E-Gas, position of the combustion chamber slider, mass flow rate, volumetric flow rate and the air flow.

4.1.4.1 Pressure measurement system

The pressures at the inlet and the exit of the turbocharger turbine and compressor are measured using piezoresistive transducers. These transducers measure static and dynamic absolute pressures. The important features of piezoresistive transducers are high output voltage, good linearity and stability as well as small dimensions. The pressure acts through a thin steel diaphragm, welded to form a tight seal with the transducer housing, onto a silicon-measuring cell. The measuring cell contains diffused piezoresistive resistors connected into a Wheatstone bridge. Through the effect of pressure the bridge is unbalanced which results in an output signal amounting to 500 mV at full measuring range. Any thermal effects on the resistors are largely compensated by connecting further resistors. These sensors measure absolute pressure i.e. the pressure referred to vacuum and not to the prevailing atmospheric pressure. The sensors can measure a pressure upto 5 bars with an accuracy of .1%.

4.1.4.2 Temperature measurement system

The temperatures on the turbine side of the turbocharger are measured by NiCrNi thermocouples. These thermocouples can withstand high temperatures and hence are suited for high temperature measurement. They can withstand high temperatures and hence are suited for high temperature measurement. They can measure temperatures up to 1300K with an accuracy of 2K.

The working principle of a thermocouple is based on the T. J. Seebeck effect also known as thermoelectric effect. It states that when two lengths of dissimilar metal wires (such as iron and

Constantan) are connected at both ends to form a complete electric circuit and one junction of two wires is at a different temperature than the other then emf is generated.

The voltage is a function primarily of the temperature difference between the two junctions and the kinds of materials used. If the temperature of the cold junction is maintained constant, or variations in that temperature are compensated for, then the voltage is the function of hot junction temperature

The temperatures on the compressor side of the turbocharger are measured by Platinum resistance thermometers (Pt100). The principle of operation is to measure the change in resistance of Platinum with temperature. The electrical conductivity of a metal depends on the movement of electrons through its crystal lattice. Due to thermal excitation, the electrical resistance of a conductor varies according to its temperature. The effect is most commonly exhibited as an increase in resistance with increasing temperature, a positive temperature coefficient of resistance. Pt100 sensors have a resistance of 100 Ω at 0°C and 138.4 Ω at 100°C. These sensors have linear characteristics (resistance with temperature) over a temperature range from 273 K to 400 K and have an accuracy of approximately 0.5 K. Its advantages include chemical stability, relative ease of manufacture, availability of wire in a highly pure form and excellent reproducibility of its electrical characteristic.

4.1.4.3 Speed measurement system

The turbocharger speed is measured by a non-contact eddy current displacement sensor. The sensor uses the eddy current loss principle to measure the turbocharger speed. A coil is housed in a sensor case and is energised by a high frequency alternating current. The electromagnetic field from the coil generates eddy currents in the turbocharger blades. Every blade generates a pulse. The controller identifies the speed by considering the number of blades. The sensor has a speed range of 0-400,000 rpm and has an accuracy of .2% of the measured value.

4.1.4.4 Air flow measurement system

The air flow is measured with the help of a hot film anemometer. The anemometer has a thin probe made of quartz rod with platinum film on the surface. The probe is heated to a higher temperature than the average temperature of the air. Since the air flowing past the probe has a lower temperature than that of the probe, the probe is continuously cooled by the air flow. The rate of cooling depends on the velocity of the air stream flowing past the probe. To keep the probe at a constant temperature level, the voltage across the probe is increased. Thus the air velocity is translated into a continuously changing voltage which has a non linear relationship with the flowing air velocity. The voltage then undergoes signal conditioning to filter out noise and improve signal/noise ratio. The anemometer available in the test cell can measure an air mass flow rate up to 2000 Kg/h with an accuracy of 1%.

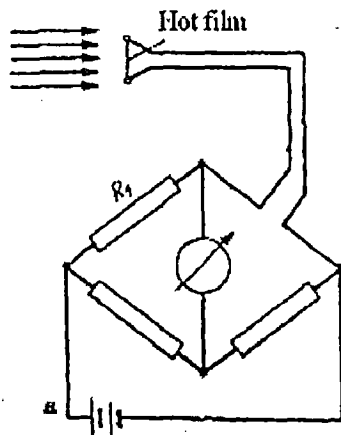The schematic diagram of a hot film anemometer is shown in the figure below

Fig 4.10 Schematic diagram of a hot film anemometer.

4.1.4.5 Location of the measuring sensors

For the experimental investigation of the turbocharger as well as for validating the numerical model, pressure and temperature sensors are located at key positions on the test cell. The locations are as follows

1. Turbine inlet (temperature and static pressure)
2. Turbine outlet (temperature and static pressure)
3. Compressor suction (temperature and static pressure)
4. Compressor outlet (temperature and static pressure)

In addition to the above mentioned measurements, the following parameters are also measured

1. Mass flow rate of the fuel and air through the turbocharger turbine.
2. Mass flow rate of the air through the turbocharger compressor.
3. Turbocharger speed.
4. Temperature and volumetric flow rate of the lubricating oil.

4.1.5 Limits of the test cell

Maximum turbine mass flow rate:

1440kg/h

Minimum air mass flow rate under operating conditions:

80 kg/h.

Minimum combustion chamber temperature under operating conditions:

400 to 500°C depending on Air mass flow rate and the Atomizer used.

Maximum combustion chamber temperature:

1200°C (momentary 1400°C)

Maximum overpressure at the turbine while using compressor 1:

1.7-1.8bar

Maximum overpressure at the turbine while using compressor 2:

2.6-2.7 bar.

4.1.6 Activation of the test cell

4.1.6.1 General arrangements:

The activation of the test cell begins with actuating the main supply to the computer cabinet (Fig 4.12), the compressor computer, the test cell computer, the monitor, the key switch BK(Fig 4.13) on the desktop and the external control system shown in the working place below (Fig 4.11).
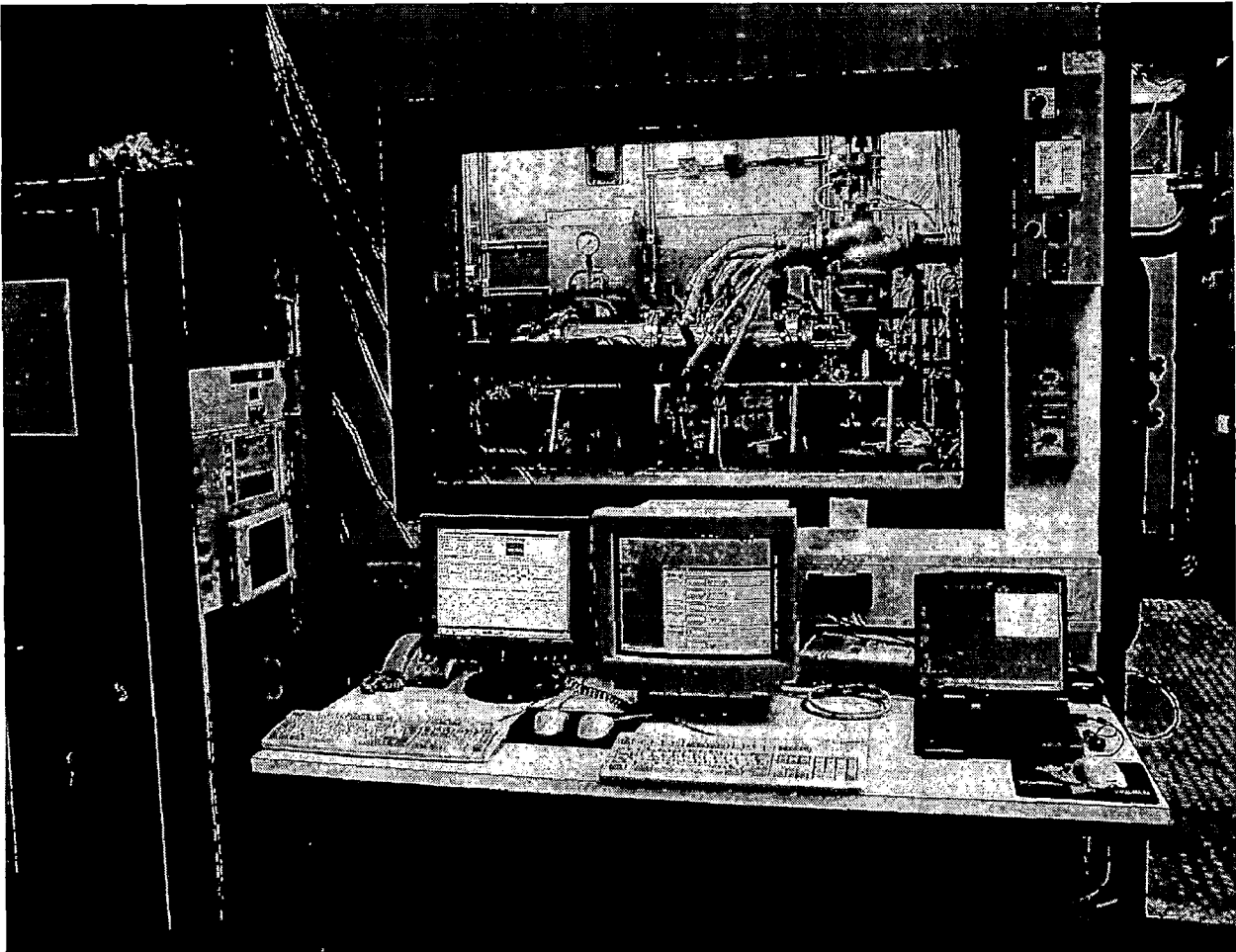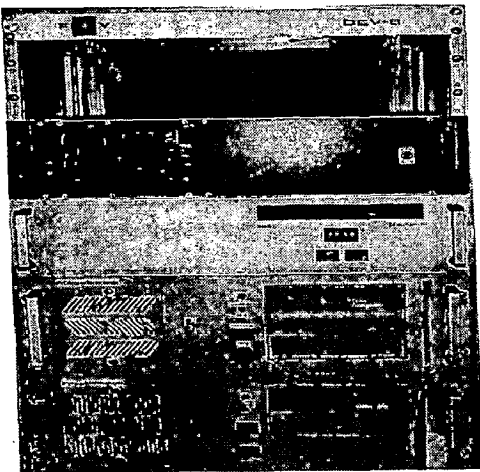

Fig 4.11 Working place
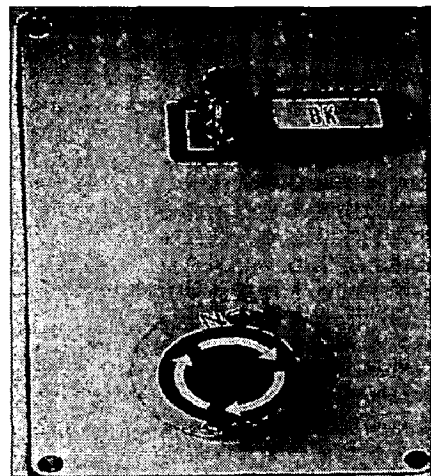

Fig 4.12 Computer cabinet

Fig 4.13 BK Switch

4.1.6.2 Arrangements at external compressor:

The decision which external compressor will be used is based upon the mode of operation. In the characteristic map operating method, for low speeds of the exhaust gas turbocharger compressor 1 is used while compressor 2 is used for high speeds. For the start of free wheel operating method both compressor 1 as well as compressor 2 can be used.

Table 4.2

	Characteristic map operating mode		Open cycle gas turbine operating mode	
	Compressor 1	Compressor 2	Compressor 1	Compressor 2
SSK1	ON		OFF	
SSK2	OFF		OFF	
MS 1	Variable		OFF	
MS 2	Variable		OFF	
MS 3	OFF		ON	
HS 1	ON		ON	
HS 2	ON		ON	
HS 3	OFF		OFF	
HS 4	OFF		OFF	
HS 5	ON		ON	
HS 6	ON	OFF	ON	OFF
HS 7	OFF	ON	OFF	ON

4.16.3 Arrangements on the test cell computer:

The control programrne is started with the command "mlx_ins"and "msPS2".Then the operation is started by clicking on the respective buttons for measurement actuation A3, for compressed air activation A5, for selecting the mode of operation A2 , for activating the corresponding compressor A1, and for heating oil A4. The oil pressure T has to be regulated carefully between 2 and 2.5 bar. The shut-off valve SSKl (F) must be opened completely before starting the external compressor. The throttle valves MSl and MS2 (D+E) are used for fine and coarse control respectively in characteristic and open cycle gas turbine operating method. If the measurements are not to be saved under the name DATA, the new name can be given in the block C3 and then the data can be saved by pressing C. The oil temperature should reach at least 56°C before starting the external compressor .In actual conditions the turbocharger in vehicles is provided with cold oil only during the initiation phase but for measurements characteristic the oil should have a constant temperature to prevent the bearing of the turbocharger from damage.
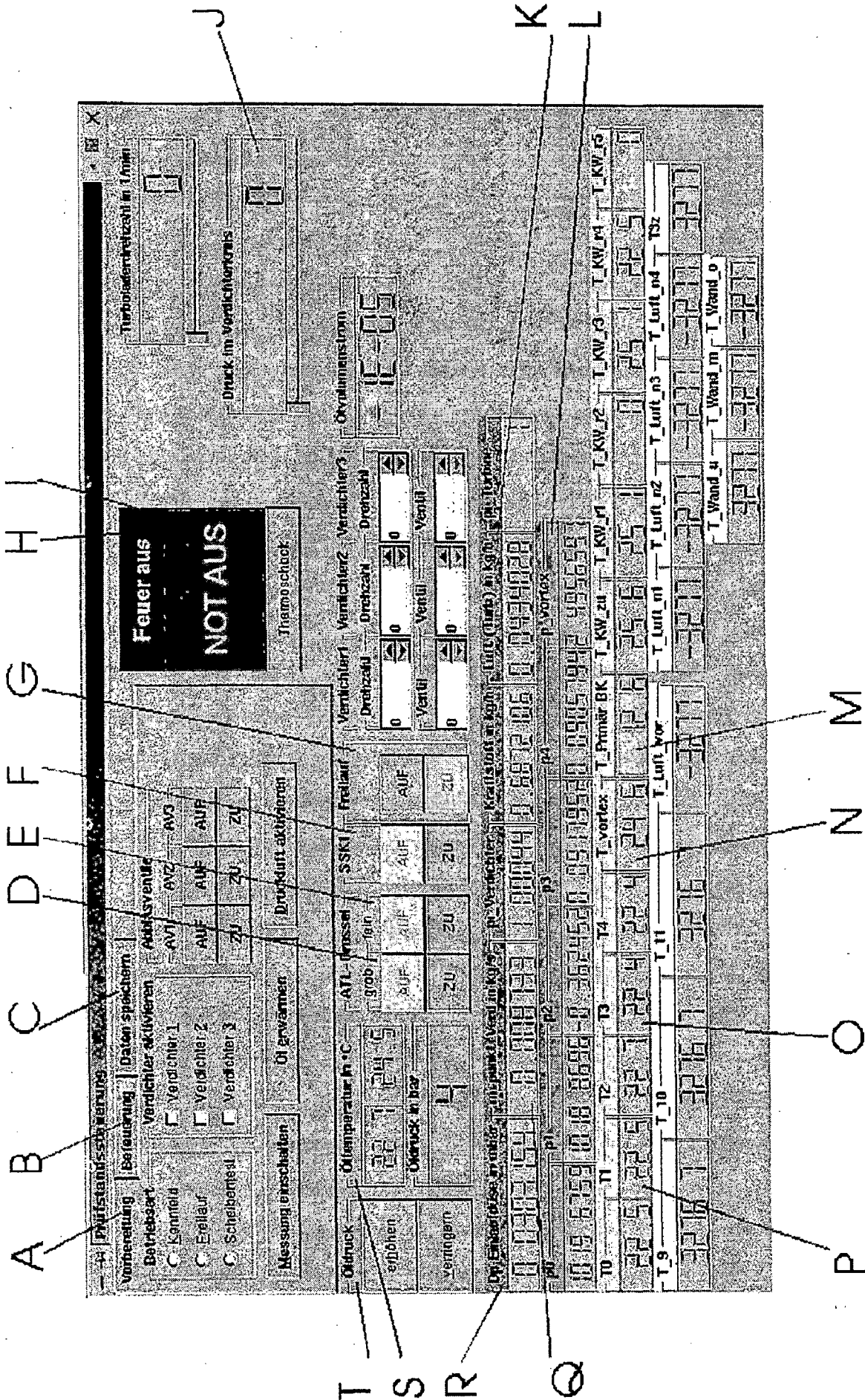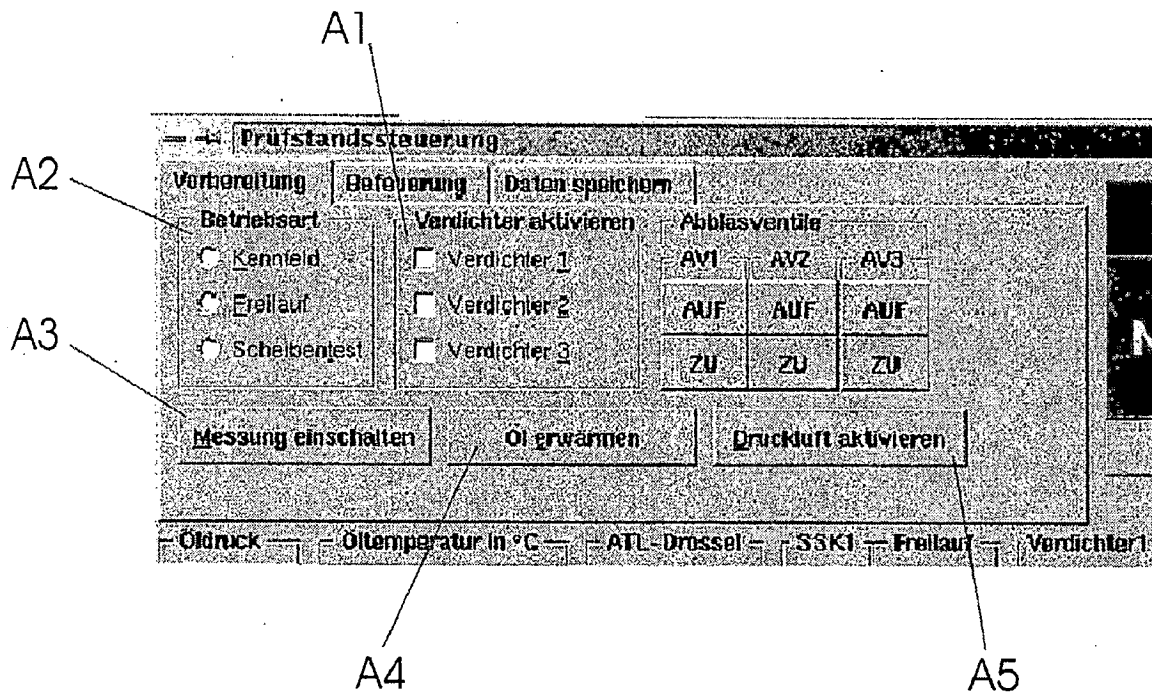
Fig 4.14 Test cell control programme
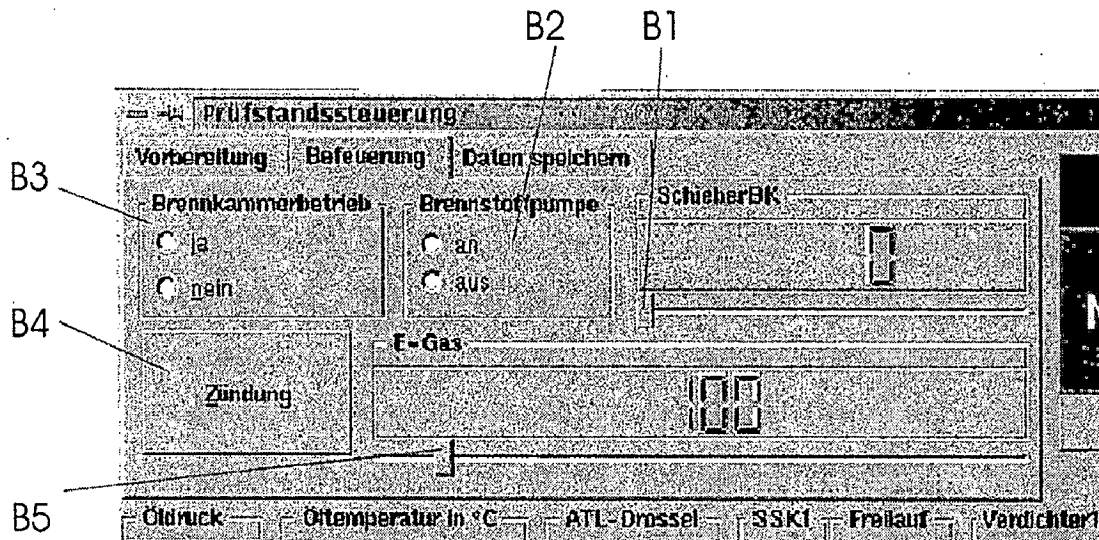
Fig 4.15 Test cell control (start)

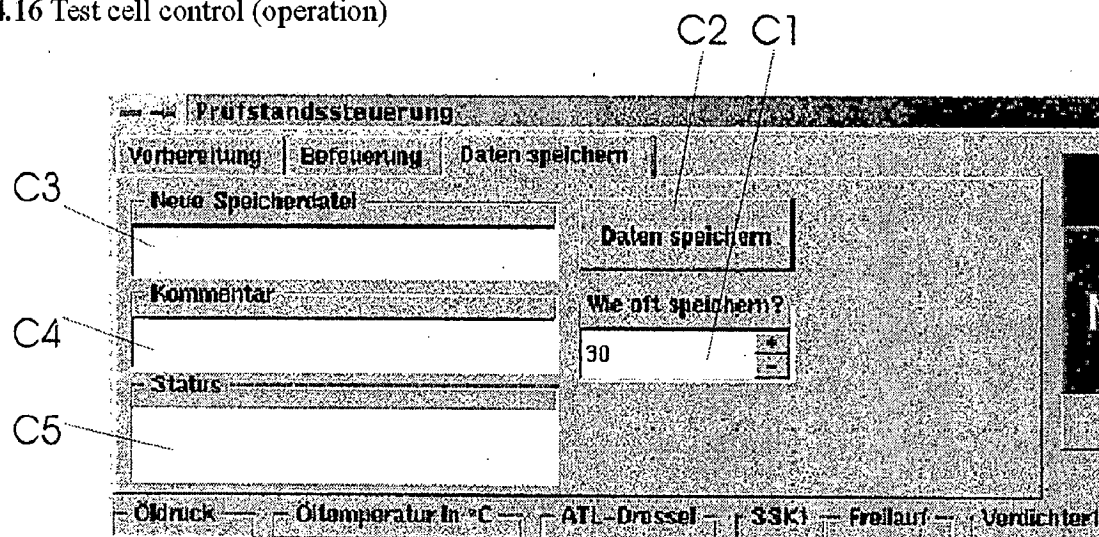Fig 4.16 Test cell control (operation)

Fig 4.17 Test cell control (saving data)

47

4.1.6.4 Arrangements on the compressor computer:

The required external compressor must be actuated in the test cell control programme before it is requested in compressor control programme .The programme initially shows for the blow-off valve 100% and for the speed 6200 min^{-1} of the requested compressor. The valve position and the speed are then controlled manually (these are reset to their initial values as the compressor is again stared).
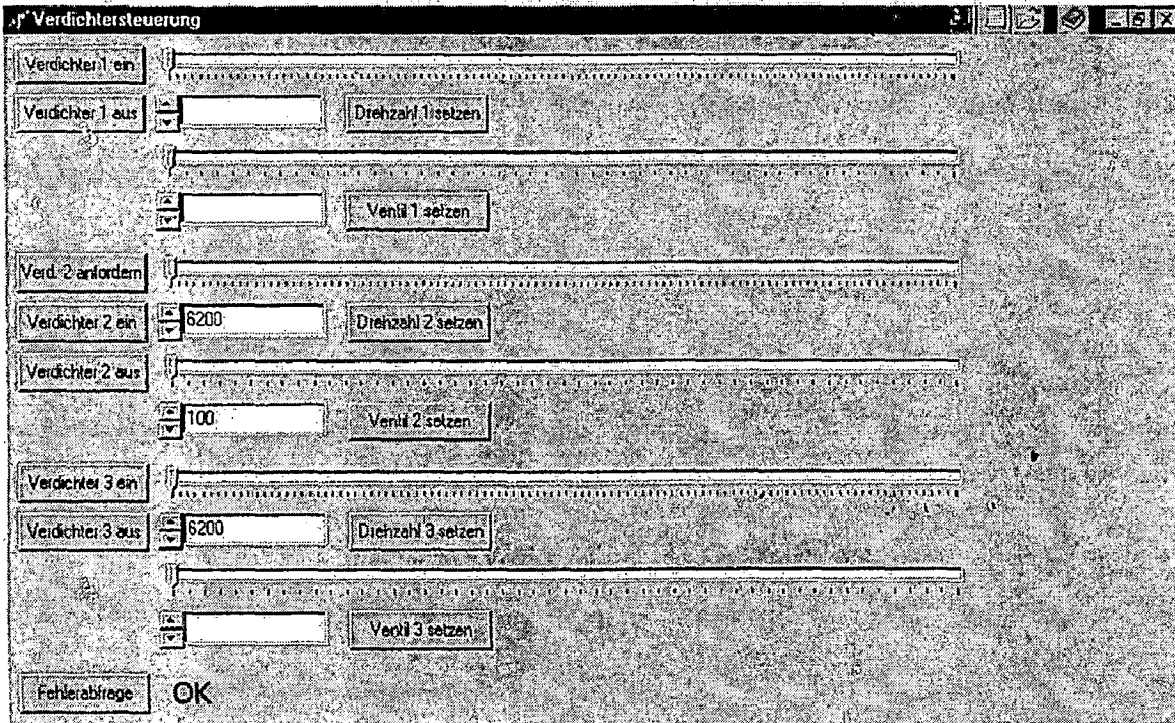

Fig 4.18 Compressor programme

4.1.7 Operating the test cell

4.1.7.1Characterstic map operating mode:

The speed of the exhaust gas turbocharger is regulated with the help of compressor speed and the position of the blow-off valve in the compressor programme. The speed of the turbocharger increases with the closing of the valve and also by increasing the compressor speed. As the desired speed is achieved, the data can be saved by pressing the button (C2).

First the gross ATL throttle (MS 1) is completely closed and the speed of the turbocharger is regulated, then the data is saved by pressing C2.For the next points the fine ATL throttle (MS2) is gradually closed by uniform intervals of mass flow rate $\overset{\bullet}{m}_{air}$ The operation is continued until the surging limit is reached. As the surging begins, the fine throttle MS1 (D) must be immediately opened .In case the speed of external compressor cannot be further lowered, the shut-off valve SSK1 (F) can be gradually closed to reduce the speed of the turbocharger. After completing one characteristic the throttle valves (MS 1 and MS2)(D+E) and the valve SSK1(F) must be completely opened and then the new speed should be adjusted to obtain more characteristic curves.

4.1.7.2 Controls during operation:

1. Increase in the fuel supply (B5) raises the temperature T_3 (O) before the turbine and the turbocharger speed n_{TBC}.

2. Opening of the combustion chamber slider (B1) reduces the primary zone temperature T_{prim} (M).

3. Increase in the compressor speed n_{comp} reduces the temperature before the turbine T_3 (O) and raises the turbocharger speed n_{TBC}.

4. Closing of the throttle valve (D+E) increases the turbocharger speed n_{TBC} and reduces the air mass flow rate $\dot{m}_{air}$ through the compressor of the turbocharger.

5. Increase in the external compressor speed n_{comp} increases the speed of the turbocharger n_{TBC} and vice versa.

6. Increase in the fuel injection pressure raises the temperature T_3 (O) before the turbine.

7. Increase in the air injection pressure reduces the temperature T_3 (O) before the turbine.

4.1.7.3 Other arrangements

A variety of fuel species are available for use in the test cell. The fuel species is regulated by opening the respective ball valve (Fig 4.19) and by selecting the corresponding control on the fuel switch (Fig 4.20). Generally diesel fuel is used in the combustion chamber. The fuel mass flow rate is indicated by the fuel balance on the computer cabinet. The mass flow rate of air through turbine is indicated either on test cell programme block K or on the digital display of the SENSYFLOW P (hot film anemometer) at the computer cabinet (Fig 4.10). The combustion chamber arrangements are done by selecting the option "ja" (B3) in the block "Brennkammerbetrieb". The fuel pump is actuated by pressing B2 .The combustion chamber slider and E-Gas are set to reasonable values and then the ignition button (B4) is pressed. It takes approximately 5-10 seconds for ignition. An abrupt rise in the turbocharger speed can be noticed. Immediately after the ignition effect the combustion chamber slider (B 1) must be raised slowly and uniformly up to 850, this can be done most suitably by using the arrow key of the key board. In case ignition does not take place. ".Feuer aus" must be pressed immediately on the test cell computer this disconnects the fuel pump, thereby avoiding the overflow of the fuel in the combustion chamber.
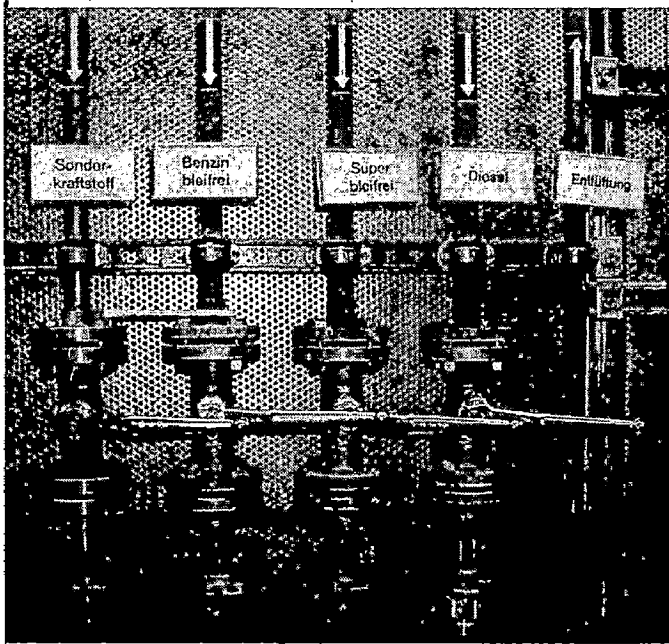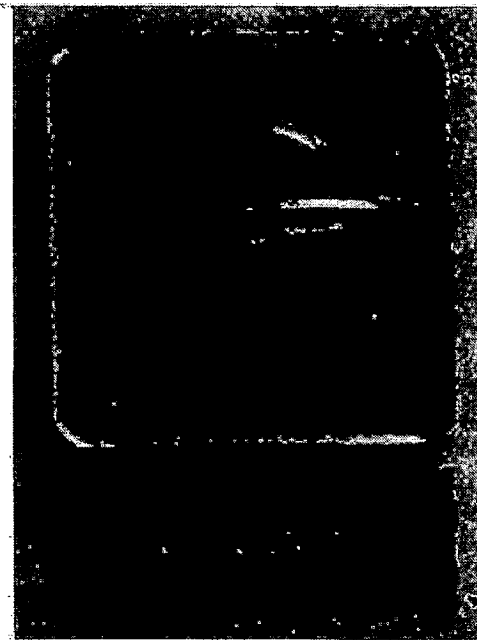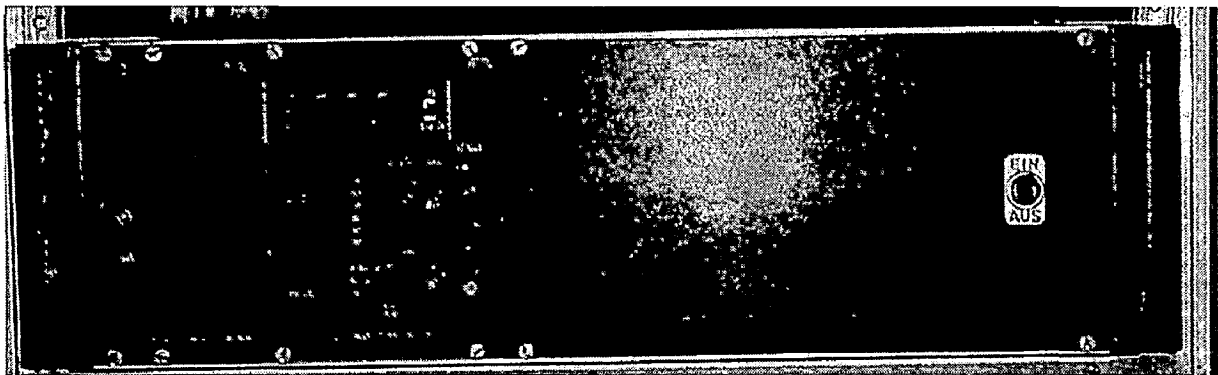
Fig 4.19 Fuel valves

Fig 4.20 Fuel switch

Fig 4.21 Fuel balance

4.1.7.4 Open cycle gas turbine operating method:

The measurements of characteristic maps are not feasible in free wheel operating method and it also requires an external compressor to actuate the process. As the pressure on the compressor side of the turbocharger equals the pressure at the exit of the external compressor, the free wheel slider (MS3)(G) is opened and then the throttle valves MS1 and MS2(D+E) as well as the fast closing valve SSK1(F) are completely closed.

4.1.7.5 Surging

Surging is an unsteady and unstable process. Surging over a longer period can lead to the destruction of turbocharger Therefore, it is important that the surging limit should not be crossed. The surging can be noticed by

1) Exhaust sounds from the test box.

2) Strong fluctuations at D_p (R)

3) Discontinuity in mass flow rate signalling (Q) or

50
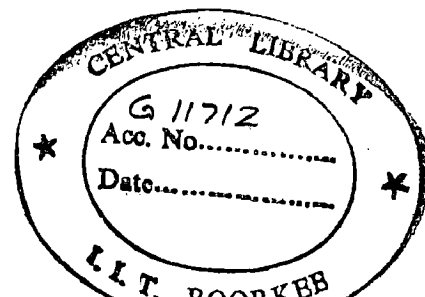
Jump in the temperature T_1 (P) before the compressor because near surging limit there is a back flow of air from high pressure side of the compressor to the low pressure side

4.1.7.5. Shutting down the test cell:

To shut down the test cell first the throttle valves (MS 1 and MS2) (D+E) and the shut-off valve SSK1 (F) are completely opened. The fuel supply (B5) is slowly and uniformly reduced to zero. The fuel pump is disconnected by pressing the button "Feuer aus" (H). Subsequently the speed of the external compressor is gradually reduced, the bleeder valve is opened, the compressor is pressed off and the programme is terminated. At the test cell computer the oil (A4) and the compressed air (A5) is pressed off and the programme is terminated. The data files containing the measured data are saved on the disk with the command "mcopy<datei> a: " After shutting down both the computers together with the monitor the test operation is switched off.

3.6 Points to be considered carefully:

1) The oil pressure must be regularly controlled.

2) While operating with compressor 1 the pressure P_{vortex} (L) should not exceed 2 bar.

3) While operating with compressor 2 the pressure P_{vortex} (L) should not exceed 3 bar.

4) The temperature T_{vortex} (N) should not exceed 90°C

5) The primary zone temperature T_{prim} (M) should not exceed 1100°C .the optimum temperature range is between 980 to 1030°C.

6) The temperature T_3 before the turbine should lie within the specified range of the required measuring temperature (for example 600±5°C).

4.2 Start-up experiments

The experiments are conducted with the turbocharger test cell on a GT-1749 turbocharger from Garrett The experiments are conducted to measure the turbine and the compressor characteristic maps with turbocharger speeds of 120000 and 16000 rpm. The temperature of the turbine exhaust gas is maintained at 600°C during the test run. The procedure for plotting the characteristic maps is explained in section 4.1.7. The turbine characteristic map gives the variation of the turbine total efficiency with the turbine pressure ratio under hot conditions. These variations are then compared with variations given by the dynamic measurements (explained in section 4.3) under cold conditions. The following graphs show the turbine and the compressor characteristic maps.
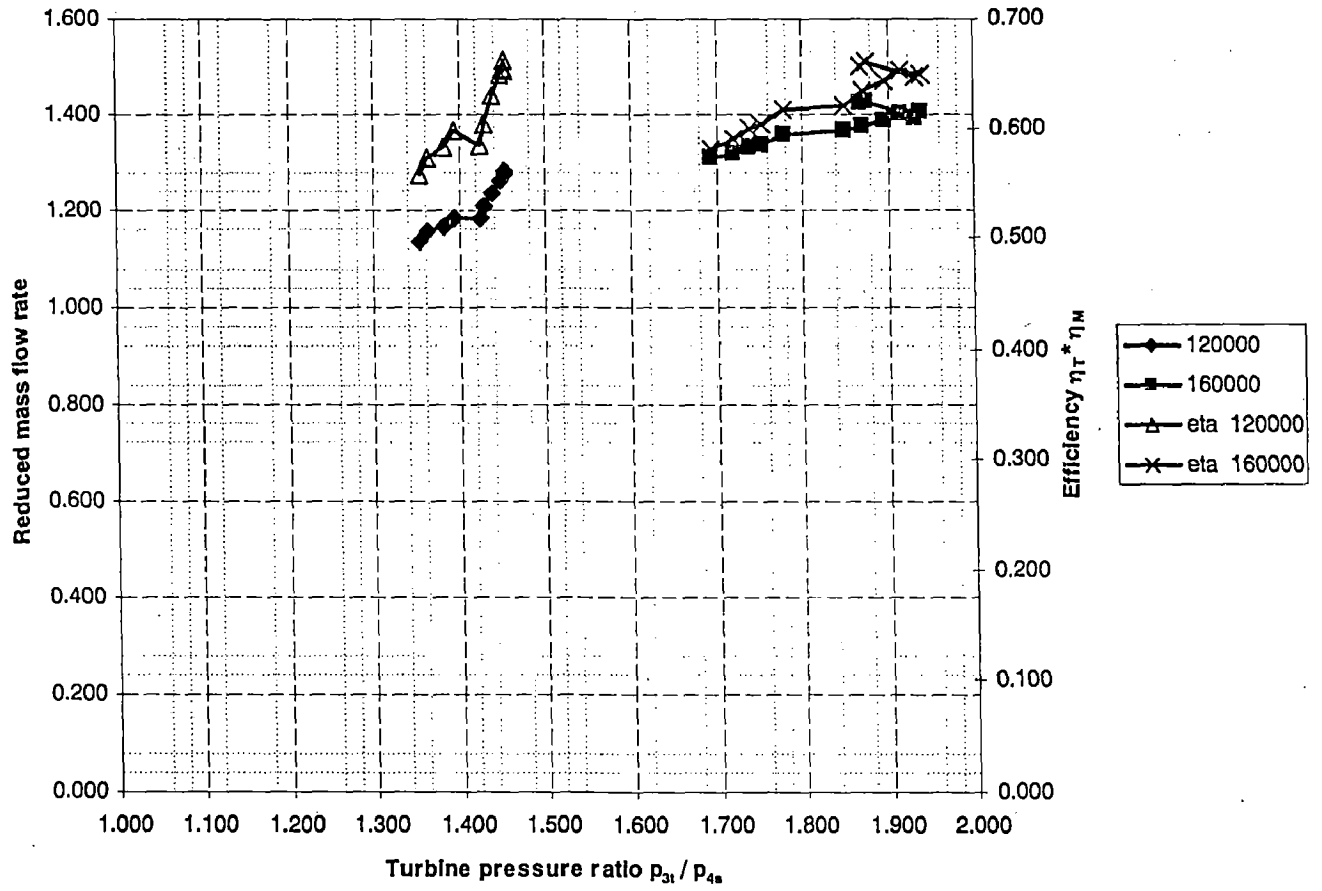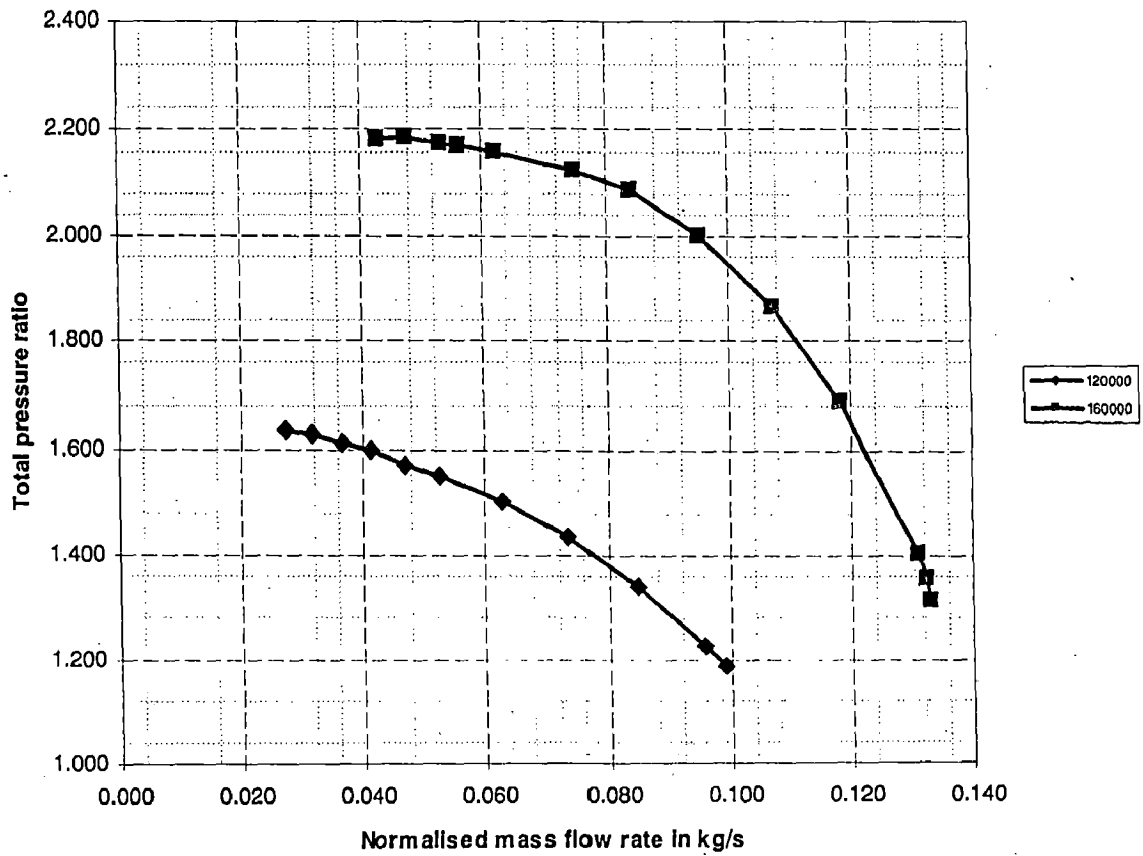
Fig 4.22 Turbine characteristics

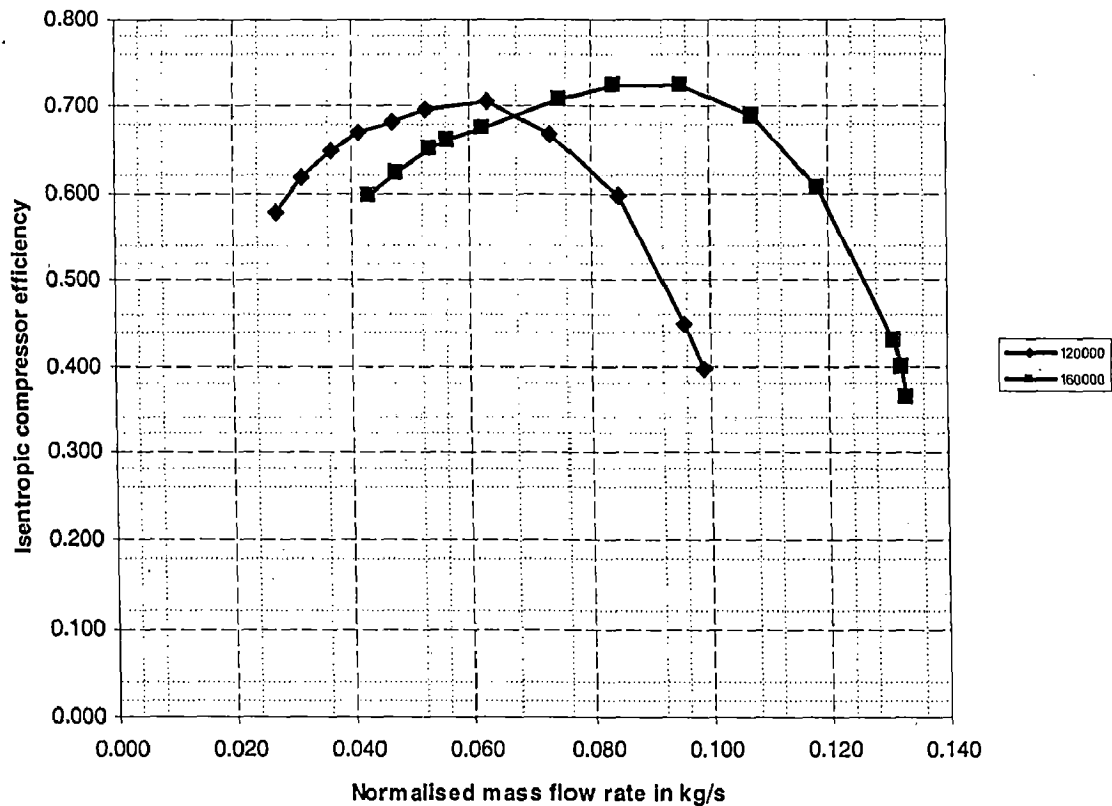**Fig 4.23** Compressor characteristics

52

Fig 4.24 Compressor efficiency

4.3 Dynamic measurements.

The dynamic measurements are done to obtain some of the inputs required in the model. These measurements are conducted on the turbocharger with different VTG positions to generate the data points required for plotting the variation of the turbine throat effective cross-sectional area and the turbine total efficiency as a function of turbine pressure ratio. These data points are then used to obtain the correlations for the turbine effective cross-sectional area and the turbine total efficiency with the turbine pressure ratio as required in the advanced model. The experiments are conducted with cold conditions (without ignition on the combustion chamber) by the dynamic variation of the speed of the external compressor and the position of the bleed-off valve. The data points are recorded with the frequency of 2 Hz. The following graphs show the variation of the above mentioned parameters with three different VTG positions 100%, 50% and 0%. The variation of the turbine total efficiency in 100% VTG case on comparison with the turbine characteristic map shows a reasonable approximation. In both the cases at a pressure ratio of 2 the turbine total efficiency is approximately 0.6. In the 100% VTG case the data points for the pressure ratio below 2 has not been used for plotting the total efficiency as due to some experimental flaws the trend shows an abnormal rise in the efficiency below this value.
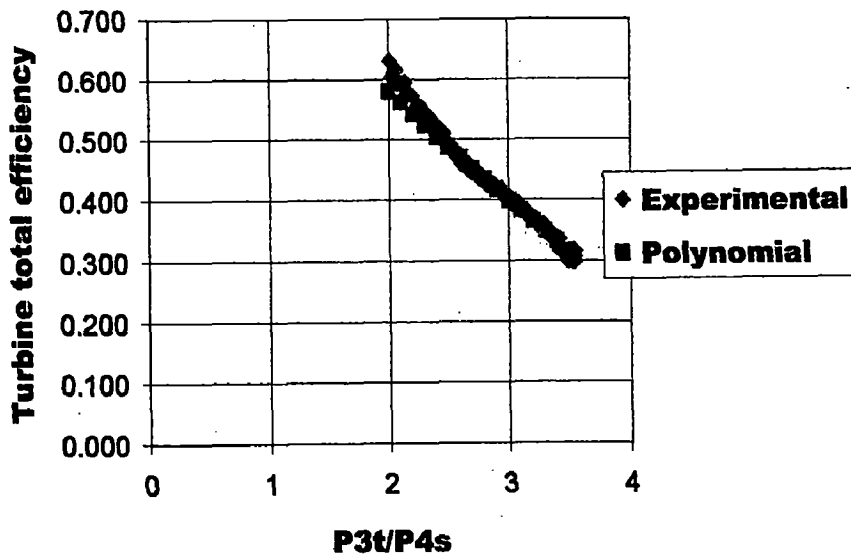
53
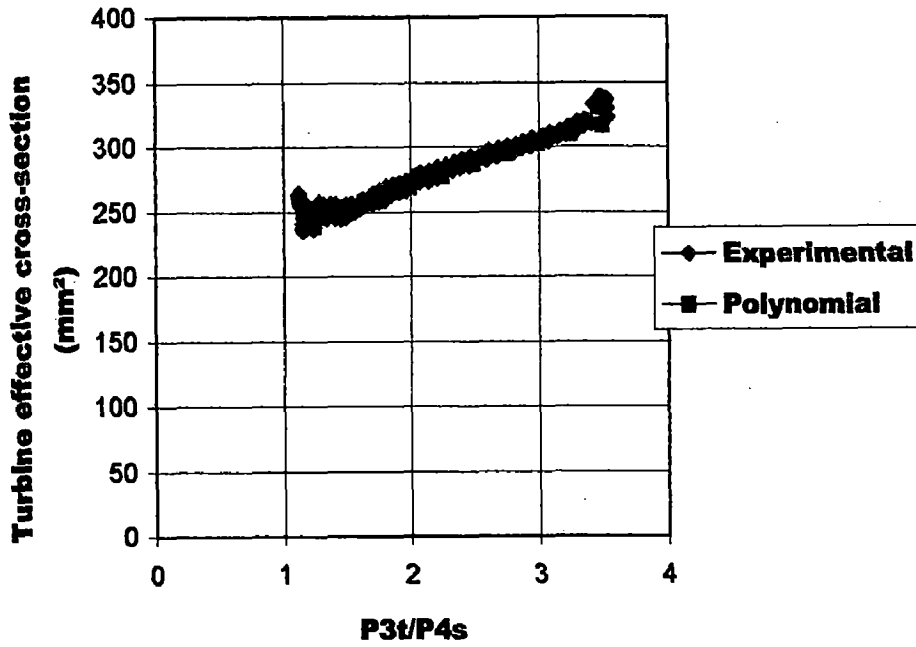
100%VTG

$$A_{eff} = -3.4 * (P_{3t}/P_{4s})^2 + 51 * (P_{3t}/P_{4s}) + 180$$
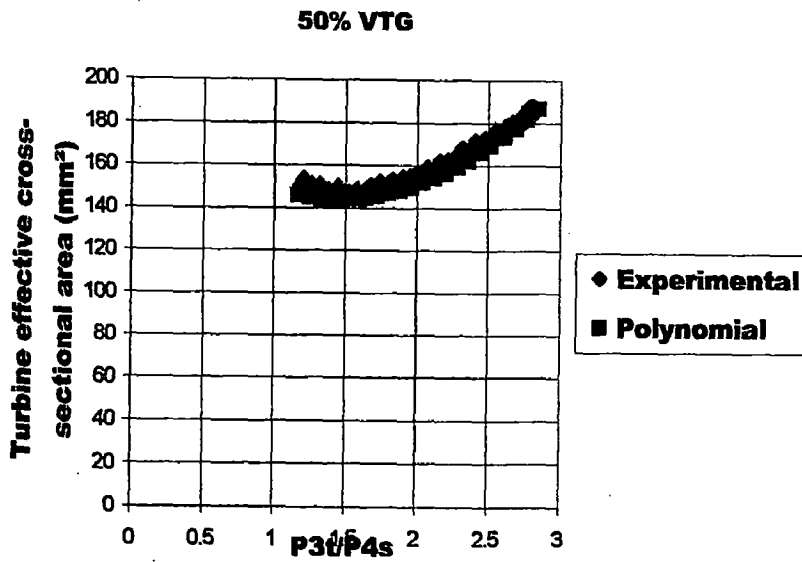
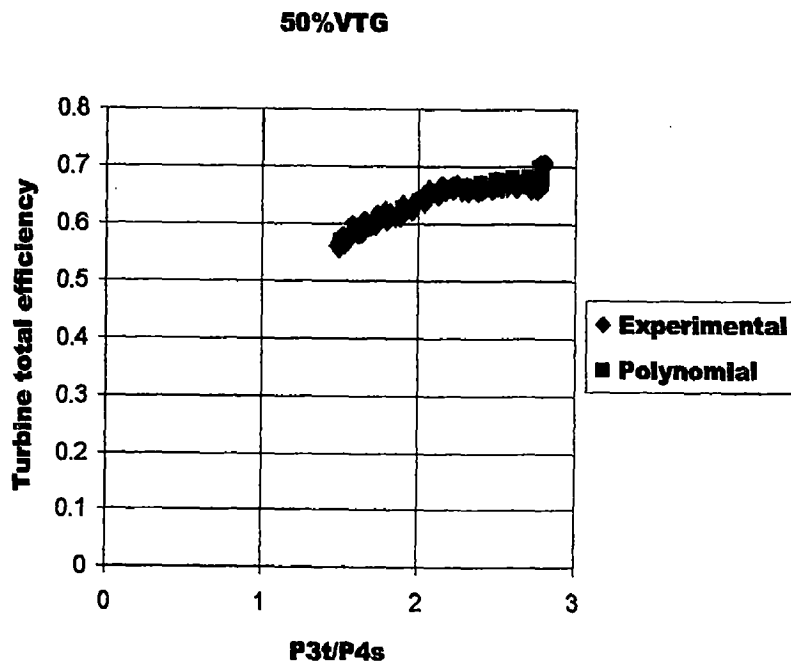Fig 4.25 Turbine effective cross-sectional area at 100% VTG

100%VTG

$$\eta_{tt} = .0077 * (P_{3t}/P_{4s})^2 - .22 * (P_{3t}/P_{4s}) + .99$$

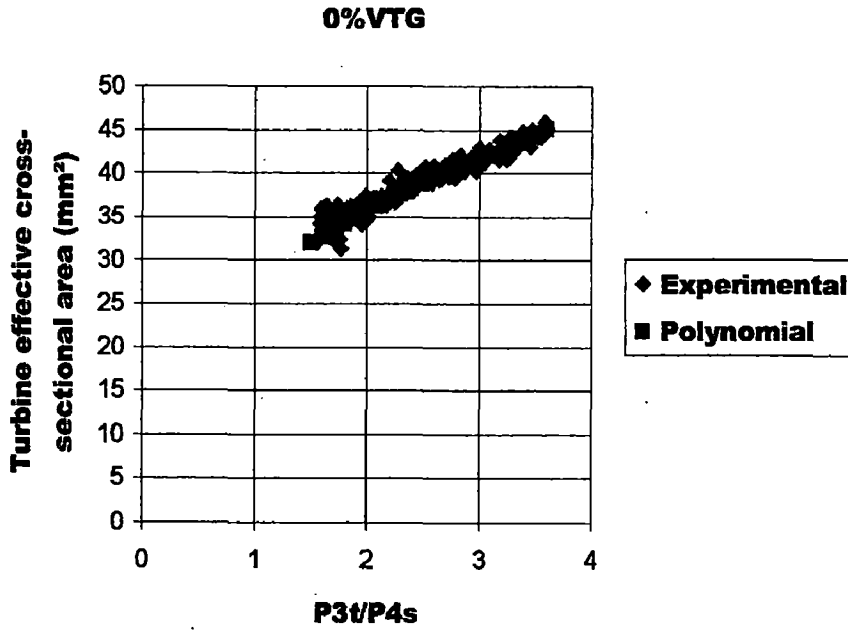Fig 4.26 Turbine total efficiency-section at 100% VTG

50% VTG

$$A_{eff} = 22*(P_{3t}/P_{4s})^2 - 64*(P_{3t}/P_{4s}) + 190$$

Fig 4.27 Turbine effective cross-sectional area at 50% VTG

50%VTG

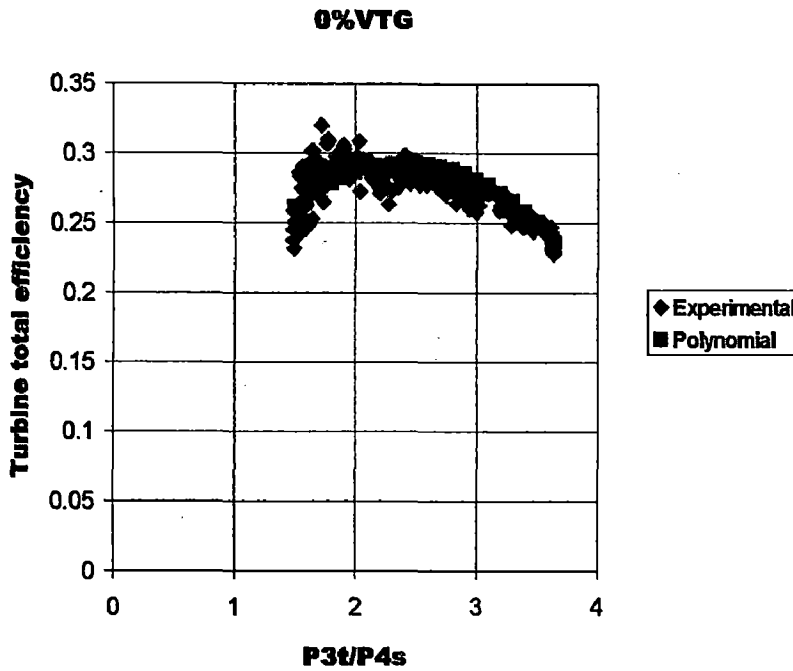$$\eta_{tt} = -.063*(P_{3t}/P_{4s})^2 + .36*(P_{3t}/P_{4s}) + .17$$

Fig 4.28 Turbine total efficiency 50% VTG

55

0%VTG

$$A_{eff} = -.74 * (P_{3t}/P_{4s})^2 - 9.8 * (P_{3t}/P_{4s}) + 19$$

Fig 4.29 Turbine effective cross-sectional area at 0% VTG

0%VTG

$$\eta_{tt} = -.037 * (P_{3t}/P_{4s})^2 + .18 * (P_{3t}/P_{4s}) + .074$$

Fig 4.30 Turbine total efficiency at 0% VTG

56

The graphs for the turbine effective cross-sectional area show that for the turbine pressure ratio of 2 the effective cross-section is 275 mm² for the 100%VTG case, whereas it reduces to 150 mm² for 50% VTG and to 35 mm² for 0% VTG. The turbine total efficiency for a pressure ratio of 1.5 is 0.55 for the 50% VTG case whereas it reduces to 0.25 for the 0%VTG case. The figure (4.30) shows that there is a sharp decrease in the turbine total efficiency at low pressure ratios (1.3 to 1.5) in the 0% VTG case.

4.4 Experiments for validation

The experiments are conducted on the turbocharger test cell to validate the transient variation of the turbine exhaust temperature, bearing housing temperature and the compressor outlet temperature under natural and forced convection conditions. The experiments are conducted with a sharp jump in the turbine inlet temperature from cold state for the three different VTG positions of the turbocharger turbine. The turbine inlet temperature is increased from 30°C to 600°C and then maintained constant by regulating the pressure of the fuel and air injected in the combustion chamber. For the forced convection experiments the turbocharger is covered by a duct of circular cross-section (diameter 315 mm) and air at a mass flow rate of 1440kg/h is made to pass through it.
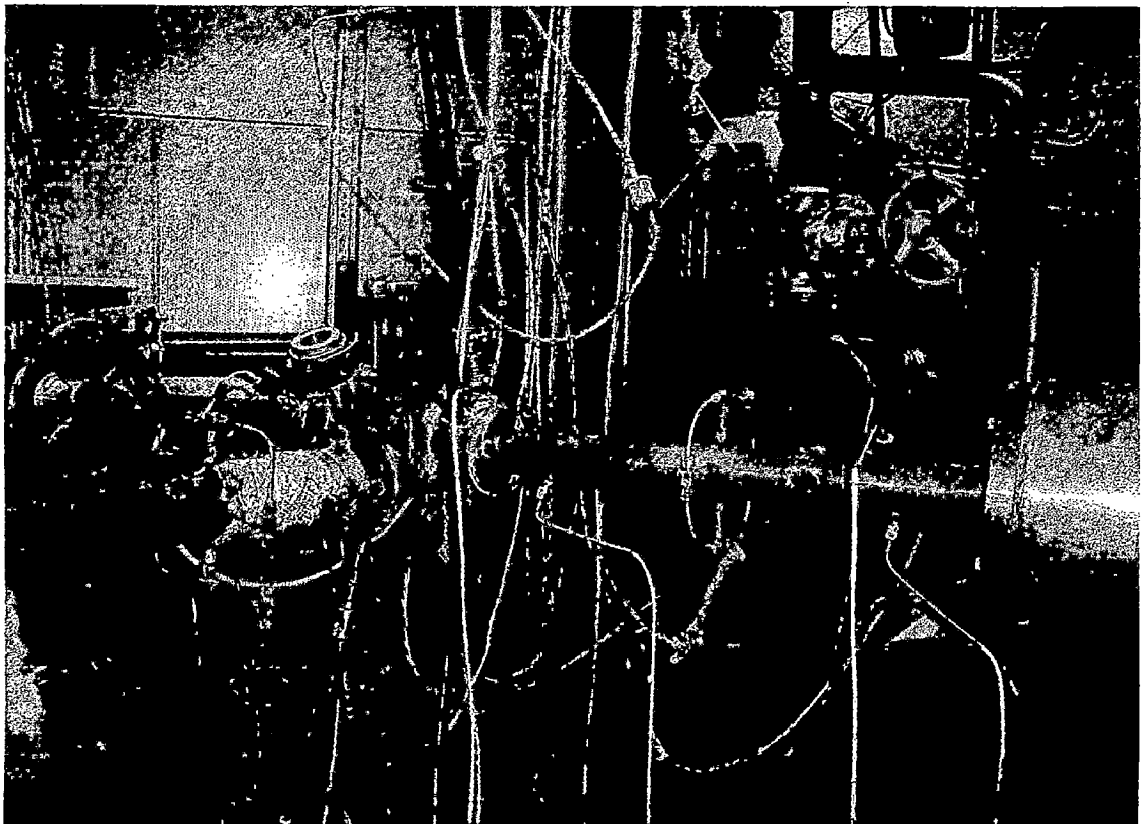

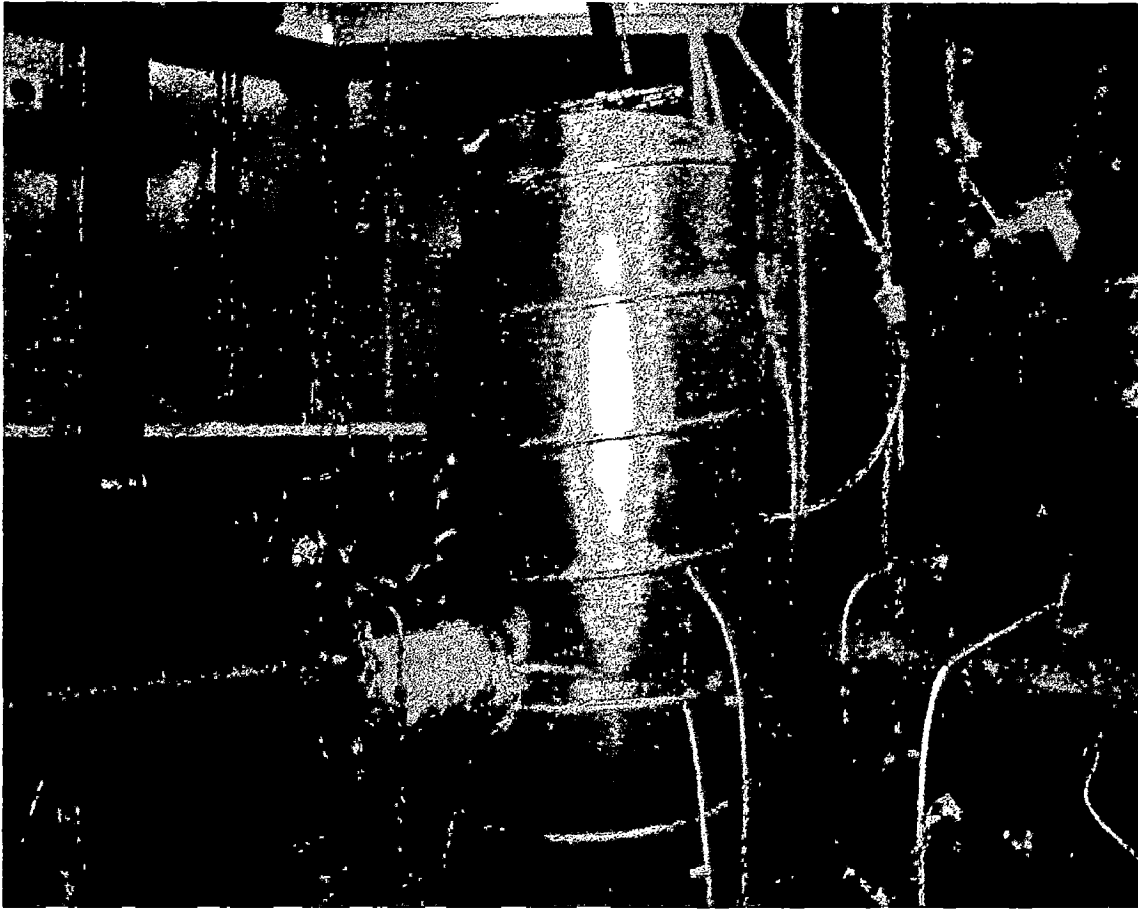Fig 4.31 Experimental set-up with natural convection.

Fig 4.32 Experimental set-up with forced convection

CHAPTER 5

Comparison Of Model And Experimental Data

5 1 Validation of the simplified model.

In the simplified model the turbine inlet conditions and the mechanical power absorbed by the compressor is taken as input from the experimental data and the model gives the turbine exhaust temperature as the output. The model has been validated under natural and forced convection conditions.

5.1.1 Natural convection

The following graph shows the experimental and the model values of the turbine exhaust gas temperature under natural convection condition.

Fig 5.1 Validation of the simplified model under natural convection.

The figure shows that the model values closely matches with the experimental values. Both the model and the experimental results show that the exhaust gases takes approximately 250 seconds to reach the maximum temperature. The following figure is the zoomed view of the above figure and it shows that the model turbine exhaust temperature is 4-5°C lower than the experimental values after 550 seconds from the start.

59
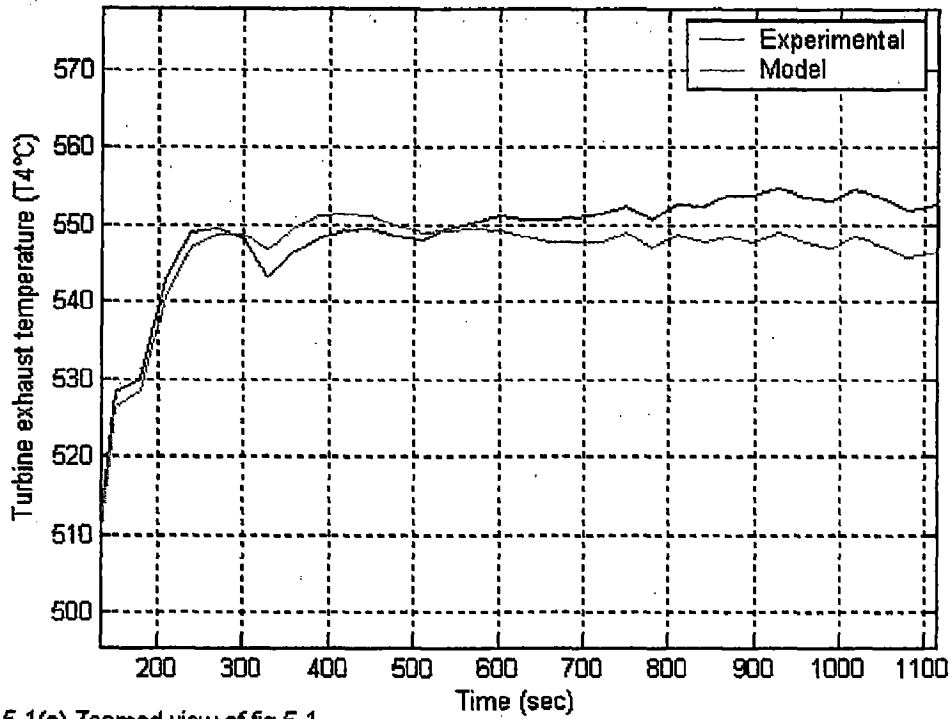
Fig 5.1(a) Zoomed view of fig 5.1

5.1.2 Forced convection

The model has been validated under natural and forced convection conditions. In natural convection the surrounding atmosphere of the turbocharger is having still air whereas in forced convection air at a velocity of 4.7m/s is made to flow across the turbocharger. The following graph shows the experimental and the model values of the turbine exhaust gas temperature for the forced convection case.

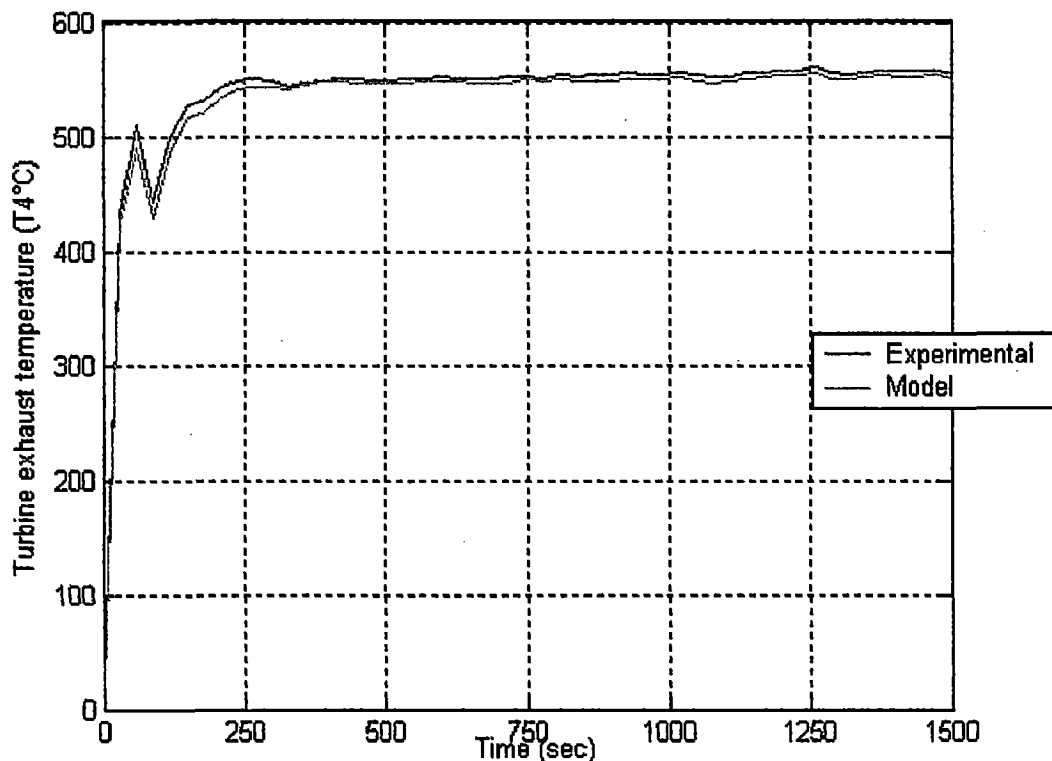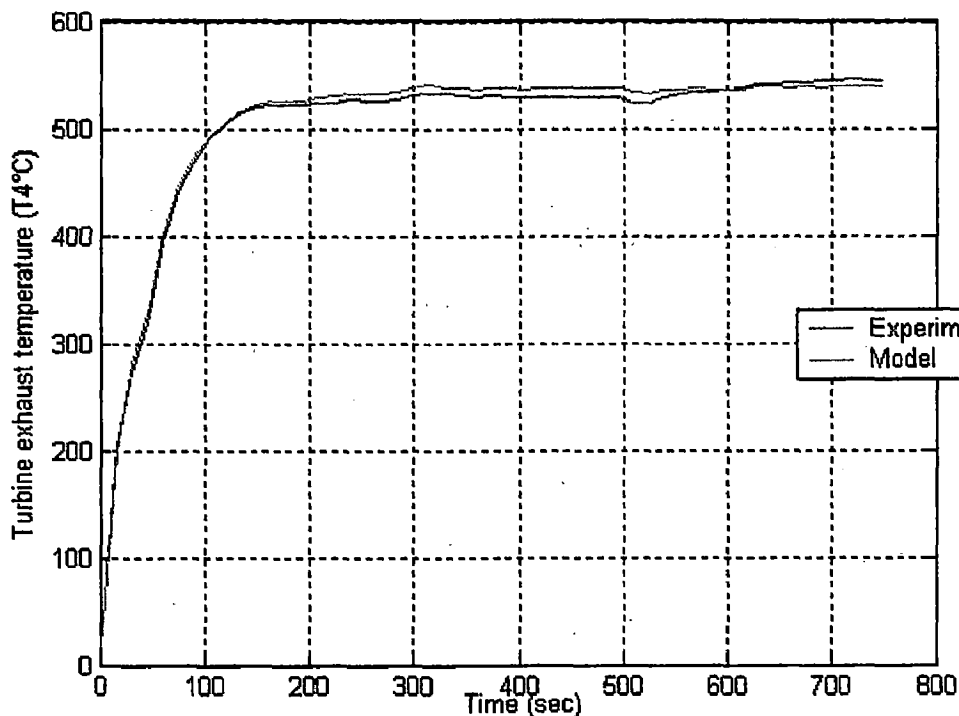Fig 5.2 Validation of the simplied model under forced convection.

The figure shows that the model turbine exhaust temperature is 5-10°C higher as compared to the experimental values. This is because of the under prediction of the heat transfer coefficient under forced convection condition. The correlation by Zhukauskas [16] used for calculating the average heat transfer coefficient for a circular cylinder in a cross flow works with an accuracy of ±25%.The following figure shows the results with a 20% increase in the heat transfer coefficient.

Fiq 5.3 Validation with increased heat transfer coefficient.
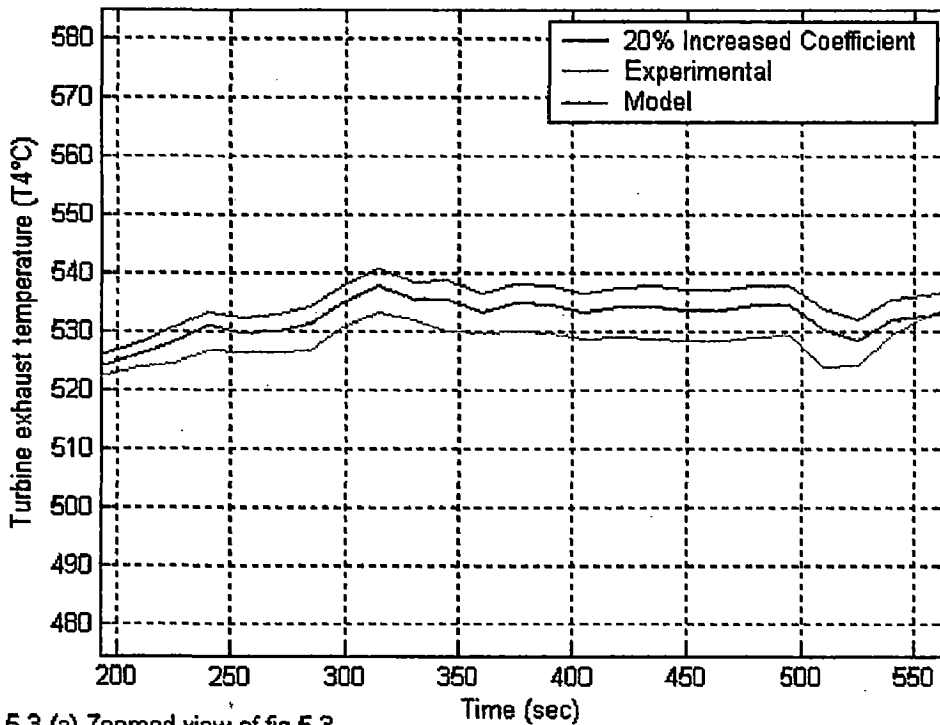
Fig 5.3 (a) Zoomed view of fig 5.3

The figure 5.3 (a) shows that on increasing the heat transfer coefficient by 20% the results come closer to the experimental values and the deviation between the two is now 3-5°C.

5.2 Validation of the advanced model

This model gives the transient variation of the turbine exhaust temperature, the bearing housing temperature and the compressor outlet temperature. The model can use the experimental data for the mass flow rate of the hot gases and can also use the correlations giving the turbine effective throat cross-sectional areas developed by conducting dynamic measurements (explained in section 4.3) for different VTG positions to calculate the mass flow rate.

5.2.1 Case I

In this case the model is validated under the natural convection condition and with the hot gas mass flow rate taken as input from the experimental data.

Fiq 5.4 Validation of the turbine exhaust temperature under natural convection.

62

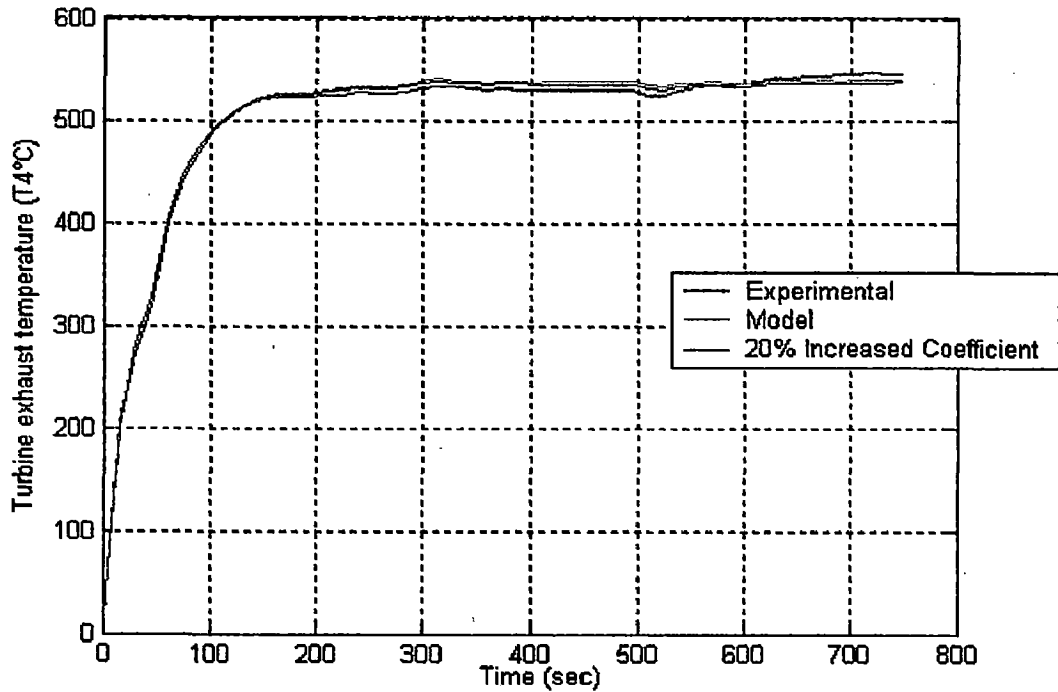Fig 5.5 Validation of the bearing housing temperature.

Fig 5.6 Validation of the compressor outlet temperature.
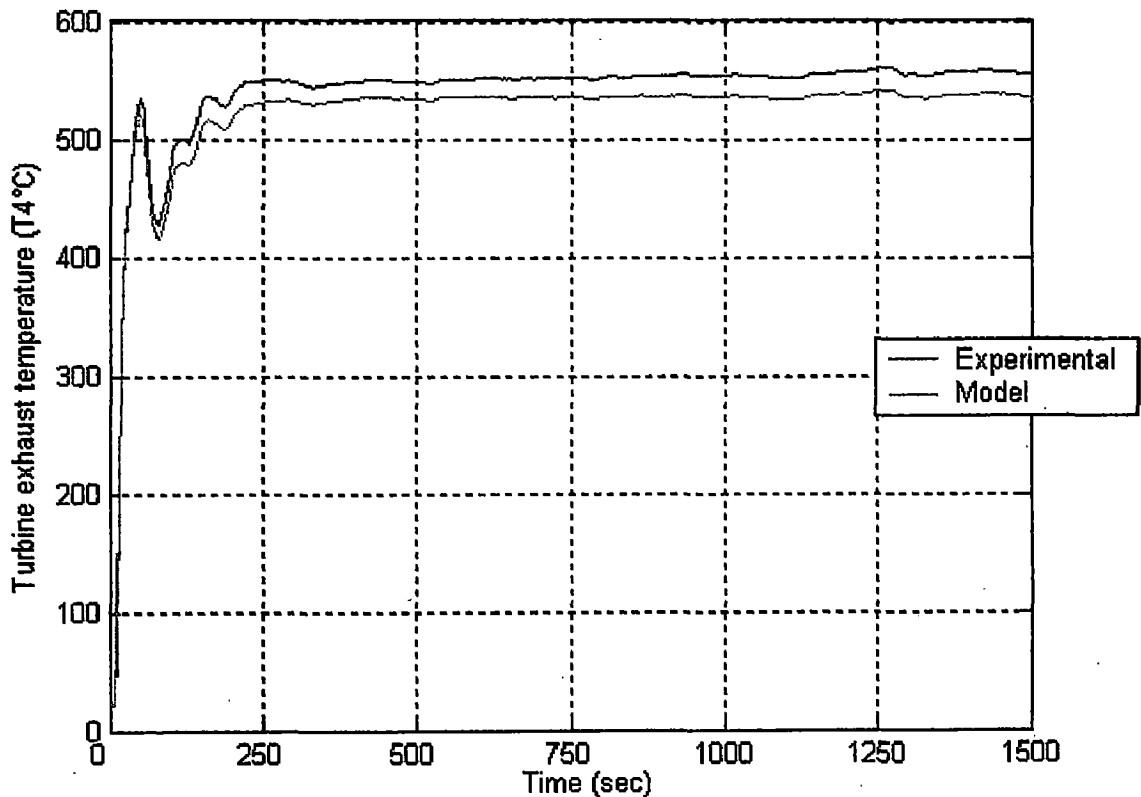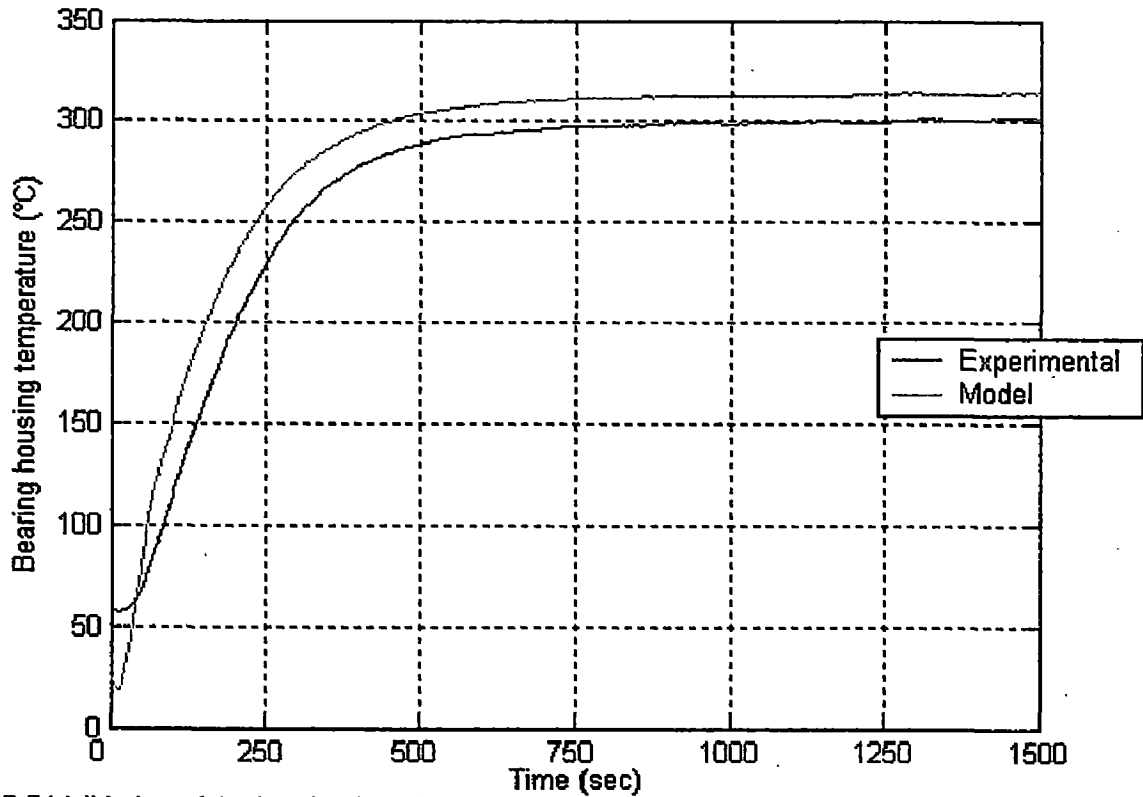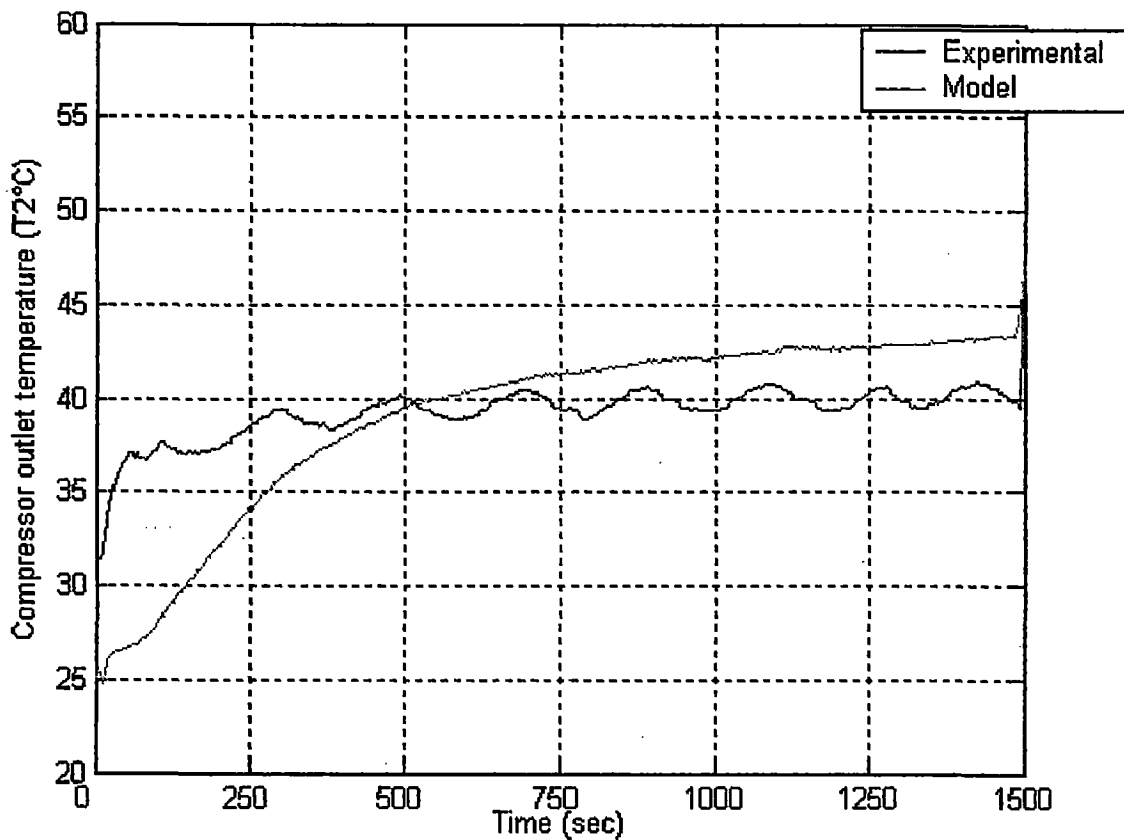
Figure 5.4 shows that the model turbine exhaust temperature is approximately 20°C lower than the experimental values and figure 5.6 shows that the model compressor outlet temperature is

63

approximately 3°C higher than the experimental values. This is because of the over prediction of the turbine total efficiency used in the advanced model to calculate the mechanical power developed by the turbine. The correlation used for calculating the turbine total efficiency was developed by using experimental data collected by conducting the dynamic measurements on the turbocharger test cell. The hot film anemometer used in the test cell to measure the turbine air mass flow rate, give the readings approximately 10% lower than the actual mass flow rate. The combined effect of the approximation by the correlation and the experimental flaw results in an over prediction of the turbine total efficiency. The over prediction of the turbine total efficiency leads to lower turbine exhaust temperature (T4) and higher compressor outlet temperature (T2). This is because of the fact that higher turbine efficiency gives a higher mechanical power developed by the turbine and this power is subtracted from the enthalpy entering the turbine to get the exhaust enthalpy which leads to a lower turbine exhaust temperature (T4). The mechanical power absorbed by the compressor is the transmission efficiency multiplied by the turbine mechanical power which is then added to the compressor inlet enthalpy to get the compressor outlet enthalpy and this leads to a higher compressor outlet temperature.

The deviation in the bearing housing temperature and the compressor outlet temperature is also due to the fact that the model does not consider the spatial effects in the analysis. The compressor casing is modelled as a hollow cylindrical lump without considering one-dimensional heat transfer effects.

Figure 5.5 shows that the transient variation of the model bearing housing temperature closely matches with the experimental variation. The deviation of temperature is approximately 20°C. The reason for this deviation is the location of the temperature sensor used. The sensor was positioned on a projected portion of the turbine casing. Moreover, the model does not consider the spatial affects of conduction. The figure shows a temperature difference of 30°C at the initial state (time is zero seconds). This is because the model uses an initial condition of 25°C to solve the differential equations involved whereas in the experiment the lubricating oil used for the bearings is initially heated to 90°C before starting the experiment. This effect of conduction heat transfer during the initial period from the heated lubricating to the bearing casing is not considered in the model.

The following graphs show the results with a 10% decrease in the turbine total efficiency. Fig 5.7 shows that by decreasing the turbine total efficiency by 10% the turbine exhaust temperature increases by approximately 5-8°C and fig 5.8 shows that the compressor outlet temperature decreases by approximately 2°C hence coming closer to the experimental data.
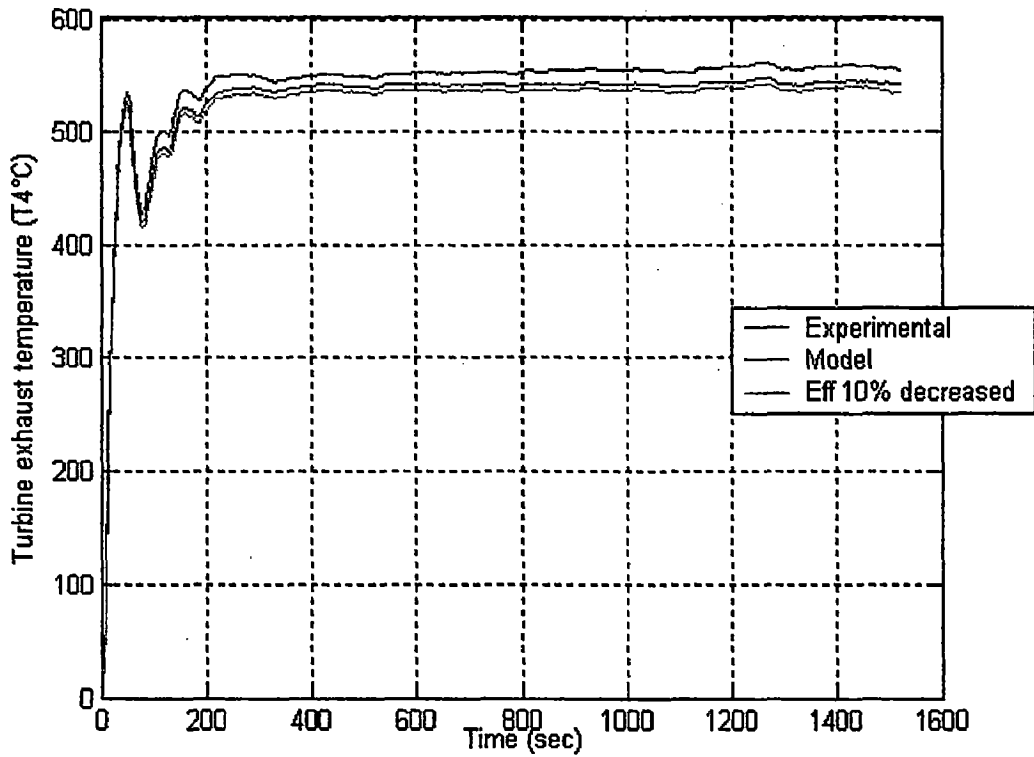
Fig 5.7 Validation of the turbine exhaust temperature with decreased total efficiency.
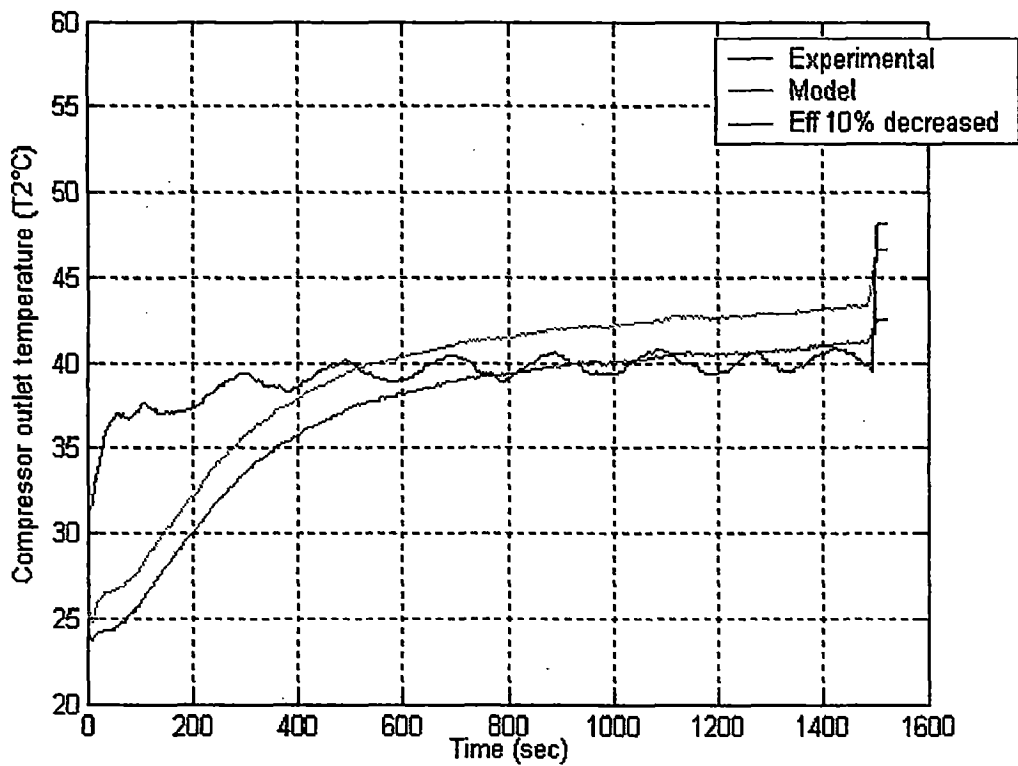
Fig 5.8 Validation of the compressor outlet temperature with the decreased total efficiency.

5.2.2 Case II

In this case the model is validated under the natural convection condition and with a correlation for 100% VTG position for estimating the effective turbine cross-sectional area and hence the hot gas mass flow rate.

Fig 5.9 Validation of the turbine exhaust temperature with 100% VTG position.

Fig 5.10 Validation of the bearing housing temperature with 100% VTG position.

Fiq 5.11 Validation of the compressor outlet temperature with 100% VTG postion.

The difference between cases I and II is that the latter uses the correlation developed in section 4.3 for estimating the turbine effective cross-sectional area which is then used to calculate the mass flow rate of the hot gases entering the turbine instead of using the value from the experimental data as done in case I. The figures 5.9 -5.11 show that the correlation used works with reasonably high accuracy and the temperature difference between the model and the experimental values is mostly due to over prediction of the total turbine efficiency.

5.2.3 Case III In this case the model is validated under the natural convection condition and with a correlation for 50% VTG position for estimating the effective turbine cross-sectional area and hence the hot gas mass flow rate. The test run is conducted for 500 seconds. The turbine inlet temperature is given a jump form cold start to 600°C and the maintained at this temperature.

67
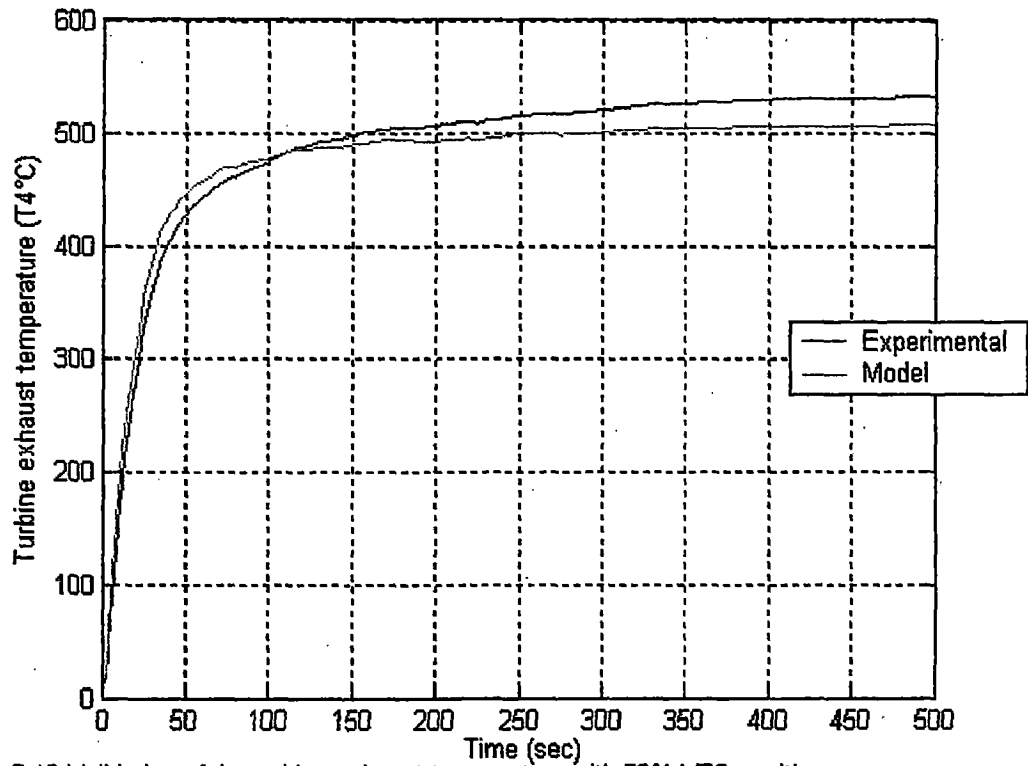
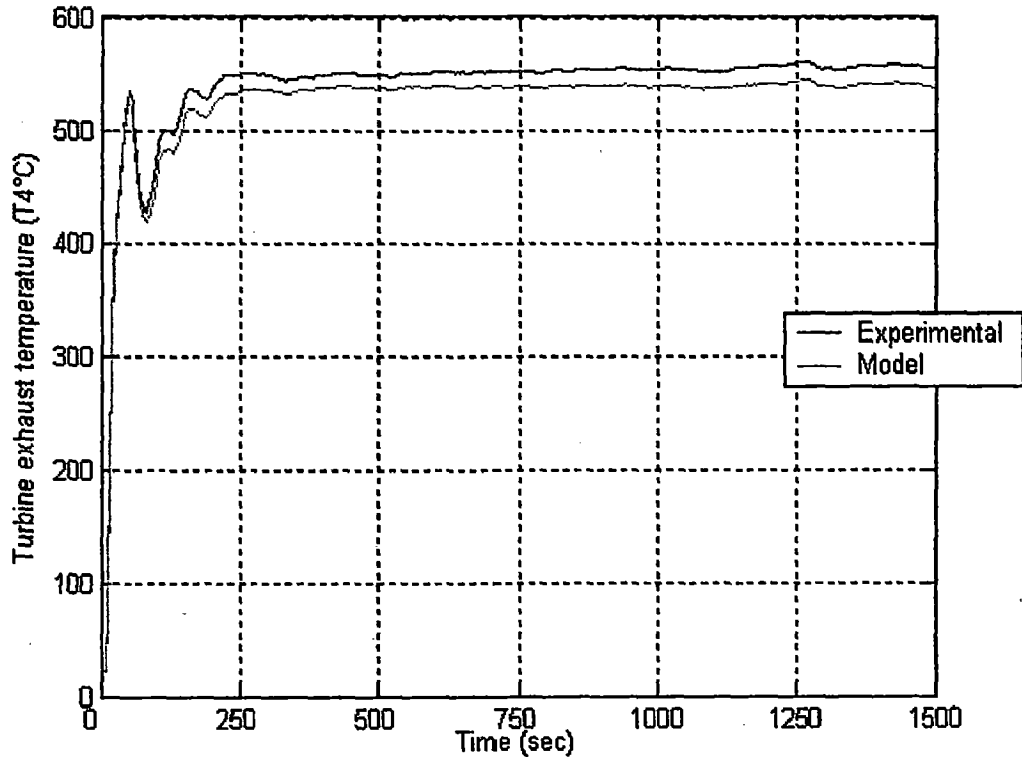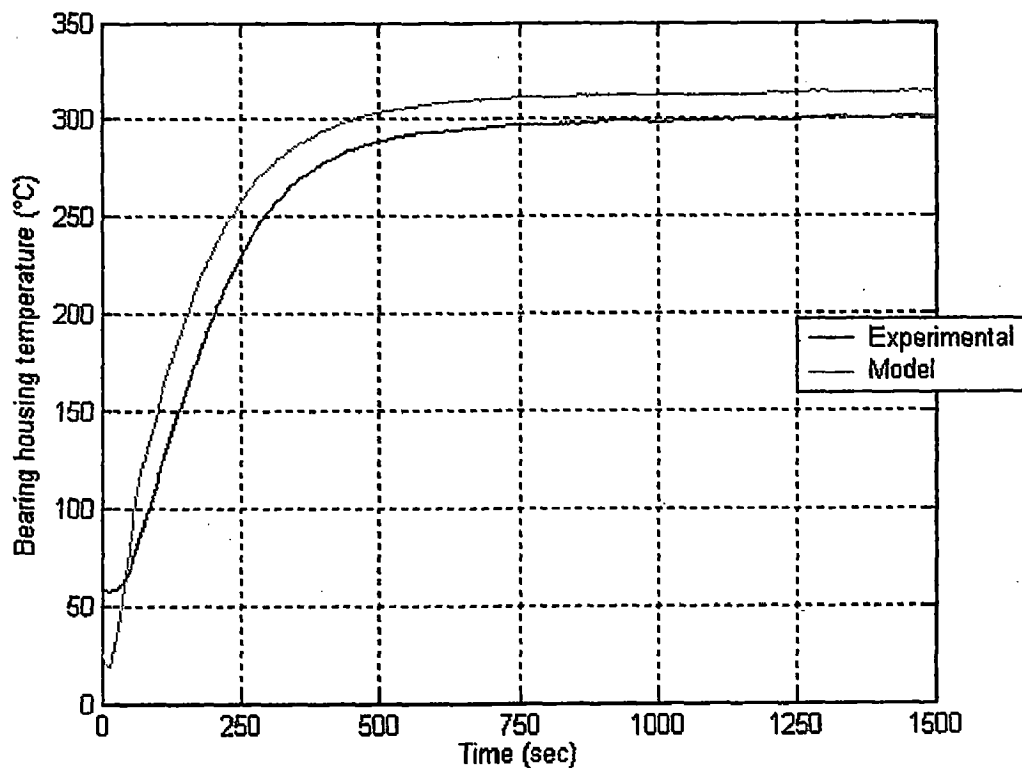the . Fig 5.12 Validation of the turbine exhaust temperature with 50% VTG position.
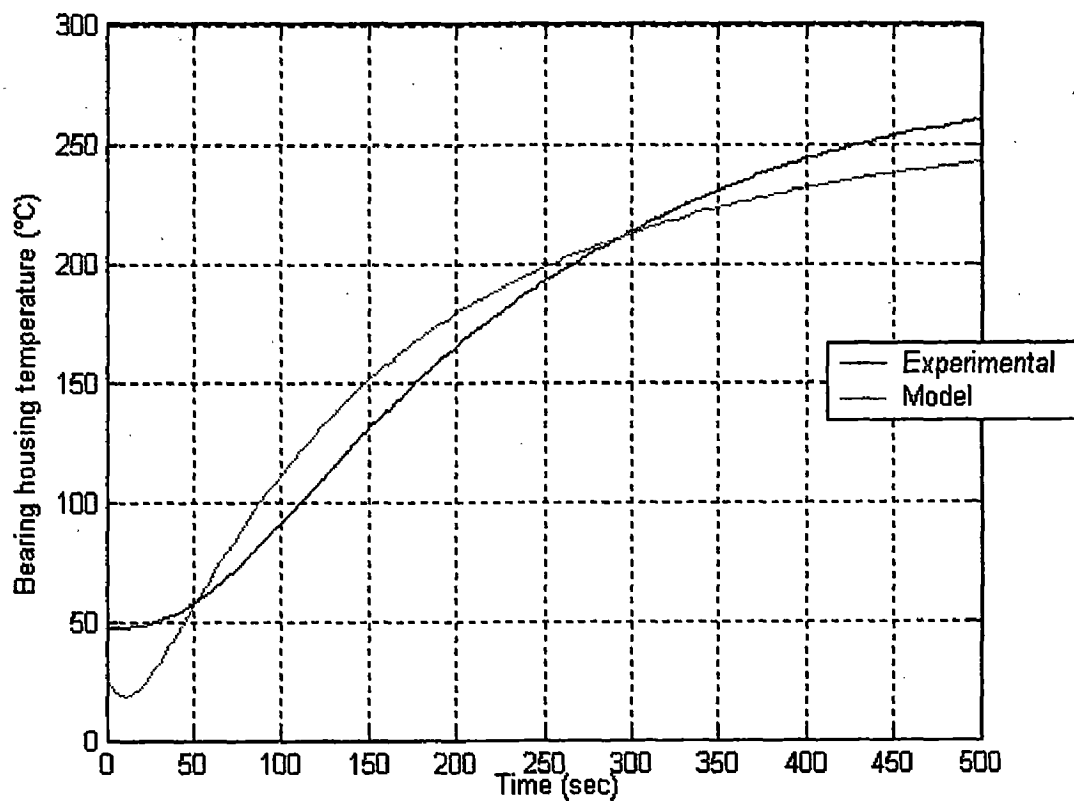
Fig 5.13 Validation of the bearing housing temperature with the 50% VTG position.
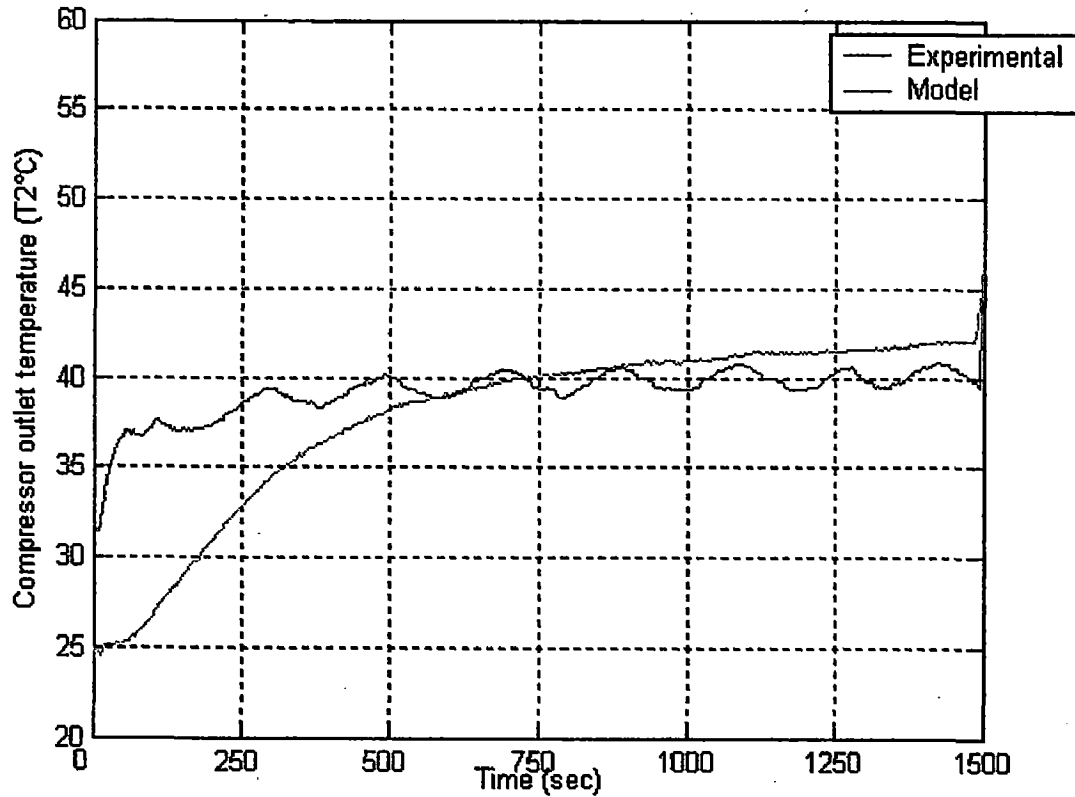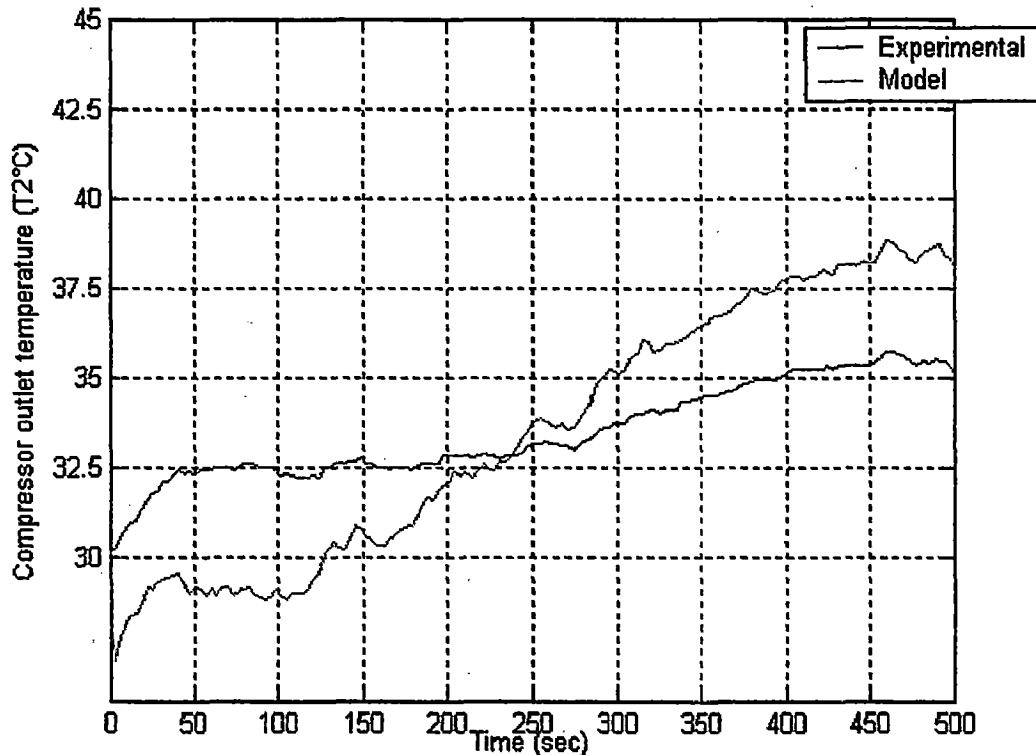
Fig 5.14 Validation of the compressor outlet temperature with 50% VTG position.

The figures above from 5.12 to 5.14 show almost the same trend as in the 100% VTG case but during the early start period the temperature variation trends differs as in the 50% VTG case the model turbine exhaust temperature is slightly higher than the experimental (shown in fig 5.12) upto 125 seconds and than it remains lower than the experimental as in 100% VTG case. The similar deviations are observed with the bearing housing temperature and the compressor outlet temperature (shown in fig 5.13 and 5.14 respectively). The probable reason for the deviations is the variations in the flow patterns with change in turbine effective cross-sectional area which further affects the thermal conductions. The model does not account these effects. Moreover, the model does not consider one-dimensional heat transfer effects.

5.2.4 Case IV

In this case the model is validated under the natural convection condition and with 0% VTG position for estimating the effective turbine cross-sectional area. The figure 5.15 below shows that the model accuracy further reduces with 0% VTG position. This reconfirms the above mentioned effect. The model cannot be validated for the bearing housing temperature and the compressor outlet temperature as at 0% VTG the mass flow rate of the air through the compressor is too low to be measured correctly by the nozzle used in the test cell. This also influences the power balance on the turbine side thereby reducing the accuracy.
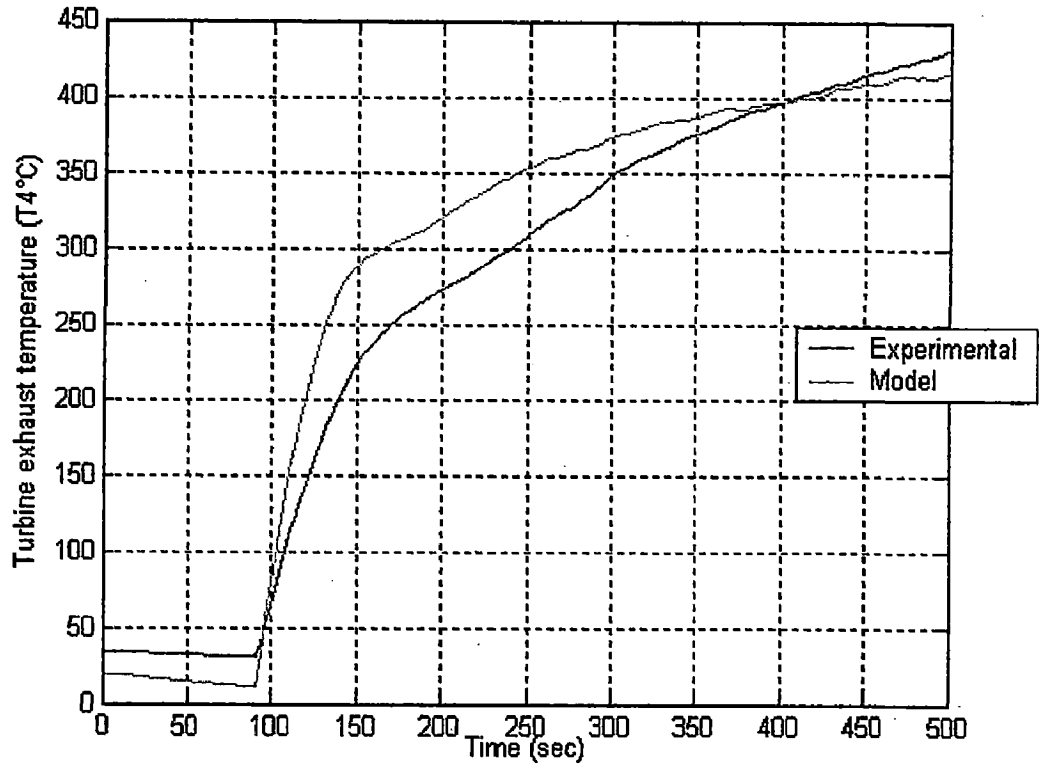
Fig 5.15 Validation of the Turbine exhaust tempertature with 0% VTG position.

5.2.1 Case V

In this case the model is validated under the forced convection condition with the air velocity of 4.7m/s and the hot gas mass flow rate is taken as input from the experimental data.
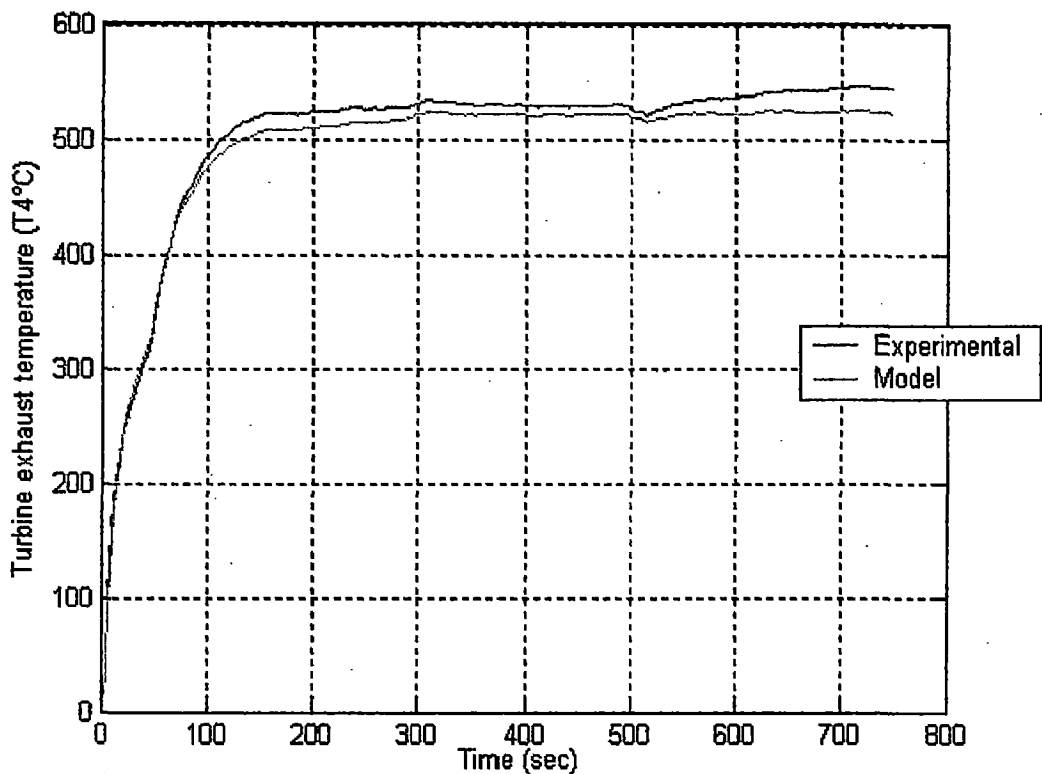
Fig 5.16 Validation of the turbine exhaust tempertature under forced convection.
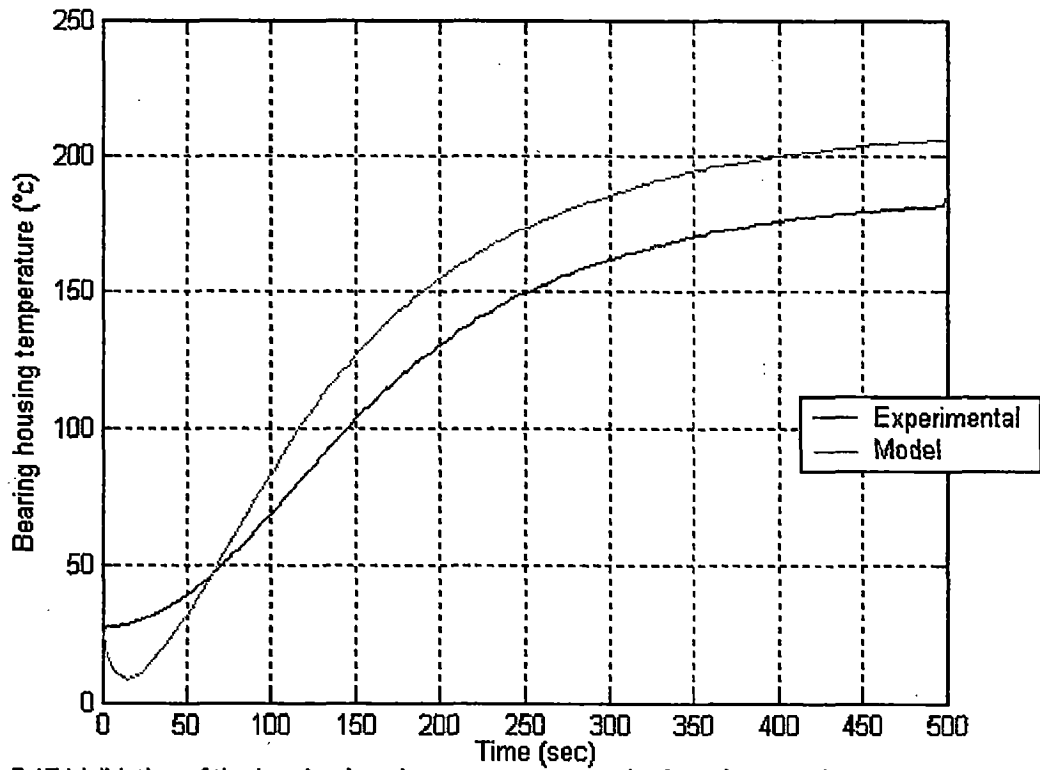
Fig 5.17 Validation of the bearing housing tempertature under forced convection.
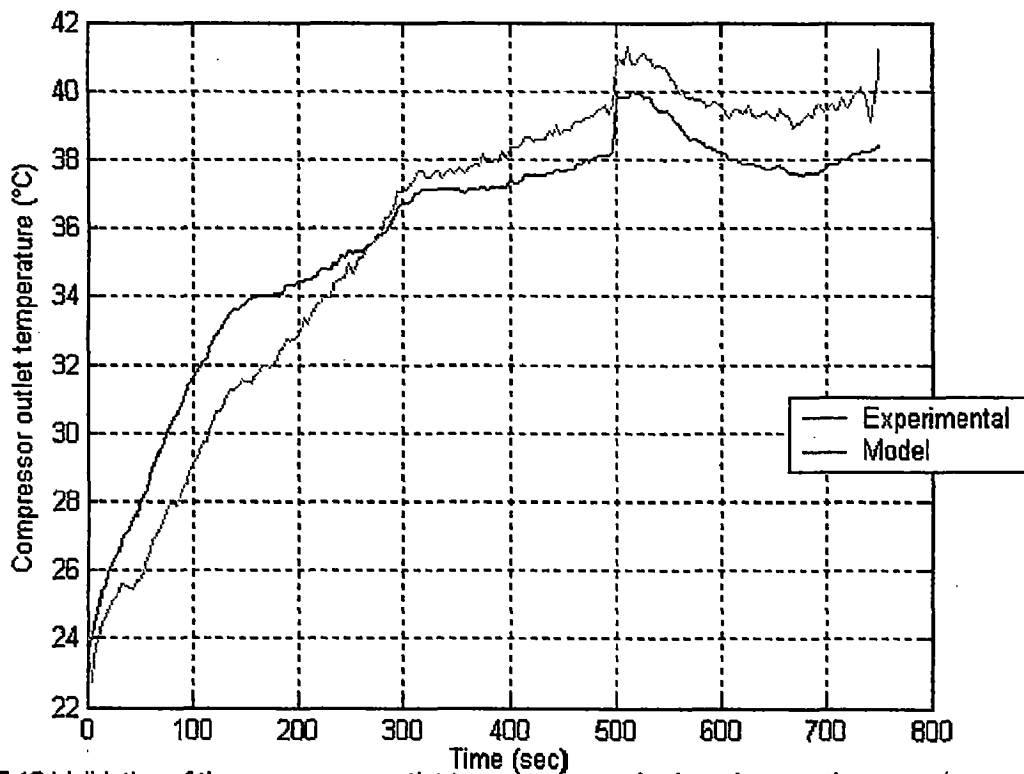
Fig 5.18 Validation of the compressor outlet tempertature under forced convection.

Figure 5.16 shows that the model turbine exhaust temperature is approximately 10°C lower than the experimental values. There are two reasons for the deviation. The first one is the under prediction of the surrounding heat transfer coefficient as mentioned earlier in validation of the simplified model and the second is the over prediction of the turbine total efficiency as mentioned in the case I. The figure shows that the over prediction of the turbine total efficiency has a more prominent affect compared to the under prediction of the heat transfer coefficient on the turbine exhaust temperature . This results in lower model turbine exhaust temperature.

The figure 5.17 shows that the model bearing housing temperature is approximately 25°C higher than the experimental. The under prediction of the heat transfer coefficient and the location of the temperature sensor used for measuring the bearing housing temperature (as mentioned in case I) are the probable reasons for the deviation. The figure shows a close approximation regarding the transient variation of the temperature.

The figure 5.18 shows that model the compressor outlet temperature is approximately 1.5 °C higher than the experimental values. The reasons for the deviation are same as for the turbine exhaust temperature along with the fact that the model does not considers the spatial effects of heat transfer. The simplified model works with high accuracy as in the model the mechanical power absorbed by the compressor is taken as input from the experimental data thus does not requires correlations for the turbine total efficiency.

CHAPTER 6

Conclusion and Suggestions for Further work

6.1 Conclusion

This work deals with mathematical modelling of the heat transfer processes in a turbocharger using the simulation tool SIMULINK and validating the model with experiments conducted under different convection conditions. The model is designed keeping in mind the suitability to be plugged into a complete engine cycle simulation model and to be used for fast online simulation.

At the first stage a simplified model is designed which takes the turbine inlet conditions and the mechanical power absorbed by the compressor as input from the experimental data and gives the transient variation of the turbine exhaust temperature as the output. In the next stage an advanced model is designed which is independent of the mass flow rate of the hot gases entering the turbine. This model takes the turbine pressure ratio and inlet temperature as input from the experimental data and calculates the transient variation of the turbine exhaust temperature, turbine casing temperature, bearing housing temperature and the compressor outlet temperature as the output. To increase the accuracy of the model the compressor inlet conditions are also given as input from the experimental data.

The models are then validated by conducting experiments on the turbocharger test cell at the TU.Berlin. First some start-up experiments are conducted to plot the characteristic maps of the turbine and the compressor at the turbocharger speed of 120000 and 160000 rpm maintaining the turbin e inlet temperature at 600°C. The maps are then are then compared with the data obtained by performing dynamic experiments on the test cell under cold conditions (without ignition of the combustion chamber) The data obtained by the dynamic measurements with different VTG positions are then used to develop the correlations for the turbine total efficiency and the effective cross-sectional area as functions of the turbine pressure ratio required in the advanced model. The simplified model is then validated by conducting experiments under forced and natural convection conditions. A cross flow of air with a velocity of 4.7 m/s is made to pass over the turbocharger to obtain the forced convection condition. To validate the advanced model the experiments are conducted with three different VTG positions (100%, 50% and 0%) of the turbocharger turbine

The results show that the simplified model works with a relatively higher accuracy under natural convection condition and the model turbine exhaust temperature is 4-5°C lower than the experimental data. In the forced convection condition the model turbine exhaust temperature is 5-10 °C higher compared to the experimental data. This is due to the under prediction of the outside heat transfer coefficient calculated by using Zhukauskas correlation which works with an accuracy of 25%. The results show that on increasing the heat transfer coefficient by 20% the difference between the model and the experimental data reduces to 3-5°C.

The results show that with the 100% VTG position the advanced model turbine exhaust temperature is 20°C lower and the compressor outlet temperature is 3°C higher as compared to the experimental

73

values. This is due to over prediction of the turbine total efficiency calculated by using the dynamic measurements conducted on the test cell and due to lack of detail in modelling the compressor. Similar trends are observed with the 50% VTG position also. The correlations developed for the turbine effective cross-sectional area works with a reasonably high accuracy. The affect of over prediction of the total turbine efficiency is more dominant than the under prediction of the heat transfer coefficient. The results show that by decreasing the turbine total efficiency by 10% the turbine exhaust temperature increases by approximately 8°C and the compressor outlet temperature decreases by approximately 2°C hence come closer to the experimental data

The model closely approximates the transient variation of the bearing housing temperature in both the cases (100 and 50%VTG). The deviation in the temperature is due to improper location of the temperature sensor used and due to fact that the model does not considers the spatial effects. The advanced model works well with the 100% and 50% VTG positions but the accuracy of the model reduces with 0% VTG position. This is due to the non existence of the compressor air mass flow rate and also due to the variations in the flow patterns with the change in effective turbine cross-sectional area which affects the thermal conduction. This effect is not accounted in the model.

The simulation model is observed to predict the turbocharger behaviour with relatively good accuracy. The models suit perfectly for fast online simulation and can be easily purged into the complete engine cycle simulation model. The model is also proved to be helpful in solving the problem of limited effectiveness of catalytic converters during the light-off period.

6.2 Suggestions for further work

The following list contains the suggestions for further work

1. In the present model the shaft and the bearing housing assembly is considered as a solid cylindrical lump divided in three parts. The model could be further improved by considering the shaft and the bearing housing as separate units.

2. In the present model the energy balance applied over the shaft and bearing housing assembly does not consider the spatial effects and determines the temperature variation with time only. The model could be further improved to determine the temperature variation with both time and one spatial coordinate by using a one dimensional solver for the temperature distribution.

3. The model could be further improved by using a one dimensional solver for the determination of the temperature distribution through the compressor casing.

4. The present model uses Zhukauskas correlation for predicting the heat transfer coefficient for a cross flow over a circular cylinder which works with an accuracy of 25%. The accuracy of the model could be further improved by developing a more appropriate correlation.

5. The present model does not accounts the effect of conduction heat transfer from the heated lubricating oil to the turbine casing during initial periods The model could be further improved by considering this effect.

Bibliography

1) Frank P. Incropera

   Fundamentals of Heat and Mass Transfer

   Second edition 1988

2) Walson N, Janota M.S.

   Turbocharging Internal Combustion Engine

   Second edition 1990

3) Steven D. Burch, Thomas F Potter

   Reducing Cold-Start Emissions by Catalytic Converter Thermal Management

   NREL 950409, 1999

4) Chow A and Wyszynki M L.

   Thermodynamic modelling of complete engine systems –a review

   August 1998

5) Jim Kerr

   Emission Control Devices

   April 2004

6) Schneider P.J.

   Conduction Heat Transfer

   Addison-Wesley, 1955

7) Touloukian Y.S, Ho C.Y.

   Thermophysical Properties of Matter, The TPRC Data series

   Plenum Press, Newyork, 1970

8) Carslaw H.S, Jaeger J.C.

   Conduction of Heat in Solids

   Second edition, Oxford University Press, London, 1959

9) Schlichting H.

   Boundary Layer Theory

   Sixth edition, McGraw-Hill, New York, 1968

10) Kays W.M, Crawford M.E.

   Convective Heat and Mass Transfer

   McGraw-Hill, New York, 1980

11) Chilton T.H, Colburn A.P.

   Transactions of AIChE

   29, 174, 1933

12) Moody L.F.

   Transactions of ASME

   66, 671, 1944

13) Jaluria Y.

Natural Convection Heat and Mass Transfer

Pergamon Press, New York, 1980

14) Siegel R, Howell J R.

Thermal Radiation Heat Transfer

Second edition, McGrawHill, New York, !981

15) Gubareff G.G, Janssen J.E, Torberg R.H.

Thermal Radiation Properties Survey

Second edition, Honeywell Research Center, Minneapolis, 1960

16) Zhukauskas A

Heat transfer from Tubes in Cross Flow

Advances in Heat transfer

Vol 8, Academic press, New York, 1972

17 Morgan V.T

The Overall Convective Heat Transfer from Circular cylinders

Advances in Heat transfer

Vol 11Academic press, New York, 1975

Appendix

A1 Thermophysical properties

Property	Correlation/value	Units
Density of CI	7854	Kg/m^3
Dynamic viscosity of gas	$(.034232 \times T + 20.501)10^{-6}$	$N\ s/m^2$
Dynamic viscosity of air	$(-2.3 \times 10^{-5} \times T^2 + .049 \times T + 17)10^{-6}$	$N\ s/m^2$
Emissivity	.85	
Prandtl No of gas	$.263 \times 10^{-4} \times T + .727$	
Prandtl No of air	.71	
Specific heat of gas	1116	J/Kg.K
Specific heat of air	1050	J/Kg.K
Specific heat of CI	$(.0019 \times T_k^2 - 1.4918 \times T_k + 767.67)$	J/Kg.K
Thermal conductivity of gas	$(.0593 \times T + 25.1903)10^{-3}$	W/m K
Thermal conductivity of air	$(-2.7 \times 10^{-5} \times T^2 + .074 \times T + 24)10^{-3}$	W/m K
Thermal conductivity of CI	$(-4.9 \times 10^{-6} \times T_k^2 - .037 \times T_k + 72)$	W/m K

In the above given table T is the temperature in degree Celsius and T_k is the temperature in degree Kelvin.

A2 Model parameters

Parameter	Correlation/value	Units
Friction factor	.038	
Heat to the lubricating oil	$7.9 \times 10^2 (P_{3t}/P_{4s}) - 680$	J/s
Surrounding heat transfer coefficient under natural convection.	5	$W/m^2\ K$
Transmission efficiency	.9	

A3 Values of the constants used in Zhukauskas correlation

Re_{DC}	C	m
1-40	.75	.4
40-1000	.51	.5
$10^3 - 2 \times 10^5$	.26	.6
$2 \times 10^5 - 10^6$	.076	.7

A4 Dimensional measurements of the turbocharger

Turbine casing inlet section horizontal diameter	.037m
Turbine casing inlet section vertical diameter	.0284m
Turbine casing outlet section diameter	.038m
Length of the spiral of the turbine casing	.365m
Thickness of the spiral casing	.012m
Width of the turbine spiral casing	.068m
Outside diameter of the turbine casing	.118m
Outside diameter of the bearing housing	.05m
Length of the bearing housing	.03m
Compressor casing inlet section horizontal diameter	.0285m
Compressor casing inlet section vertical diameter	.0238m
Compressor casing outlet section diameter	.0337m
Length of the spiral of the compressor casing	.325m
Width of the compressor spiral casing	.035m
Outside diameter of the compressor casing	.111m

A5 Data available from the experiments

Entity	Symbol	Units
Turbocharger speed	Speed	RPM
Atmospheric temperature	T0	°C
Compressor inlet temperature	T1	°C
Compressor outlet temperature	T2	°C
Turbine inlet temperature	T3	°C
Turbine outlet temperature	T4	°C
Bearing housing temperature	TGehause	°C
Atmospheric pressure absolute	P0	mbar
Compressor inlet pressure absolute	P1	mbar
Compressor outlet pressure relative	P2	mbar
Turbine inlet pressure relative	P3	mbar
Turbine outlet pressure relative	P4	mbar
Nozzle pressure difference	Dp	mbar
Turbine air mass flow rate	Luft(Mair)	Kg/h
Fuel mass flow rate	Krafstoff(Mf)	Kg/h

A6 Data processed for characteristic maps, model inputs and validation.

Entity	Symbol	Equations used	Units
Compressor inlet density	rho1	$P1*100/287*(T3+273)$	Kg/m³
Compressor outlet density	rho2	$(P2+P0)*100/287*(T2+273)$	Kg/m³
Turbine inlet density	rho3	$(P3+P0)*100/287*(T3+273)$	Kg/m³
tauE	E	$P0-Dp/p0$	
EpsilonE	a	$SQRT((1.4*E^{(2/1.4)})/(1.4-1)*((1-E^{((1.4-1)/1.4)})/(1-E)))$	
Compressor mass flow rate	Mcom	$1.0309*a*.00159*WURZEL((2*P0*100*Dp*100)/(287*(273.15+T0)))$	Kg/s
Normalised massflow rate	Mnor	$Mcom*981/P1*SQRT((273.15+T1)/293)$	Kg/s
Compressor volumetric flow	Qcom	$Mnor*287/(P1*100)*SQRT((T1+273.15)*293)$	m³/sec
Compressor inlet velocity	V1	$Mcom/(rho1*.00196)$	m/s
Compressor outlet velocity	V2	$Mcom/(rho2*.00057)$	m/s
Turbine inlet velocity	V3	$(Mair+Mf+2)/3600/(rho3*.00419)$	m/s
Compressor inlet total pressure	P1t	$P1*100+rho1*V1^2/2$	N/m²
Comp outlet total pressure	P2t	$(P0+P2)*100+rho2*V2^2/2$	N/m²
Turbine inlet total pressure	P3t	$(P3+P0)*100+(rho3*V3^2)/2$	N/m²
Turbine outlet static pressure	P4s	$(P4+P0)*100$	N/m²
Hot gas mass flow rate	Mtur	$(Mair+Mf+2)/3600$	Kg/sec
Compressor pressure ratio	Pi	$P2t/P1t$	
Comp T2 isentropic	T2isen	$(273.15+C6)*Pi^{((1.4-1)/1.4)}$	°K
Comp isentropic	Effc	$(T2isen-(T1+273.15))/(T2-T1)$	

efficiency			
Turbine pressure ratio	Pit	P3t/P4s	
Reduced mass flow rate	Mred	(Mair+Mf+2)*SQRT(T36+273.15)/(P3t*3600/100000)	kg*SQRT(K)/bar*s
Comp isentropic enthalpy rise	hcom	1012*(T1+273.15)*(BA7^((1.4-1)/1.4)-1)	J/kg
Turbine isen enthalpy drop	htur	1160*(T3+273.15)*(1-(P4s/P3t)^((1.33-1)/1.33))	J/kg
Turbine total eff	Efftt	hcom*Mcom/(htur*Mtur*Effc)	

A7 Derivation of the equation used for calculating the mass flow rate of the hot gases through turbocharger turbine.

Equating the total enthalpy per unit mass across an open system

$$h_{1t} = h_{2t}.$$ (A.1)

Here h_{1t} and h_{2t} are the total enthalpies per unit mass flow at state points 1 and 2 respectively

$$h_{2t} = h_{2s} + \frac{w_2^2}{2}.$$ (A.2)

Here h_{2s} is the static enthalpy and w_2 is the flow velocity at the state point 2

Substituting equation 1.2 in equation 1.1 gives

$$h_{1t} = h_{2s} + \frac{w_2^2}{2}.$$ (A.3)

$$w_2 = \sqrt{2(h_{1t} - h_{2s})}.$$ (A.4)

Subsituting $h = c_p T$ and $p = \rho RT$ in equation 1.4 gives

$$w_2 = \sqrt{2(c_p T_{1t} - c_p T_{2s})}.$$ (A.5)

$$w_2 = \sqrt{2c_p \left(\frac{p_{1t}}{\rho_{1t}R} - \frac{p_{2s}}{\rho_{2s}R} \right)}.$$ (A.6)

$$w_2 = \sqrt{\frac{2c_p}{R} \frac{p_{1t}}{\rho_{1t}} \left(1 - \frac{\rho_{1t}}{p_{1t}} \frac{p_{2s}}{\rho_{2s}} \right)}.$$ (A.7)

Here $\gamma = \dfrac{c_p}{c_v}$ and $R = c_p(1-\frac{1}{\gamma})$

$$w_2 = \sqrt{\frac{2}{1-\frac{1}{\gamma}}\frac{p_{1t}}{\rho_{1t}}\left(1-\frac{p_{2s}}{p_{1t}}\frac{\rho_{1t}}{\rho_{2s}}\right)}\,.$$ (A.8)

For an isentropic processes

$$\frac{p_2}{\rho_2^{\gamma}} = \frac{p_1}{\rho_1^{\gamma}} = C\,.$$ (A.9)

$$\left(\frac{p_2}{p_1}\right)^{-\frac{1}{\gamma}} = \frac{\rho_1}{\rho_2} = C\,.$$ (A.10)

Subsituting equation 1.10 in equation 1.8 yields

$$w_2 = \sqrt{\frac{2}{1-\frac{1}{\gamma}}\frac{p_{1t}}{\rho_{1t}}\left[1-\frac{p_{2s}}{p_{1t}}\left(\frac{p_{2s}}{p_{1t}}\right)^{-\frac{1}{\gamma}}\right]}\,.$$ (A.11)

$$w_2 = \sqrt{\frac{2}{1-\frac{1}{\gamma}}\frac{p_{1t}}{\rho_{1t}}\left[1-\left(\frac{p_{2s}}{p_{1t}}\right)^{1-\frac{1}{\gamma}}\right]}\,.$$ (A.12)

$$w_2 = \sqrt{\frac{2}{1-\frac{1}{\gamma}}\frac{p_{1t}}{\rho_{1t}}\left(\frac{p_{2s}}{p_{1t}}\right)^{-\frac{2}{\gamma}}\left[\left(\frac{p_{2s}}{p_{1t}}\right)^{\frac{2}{\gamma}}-\left(\frac{p_{2s}}{p_{1t}}\right)^{1+\frac{1}{\gamma}}\right]}\,.$$ (A.13)

For mass flow rate

$$m = w_2 A\rho_2\,.$$ (A.14)

Here A is the effective turbine cross-section area.

Subsituting equation 1.13 in equation 1.14 yields

$$m = A\rho_2\sqrt{\frac{2}{1-\frac{1}{\gamma}}\frac{p_{1t}}{\rho_{1t}}\left(\frac{p_{2s}}{p_{1t}}\right)^{-\frac{2}{\gamma}}\left[\left(\frac{p_{2s}}{p_{1t}}\right)^{\frac{2}{\gamma}}-\left(\frac{p_{2s}}{p_{1t}}\right)^{1+\frac{1}{\gamma}}\right]}\,.$$ (A.15)

$$m = Ap_{1t}\sqrt{\frac{2}{1-\frac{1}{\gamma}}\frac{1}{RT_1}\left[\left(\frac{p_{2s}}{p_{1t}}\right)^{\frac{2}{\gamma}}-\left(\frac{p_{2s}}{p_{1t}}\right)^{1+\frac{1}{\gamma}}\right]}\,.$$ (A.16)

The equation 1.16 is used for calculating the mass flow rate of the gas through the turbocharger turbine.